AD-A118 963 FOREIGN TECHNOLOGY DIV WRIGHT-PATTERSON AFB OH F/G 3/2
RADIO-ASTRONOMICAL INSTRUMENTS OBSERVATIONS (SELECTED ARTICLES)--ETC(U)
AUG 82 L I MATVEYENKO, G S MISEZHNIKOV
UNCLASSIFIED FTD-ID(RS)T-0564-82 NL

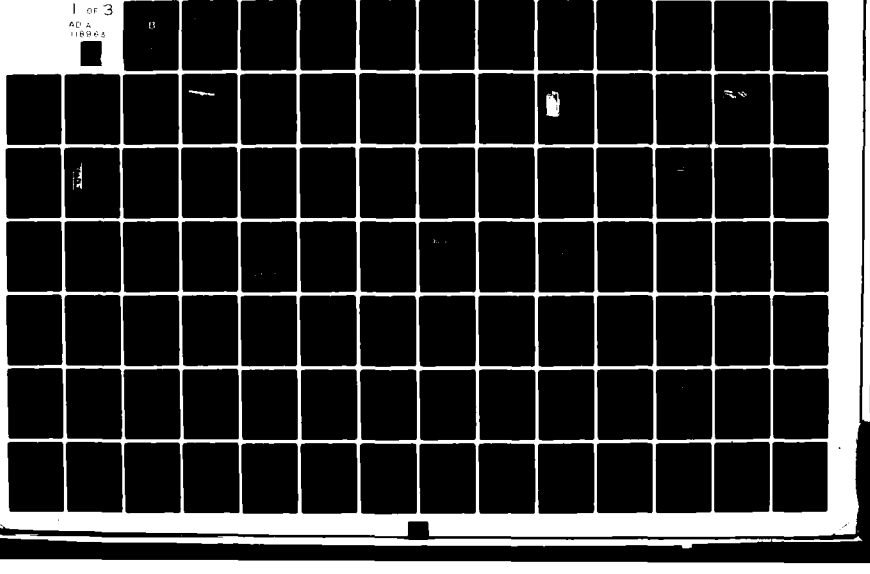

FTD-ID(RS)T-0564-82

FOREIGN TECHNOLOGY DIVISION

RADIO-ASTRONOMICAL INSTRUMENTS OBSERVATIONS

(Selected Articles)

Approved for public release;
distribution unlimited.

UNEDITED MACHINE TRANSLATION

FTD-ID(RS)T-0564-82 2 August 1982

MICROFICHE NR: FTD-82-C-001039

RADIO-ASTRONOMICAL INSTRUMENTS OBSERVATIONS
(Selected Articles)

English pages: 266

Source: Trudy Fizicheskogo Institut im. P.N. Lebedeva, Radioastronomicheskiye Instrumenty i Nablyudeniya, Publishing House "Nauka", Moscow, Vol. 47, 1969, pp. 25-84; 117-136; 149-162; 173-182; 201-211

Country of origin: USSR
This document is a machine translation.
Requester: FTD/SDSY

PREPARED BY:

TRANSLATION DIVISION
FOREIGN TECHNOLOGY DIVISION
WP-AFB, OHIO.

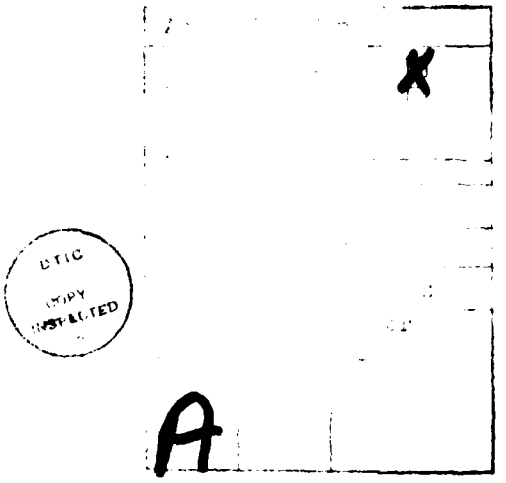

Table of Contents

U. S. BOARD ON GEOGRAPHIC NAMES TRANSLITERATION SYSTEM

Block	Italic	Transliteration	Block	Italic	Transliteration
А а	*А а*	A, a	Р р	*Р р*	R, r
Б б	*Б б*	B, b	С с	*С с*	S, s
В в	*В в*	V, v	Т т	*Т т*	T, t
Г г	*Г г*	G, g	У у	*У у*	U, u
Д д	*Д д*	D, d	Ф ф	*Ф ф*	F, f
Е е	*Е е*	Ye, ye; E, e*	Х х	*Х х*	Kh, kh
Ж ж	*Ж ж*	Zh, zh	Ц ц	*Ц ц*	Ts, ts
З з	*З з*	Z, z	Ч ч	*Ч ч*	Ch, ch
И и	*И и*	I, i	Ш ш	*Ш ш*	Sh, sh
Й й	*Й й*	Y, y	Щ щ	*Щ щ*	Shch, shch
К к	*К к*	K, k	Ъ ъ	*Ъ ъ*	"
Л л	*Л л*	L, l	Ы ы	*Ы ы*	Y, y
М м	*М м*	M, m	Ь ь	*Ь ь*	'
Н н	*Н н*	N, n	Э э	*Э э*	E, e
О о	*О о*	O, o	Ю ю	*Ю ю*	Yu, yu
П п	*П п*	P, p	Я я	*Я я*	Ya, ya

*ye initially, after vowels, and after ъ, ь; e elsewhere.
When written as ё in Russian, transliterate as yё or ё.

RUSSIAN AND ENGLISH TRIGONOMETRIC FUNCTIONS

Russian	English	Russian	English	Russian	English
sin	sin	sh	sinh	arc sh	$\sinh^{-1}$
cos	cos	ch	cosh	arc ch	$\cosh^{-1}$
tg	tan	th	tanh	arc th	$\tanh^{-1}$
ctg	cot	cth	coth	arc cth	$\coth^{-1}$
sec	sec	sch	sech	arc sch	sech^{-1}
cosec	csc	csch	csch	arc csch	csch^{-1}

Russian	English
rot	curl
lg	log

GRAPHICS DISCLAIMER

All figures, graphics, tables, equations, etc. merged into this translation were extracted from the best quality copy available.

RADIO-ASTRONOMICAL INSTRUMENTS OBSERVATIONS.

Page 25.

Radiometer with the quantum paramagnetic amplifier to the wave 8 cm.

L. I. Matveyenko, G. S. Misezhnikov, M. M. Zhukhina, V. B. Shteynshleyger.

Introduction.

In recent years in astrophysics wide acceptance received the radio-astronomical methods of study. These methods make it possible to record the radiation/emission of space objects over a wide range of radio waves and by it to judge about their physical properties. In the majority of the cases the intrinsic emission of radio sources is small, which imposes heavy demands on the sensitivity of radiotelescopes. The minimally revealed/detected density of flow is connected with the parameters of radiotelescope with the following relationship/ratio:

$$\delta S \sim \frac{\delta T}{A_{эфф}}, \qquad (1)$$

where δT - fluctuation sensitivity of radiometer, $A_{эфф}$ — effective antenna area.

As is known, the fluctuation sensitivity of radiometer the

higher, the lower the noise temperature at its input. Because of the successes of quantum radiophysics in recent years were developed the low-noise quantum paramagnetic amplifier (KPU). In particular, were developed by KPU of traveling wave 5- and 8-centimeter ranges, analogous in construction/design [1, 2]. However, there was no experiment on their use/application for the radio-astronomical measurements in the USSR. In 1962 were initiated the developments of radiometer with the quantum paramagnetic traveling-wave amplifier of 8-centimeter range. To the description of this radiometer and to the first results of observations and is dedicated this work

1. Selection of the diagram of radiometer.

The fluctuation sensitivity of radiometer, caused by the statistical fluctuations, is determined by the expression

$$\delta T = \alpha \frac{T_m}{\sqrt{\Delta f \tau}}, \qquad (2)$$

where T_m — noise temperature, led to the input of radiometer; Δf - passband of radiometer to the square law detector; τ - time constant of the integrating chain/network; α - coefficient, determined by the type of radiometer.

Page 26.

In the radio astronomy for the measurements in the continuous

spectrum obtaine use/application the following fundamental types of radiometers: compensative, correlation and modulation.

Maximum fluctuation sensitivity possesses compensation method $\alpha=1/\sqrt{2}$. Minimum - modulation, depending on the form of modulation and demodulation α it lies/rests within the limits $\pi^2/8-2$. Correlation type in the case $\alpha=1$ [3]. However, in spite of high fluctuation sensitivity, compensation method has a number of deficiencies/lacks, namely for the realization of its sensitivity it is necessary to ensure the stability of factor of amplification $\Delta k/k$, which corresponds $\frac{\Delta k}{k} < \frac{\delta T}{T_m} \approx 10^{-4}$, and since $\delta T \ll T_m$, its amplitude characteristic must be linear in the broad dynamic band. In the correlation method the recorded signal is proportional to the correlated part of two independently taken signals, which substantially weakens/attenuates the effect of the instability of amplification factor. However, in this case is retained requirement for the linearity of amplitude characteristic and, furthermore, additionally is superimposed the condition of the high decoupling between the inputs of radiometer. Modulation method is deprived of the deficiencies/lacks indicated, but it imposes heavy demands on modeling device/equipment. Ferrite switches and the valves/gates, which obtained wide acceptance in recent years, make it possible comparatively simply to exclude "parasitic" effects and to realize the fluctuation sensitivity of this method. Thus, the radiometer with

it is amplitude the modulation, which has higher technical sensitivity, it was accepted as the base.

2. Radiometer with the quantum paramagnetic amplifier.

Radiometer consists of the following fundamental assemblies: amplitude modulator, quantum paramagnetic amplifier, block of conversion, low-frequency part and feed. The block diagram of radiometer is shown in Fig. 1. For the larger reliability the schematics of the construction/design of nodes are maximally simplified. Schematic diagrams and requirements for them are examined below.

Input circuits of radiometer. Primary attention for an improvement in the fluctuation sensitivity of radiometer must be turned to a decrease in its noise temperature. The noise temperature of radiometer according to block diagram, is assumed that the high-frequency circuit is sufficiently well matched and the effect of disagreement/mismatch on the noise temperature can be disregarded/neglected):

$$T_ш = m\left\{T_а - T_0 + \frac{\beta_{м.0}+\beta_{м.а}}{\beta_{м.э}\beta_{м.а}}\left[\frac{T_{см}}{G3} + \frac{T_{кпу}}{3} + (1-3)\,T_0\right] + \right.$$
$$\left. + T_0\,(2-\beta_{м.а}-\beta_{м.э})\right\} + (0{,}5-m)\,T'_э \qquad (3)$$

where $T_а$, $T_э$, T_0 — noise temperatures of antenna, equivalent and

environment respectively; $T_{см}$ and $T_{КПУ}$ — noise temperatures of mixer and quantum paramagnetic amplifier; $\beta_{м.а}$, $\beta_{м.э}$ — straight/direct passage of modulator on the input of antenna and equivalent respectively; β - transmission factor of the high-frequency circuit between the modulator and the quantum paramagnetic amplifier; G - factor of amplification KPU in the power; m - coefficient, determined by the relative time of the inclusion/connectionof antenna and equivalent; T' - noise temperature of radiometer at the moments of switching.

Page 27.

The noise temperature of the antenna, advanced into the zenith, T_a is determined by its irradiation and temperature of the background of cosmic radio-frequency radiation. The temperature of equivalent $T_э$, as follows from [4], for weakening of the effect of the instability of the coefficient of radiometer it must be equal to the temperature of antenna. Thus, thenoise temperature of radiometer can be lowered due to the decrease of the noise temperature of mixer, losses of high-frequency circuit and use/application of the low-noise high gain amplifier. Modulator must have short switch time. In the case of the high temperature T' at the moments of switching the radiometer can be disconnected with the aid of suppressor pulses. The requirements indicated were taken into consideration during the

construction of the high-frequency part of the radiometer

Modulator. Amplitude modulator is in the radiometer the most critical element/cell on which depends the realization of fluctuation sensitivity. The investigations of the work of the amplitude modulators, constructed on crystal diodes and ferrite, which works in the longitudinal magnetic field, showed that the attenuation of the latter significantly does not exceed the attenuation of the first, but modulator on the ferrite is more stable in the work, it does not require tuning but the level of "parasitic" modulation is significantly below and virtually it does not depend on ambient temperature. In connection with this in the radiometer was established/installed the modulator on the ferrite.

Let us examine how is connected "parasitic" signal with the parameters of modulator. Let us represent modulator in the form of four-leg circulator connected according to the diagram, shown in Fig. 2. Let us designate β_{nm} the straight/direct transmissionbetween the nearest inputs, γ_{nm} — reverse/inverse weakening, T_n — noise temperatures at its inputs and $\Gamma_n = (k_n - 1)/(k_n - 1)$ — reflection coefficients.

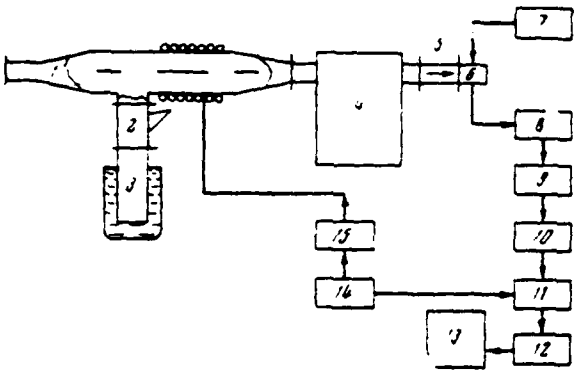

Fig. 1. Block diagram of radiometer with KPU. 1 - amplitude modulator; 2 - smooth attenuator; 3 - load equivalent; 4 - KPU; 5 - insulator; 6 - mixer; 7 - heterodyne; 8 - PUPCh [intermediate-frequency preamplifier]; 9 - UPCh and detector; 10 - UNCh; 11 - synchronous detector; 12 - UPT; 13 - recorder; 14 - GMC; 15 - power amplifier.

Page 28.

If we disregard/neglect interference terms and terms, which correspond to dual reflection, then signals at the output KPU will be equal to:

is connected the antenna

$$P_1 \propto [T_a(1-\Gamma_a^2)\beta_{a\,вых} - T_э(1-\Gamma_э^2)\gamma_{э.вых} - T_н(1-\Gamma_н^2)\Gamma_{а}^{2}\beta_{н.а}\beta_{а.вых} + + T_{КПУ}(1+2\Gamma_э\sqrt{\beta_{э.вых}\gamma_{э.вых}} + \Gamma_{э}^{2}\beta_{э.вых}\gamma_{э.вых}) - T_0(1-\beta_{а.вых})]G_a, \quad (4)$$

is connected the equivalent

$$P_1 \sim [T_1(1-\Gamma_1^2)\beta_{э.вых} - T_a(1-\Gamma_a^2)\gamma_{а.вых} + T_н(1-\Gamma_н^2)\Gamma_э^2\beta_{н.э}\beta_{э.вых} + \\ - T_{КПУ}(1-2\Gamma_э\sqrt{\beta_{э.вых}\gamma_{а.вых}} - \Gamma_а^2\beta_{а.вых}\gamma_{а.вых}) - T_0(1-\beta_{э.вых})]G_э. \quad (5)$$

It is obvious, signal at the output of radiometer in the case of square-law detection will be proportional to a difference in the values indicated, i.e.,

$$P = T_a(1-\Gamma_a^2)\beta_{а.вых} - T_э(1-\Gamma_э^2)\beta_{э.вых}\frac{G_э}{G_а} + T_1(1-\Gamma_1^2)\gamma_{э.вых} - \\ - T_a(1-\Gamma_a^2)\gamma_{а.вых}\frac{G_1}{G_а} + T_н(1-\Gamma_н^2)\left(\Gamma_а^2\beta_{н.а}\beta_{а\ вых} - \Gamma_э^2\beta_{н.э}\beta_{э.вых}\frac{G_э}{G_а}\right) + \\ + T_{КПУ}\left[(1-2\Gamma_э\sqrt{\beta_{э\ вых}\gamma_{э.вых}} - \Gamma_э^2\beta_{э\ вых}\gamma_{э.вых}) - \right. \\ \left. - (1-2\Gamma_а\sqrt{\beta_{а.вых}\gamma_{а.вых}} - \Gamma_а^2\beta_{а.вых}\gamma_{а.вых})\frac{G_1}{G_а}\right] + \\ + T_0\left[(1-\beta_{а.вых}) - (1-\beta_{э.вх})\frac{G_э}{G_а}\right]. \quad (6)$$

As can be seen from present expression, when $T_a = T_э$ the signal a the output of radiometer is not equal to zero. This "parasitic" signal in the general case is caused by the following reasons: a) by the disagreement/mismatch of the inputs of modulator, b) by a difference in the parameters of modulator in different arms, c) by the dependence of factor of amplification of KPU on the agreement of its input.

"Parasitic" signal can be compensated by the appropriate change in the temperature it is equivalent, but, since its value changes with change in the parameters of modulator, high-frequency circuit and amplification factor, balance will be unstable. Let us assume

that the antenna and equivalent are matched, modulator symmetrical and has low losses, and $T_a = T_э$. In this case, as it follows from (6), spurious signal will be determined by the value, approximately/exemplarily equal to $(T_a - T_{КПУ})$ $\Delta G/G$. Since $T_a - T_{КПУ} \approx 100°$ K, the obviously spurious signal can reach the significant magnitude. We have used KPU of the traveling wave, which work in the saturation mode on the signal of pumping and with the high decoupling in the opposite direction.

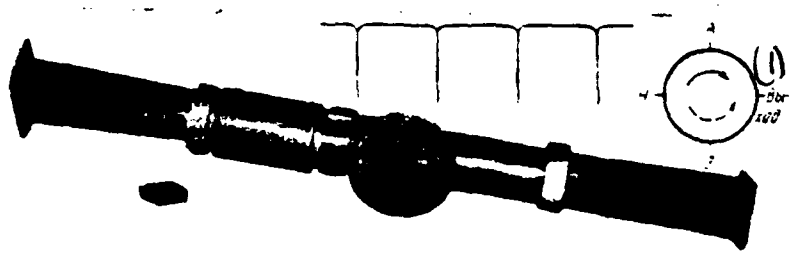

Fig. 2. Amplitude modulator (appearance, equivalent diagram and the form of modulation).

Key: (1). output.

Page 29.

As it is easy to show, in this case

$$\Delta G/G \approx 2(\Gamma_a - \Gamma_э)\sqrt{GL\gamma}\,\Gamma_{вых\ КПУ}.$$

where L and γ - fading signal in the opposite direction in KPU and modulator respectively. With L=-40 dB, γ=25 dB, $\Gamma_{вых\ КПУ} = 0.2$ and KSV of the outputs of modulator, equal to approximately/exemplarily 1.2, the effec ΔG can be disregarded/neglected.

In this case after simple conversions "parasitic" signal can be represented in the form

$$P \approx (T_a - T_0)(\beta_{a.вых} - \beta_{э.вых}) + T_a(\gamma_{э.вых} - \gamma_{э.вых}) + T_н(\Gamma_a^2 - \Gamma_э^2) + \\ + T_{КПУ}[(\Gamma_э^2\gamma_{э.вых} - \Gamma_a^2\gamma_{a.вых}) + 2(\Gamma_э\sqrt{\gamma_{э.вых}} - \Gamma_a\sqrt{\gamma_{a.вых}})].$$

As it follows from this expression, with the sufficiently good decoupling of modulator (about 20 dB) the effect of the second and fourth terms can be disregarded/neglected. In this case fundamental "parasitic" signal will be determined by the third term of equation, since $T_н = 300°$ K.. For weakening of its effect, obviously, it is necessary to thoroughly match the input of antenna and equivalent, also, as far as possible to make their identical. So that the contribution of this term would not exceed 0.5°K, the agreement of the inputs must be of order KSV~~1.2 and differ from each other not more than by several percentages. So that the effect of the first term it would be possible to disregard/neglect, when $\beta_н = 0.96$ a difference in the attenuations must not exceed several percentages. The conditions examined were taken into consideration during the construction of modulator.

The general view of modulator is shown in Fig. 2. Ferrite is arranged/located in the circular waveguide, in the magnetic field of solenoid. A change in the magnetic field with the modulation frequency as a result of the Faraday effect leads to the rotation of the plane of polarization of signal in +-45°. The length of ferrite is selected in such a way that the rotation would achieve saturation at angle of 45° and, thus, would create modulation, close to the rectangular (it was shown in Fig. 2), with the sine voltage of modulation. So increases sensitivity and is eliminated the effect of

the instability of the amplitude of the modulating voltage/stress. Tuning modulator achieved/reached the decoupling between its inputs not less than 25 dB and agreement on antenna input KSV=1.02 and on the input of equivalent KSV=1.045 in the transmission band of radiometer 20 MHz. For decreasing the losses the ferrite was dried up and placed into the sealed/pressurized polystyrene shell. Losses in the modulator on the antenna input were distributed as follows: waveguides - 0.06 dB, the absorbing plate - 0.01 dB, ferrite - 0.08 dB. Total losses 0.15 dB. Attenuation on the input of equivalent did not exceed 0.18 dB. The measured noise temperature of modulator proved to be equal to 10-15°K. The power of the modulating voltage/stress is 6.5 W.

Load - equivalent. The temperature of equivalent must be equal to the noise temperature of antenna. In our case the noise temperature of antenna at the mean angles of place is approximately 80°K. The conventional equivalent in the form of small horn antenna little is acceptable in this case due to its small directivity, which leads to the reception/procedure of interferences and deterioration in the sensitivity. In connection with this the equivalent was made in the form of waveguide by the section 10x60, loaded with key from polyiron. For decreasing of thermal conductivity and attenuation the waveguide is prepared from metallized silver-plated Getinax [laminated paper-Bakelite insulating material]. The collar of load

is ground/wiped and for guaranteeing its airtightness is connected to the modulator through the thin Teflon film. The measurement of the absorption of waveguide by the method of short circuit showed that it does not exceed 0.5o/o. Load is submerged in liquid nitrogen the boiling point of which composes 78°K.

Page 30.

For the exception/elimination of a change in the impedance of load in view of the liquefaction of air located within it the load is filled with the helium gas, which enters from the small rubber ball/sphere through the opening/aperture in the wide wall of waveguide. KSV of load in the range of the frequencies of the radiometer not are worse than 1.05. Thus, the noise temperature of load on its output collar did not exceed 80°K. The control of the temperature of equivalent was conducted with the aid of the smooth attenuator with the small attenuation 0-0.5 dB. The agreement of entire system is not worse KSV$\leq$1.15.

The noise temperatures of radiometer and gauging step were measured with the aid of the load, analogous to equivalent. The temperature of load changed with its insertion/immersion into liquid nitrogen, melting ice and boiling water. KSV of load in the band of radiometer are less than 1.05 and virtually it is not changed with a

change in its temperature.

Quantum paramagnetic amplifier. For decreasing the noise temperature in the radiometer is used quantum paramagnetic traveling-wave amplifier; its appearance is shown in Fig. 3. Amplifier is established/installed in the horizontal position and is connected with the modulator through the rotating transition. KPU in comparison with resonator type amplifier has wider passband (~20 MHz), smaller inherent noise level as a result of the absence of circulator on the input and more stable amplification factor. As the active material is utilized the ruby. The angle between the direction of trigonal crystal index and the direction of external magnetic field is equal to 90°. Signal frequency corresponds to transition/junction between the first and second energy levels, while the frequency of pumping - between the first and the fourth. This mode/conditions makes it possible to obtain maximum factor of amplification [1].

The investigation of the dependence of amplification factor on chromium concentration in the ruby showed that in this mode/conditions the greatest amplification on the wave 8 cm is achieved at concentration Cr^{3+}, the equal to 0.036o/o; the coefficient of inversion in this case it is equal to 4.5. The crystals of ruby are located in both sides of the bolt circuit whose

length is equal to 165 mm. In the band of the transparency of system (~150 MHz) the delay/retarding/deceleration of wave on the group velocity is equal to 100, and their own losses are 5 dB. At a temperature of 4.2°K agreement of input and output is equal KSV~~1.5.

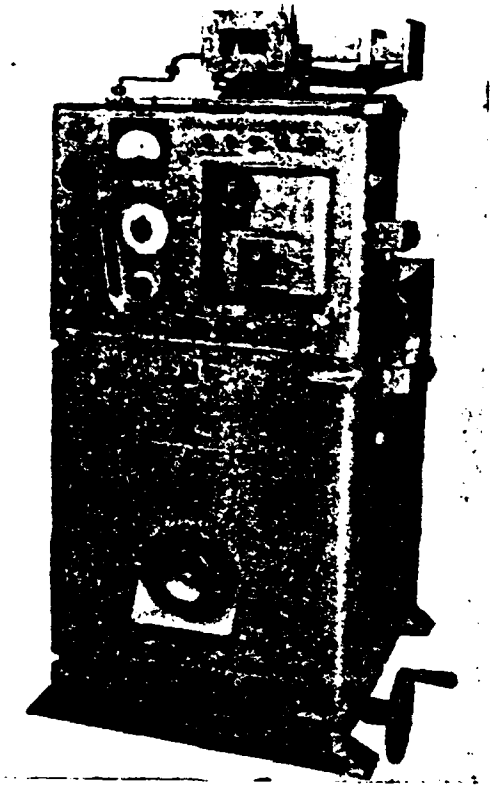

Fig. 3. Quantum paramagnetic amplifier of the traveling wave.

Page 31.

For absorbing backward wave is utilized ferrite valve element/cell in the form of the plates, situated under the ruby rods from both sides of circuit. The best valve properties at liquid-helium temperatures in the range 8 cm, as showed measurements, possesses polycrystalline

iron-yttrium ferrite with the structure of garnet. Circuit with supplying coaxial cables is placed in the metallic cryostat between the poles of external permanent magnet. Cryostat provides continuous operation of KPU for 8 hours.

The bilateral filling of circuit with ruby made it possible to raise amplification of KPU to 40o/o in comparison with the one-sided and to obtain with T=4.2°. To the amplification, equal to 32 dB with the losses in the circuit for direct wave 12 dB. The overall gain of KPU is 20 dB in the band of approximately 20 MHz. Reverse attenuation of KPU is equal to 40 dB. Its own noise temperature of KPU does not exceed 15° K. If necessary the amplification factor can be increased to 35 dB in the band of approximately 15 MHz by lowering the boiling point of liquid helium to 2° K by the evacuation of its vapors. Amplifier it allows/assumes retuning on +-50 MHz by the corresponding change in the magnetic intensity, without a change in the frequency of pumping.

The unit of converter (Fig. 4) consists of mixer, heterodyne, preliminary and fundamental IF amplifiers. On the output of the latter is located the square law detector. Unit is established/installed directly on the quantum paramagnetic amplifier, which decreases the additional losses in the high frequency and eliminates those rotating or flexible connections both on the high

and on the intermediate to frequencies. The inherent noise of the unit of conversion together with second channel are equal to 1350°K. Frequency characteristic is close to the rectangular and provides passband on the level of the half power of approximately/exemplarily 25 MHz. Mixer single-cycle, works on diode D405. The signal of heterodyne is supplied to the mixer through the directional coupler. At the input of mixer as the valve/gate is established/installed the circulator, which eliminates the incidence/impingement of the signal of heterodyne on KPU. Is directly to the output plug of mixer connected intermediate-frequency preamplifier. The input cascades/stages of this amplifier are assembled on the tubes 6S3P and 6S4P, connected on the cascade circuit.

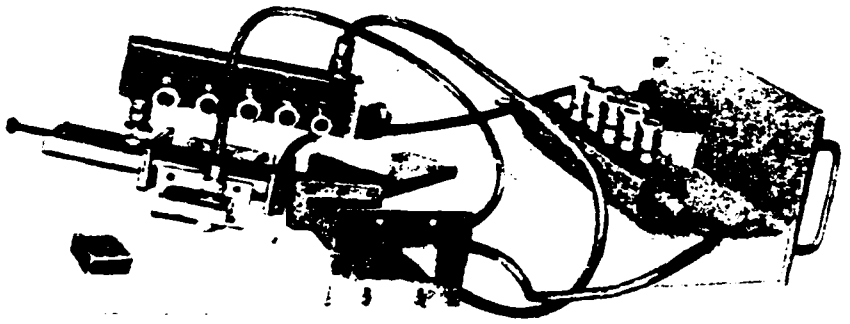

Fig. 4. The general view of the unit of frequency conversion.

Page 32.

As the square law detector is utilized the electron tube 6Zh1P in the diode inclusion/connection. The linearity of the amplitude characteristic of detector is retained to 0.1 V at its input. Checking the linearity of radiometer as a whole was conducted in the matched load, analogous to a load-equivalent whose temperature was equal to the temperature of liquid nitrogen, melting ice and boiling water, and also on the radio sources with the known flux of radio emission.

Low-frequency part of the radiometer. The general view of the low-frequency part of the radiometer is shown in Fig. 5. It consists of narrow-band amplifier of low frequency, tuned to a frequency of

modulation F=178 Hz. The expansion of the passband of low-frequency amplifier for guaranteeing complete transmission of the modulated signal, as shows practice, it does not lead to the expected gain in the sensitivity both because of the focusings/inductions and the complexity of guaranteeing the cophasality of the harmonics of signal and reference voltage. Therefore the passband of amplifier is made sufficiently narrow: Δf=10 Hz. Further contraction of band is inexpedient, since in this case can appear the instability of the phase of the intensive voltage/stress, especially with the change amplification factor with the aid of the attenuators. In this case grow/rise also the requirements for the stability of the generator of modulation frequency. Syncnronous detector is assembled on the double diode 6Kh2P. Its balancing/trimming eliminates the effect of the instability of reference voltage. Thus, a change in reference voltage ($U_{\text{ампл}}$ =11 V) on 3 dB virtually is not detected at the output of radiometer.

Dc amplifier is assembled on usual bridge circuit. Reference generator and power amplifier generate the sine voltage of modulation frequency F=178 Hz. Modulation frequency is selected from the point of view of the exception/elimination of focusings/inductions from the network/grid. The sinusoidal form of voltage/stress simplifies phasing and symmetrization of voltage/stress.

Power supply units. Radiometer, with exception of the unit of the generator of modulation frequency, is fed from the specially developed stabilizers of anode voltage with the stabilization factor, equal to 2500, with a change in the line voltage on 10o/o. The appearance of stabilizer is given in Fig. 5, and its diagram - 6. For decreasing the focusings/inductions from the network/grid in the radiometer is utilized the stabilizer of the filament DC voltage of the type VS25. The generator of modulation frequency is supplied on the anode from the stabilizer with the stabilization factor, equal to approximately/exemplarily 200.

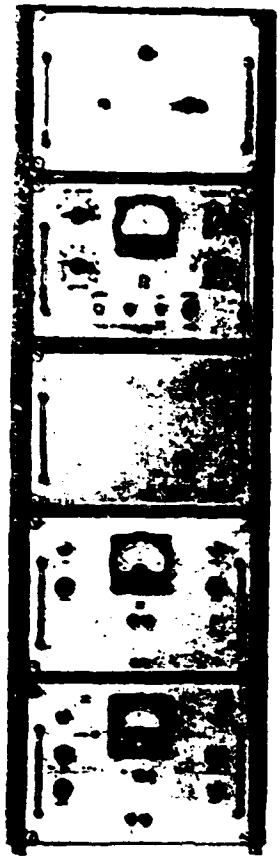

Fig. 5. The general view of the low-frequency part of the resonator.

Page 33.

Inclusion/connection of KPU significantly lowered the inherent noise of radiometer. Thus, if the noise temperature of radiometer without KPU (without second channel) was equal to 2700°K, then radiometer with KPU had a temperature, equal to 50°K, i.e., it is

more than 50 times lower. As one would expect, this decrease in the noise temperature came to light/detected/exposed effects ("parasitic" modulation, focusings/inductions, etc.), previously hidden in the noises. Supplementary tuning of high-frequency circuit KSV<1.15, filling of the waveguide of a load-equivalent with helium gas, the feed of the units of radiometer on the incandescence/filament by the DC voltage and high stability made it possible to lower these effects to the level of noise path/track and to raise the stability of amplification factor to 2o/o per hour of work.

In the process of tuning radiometer it was discovered, that the sensitivity of radiometer with KPU with a change in the time constant τ from 0.5 to 2 s increases more rapidly (about 30o/o), than this follows from the dependence $\tau^{-1/2}$. This special feature/peculiarity, apparently, is connected with the high-frequency component of the fluctuations (>1 Hz), caused by boiling helium in the cryostat.

In the radiometer was realized the fluctuation sensitivity, which according to the calculation was equal to $\delta T_p = 0{,}024^\circ$ K. In this case the general/common/total noise temperature of radiotelescope, according to measurements, took as equal to $T_m = 120^\circ$ K. the passband of radiometer Δf=20 MHz, τ=3.2 s, modulation rectangular, and demodulation sinusoidal. The measured sensitivity according to the sources with the known densities of the fluxes of radio emission and the calibration on the standard load proved to be equal to δT= (0.024+0.003)° K.

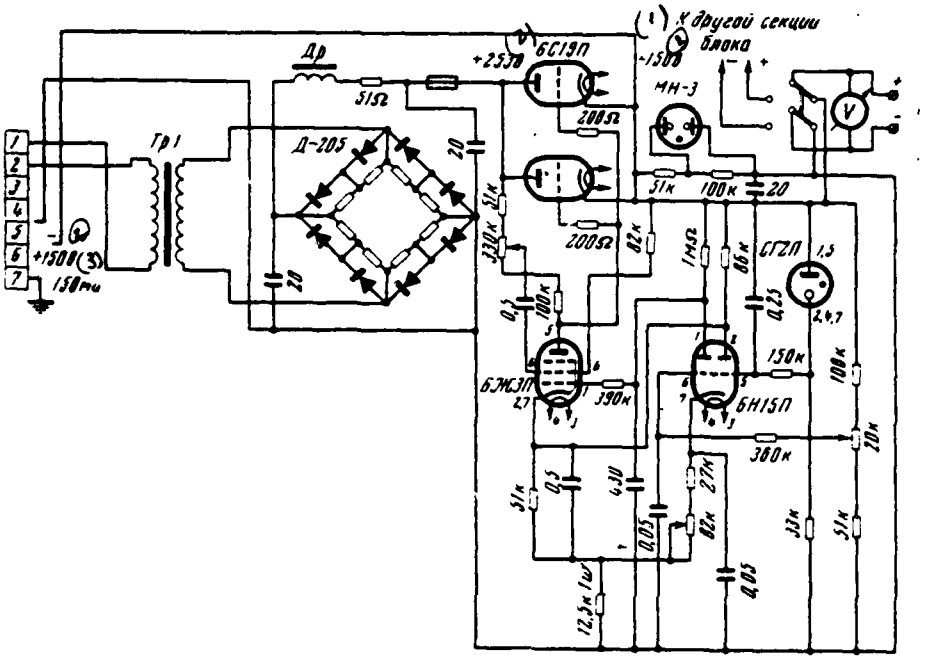

Fig. 6. Schematic diagram of the stabilizer of anode voltage.

Key: (1). To another section of unit. (2). V. (3). mA.

3. Results of observations.

The use/application of KPU raised the fluctuation sensitivity of radiotelescope along the flow approximately/exemplarily 10 times. Its sensitivity proved to be close to calculated and equal to $\delta s = 1.5 \cdot 10^{-21}$ W/m^2·Hz with the time constant of the integrating [5] device/equipment $\tau = 3.2$ s.

Page 34.

For an example Fig. 7 shows the recordings of the radio sources 3C 84 and 3C 273, the densities of the fluxes of radio emission [6] of which compose 7+-0.3 and 31 respectively. During October 1963 were initiated radio-astronomical observations. The recordings of the Crab Nebula showed that its right ascension, converted to epoch 1950.0 is equal to $\alpha = 5^h31^m29{,}7^s \pm 0{,}7^s$. i.e. it is displaced relative to the center of binary star to the west by $\Delta\alpha$=-25+-10". The size/dimension of nebula on half intensity level under the assumption of Gaussian distribution proved to be equal to φ=3.27+-0.05'. However, the total extent of the region of radio emission in the direction of right ascension (on level 1o/o) is equal to 6+-1' and with an accuracy to measuring error coincides with that optically seen.

High sensitivity and accuracy of tracking radiotelescope made it possible to for the first time conduct the observations of coating with the Moon [7] the sources of radio emission on the wave 8 cm. The investigations of the Crab Nebula by this method showed that in it, including in the predicted location of the remainder/residue of the supernova explosion of star, there are no sources of small angular dimensions (<2"), the contribution of radio emission of which would

comprise more than 2o/o. The center of gravity of nebula is displaced in the northwestern direction relative to the center of binary star on $\Delta\alpha$=-12+-5" and $\Delta\delta$=+17+-5". This displacement is caused by the presence in the northwestern part of the nebula, in the location of local formation/education [8], seen in the optic/optics, part No 3, whose sizes/dimensions are equal to approximately/exemplarily 30", and the contribution of its radio emission is approximately 8o/o. However, the region of radio emission does not fall outside the optically visible boundaries and virtually with them it coincides.

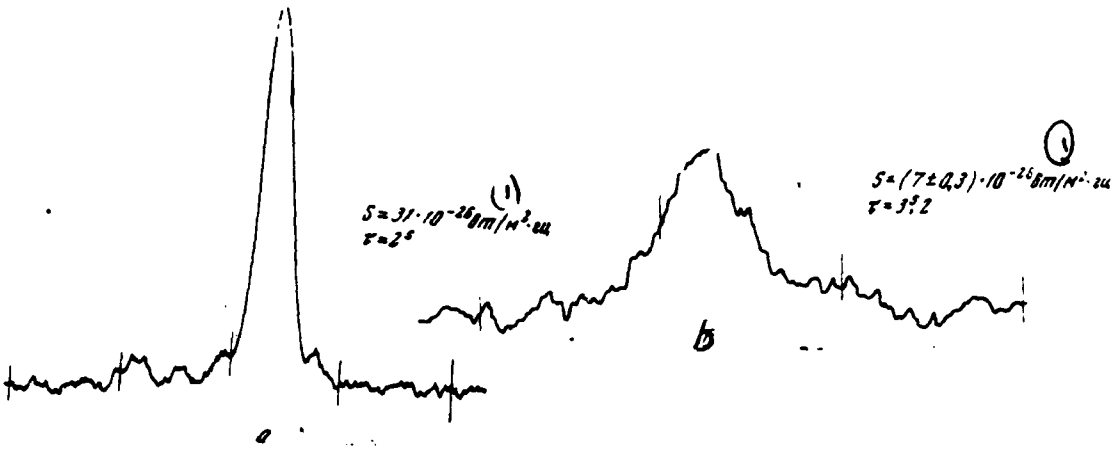

Fig. 7. Recording of radio sources 3C 273 (a) and 3C 84 (b).

Key: (1). W/m²·Hz.

Page 35.

The observations of coating radio source 3C 273 made it possible to divide the components of the radiation/emission of this source. It turned out that the ratio of the densities of the flows of these components [9] on the wave 8.2 cm is equal to 0.31.

The authors express deep gratitude to G. Ya. Gus'kov, A. D. Kuzmina and A. Ye. to Salomonovich for the attention to the work.

REFERENCES.

1. В. Б. Штейншлейгер, Г. С. Мисеженков, О. А. Афанасьев. Радиотехника и электроника, 7, 874 (1962).
2. В. Б. Штейншлейгер, О. А. Афанасьев, Г. С. Мисеженков, Я. И. Розенберг. ПТЭ, 5, 136 (1964).
3. B. J. Robinson. Ann. Rev. Astron. and Astrophys., 2, 401 (1964).
4. Ф. В. Бункин, Н. В. Карлов, ЖТФ, 25, 733 (1955).
5. Л. И. Матвеенко, Г. С. Мисеженков, М. М. Мухина, В. Б. Штейншлейгер. Докл. АН СССР, 161, 810 (1965).
6. В. И. Костенко. Л. И. Матвеенко. Астрон. ж., 43, 280 (1966).
7. Л. И. Матвеенко. Астрон. цирк., № 358, 5 (1966).
8. Л. И. Матвеенко. Астрон. цирк., № 343, 1 (1965).
9. Г. Б. Шоломицкий, Л. И. Матвеенко, Н. Ф. Слепцова. Астрон ж., 6, 1135 (1965).

Page 36.

METHOD OF STATIC COMPUTATION OF A PARABOLIC REFLECTOR ON A MULTIPLE-SUPPORT SUSPENSION.

P. D. Kalachev.

Introduction.

Radiotelescopes with the full-turn antennas in the form of parabolic reflector are at present the basic type of radiotelescopes. This is explained by the fact that the full-turn parabolic antenna successfully combines in itself the series/row of the positive qualities: the possibility of tracking the observed object and the accumulation of signal, the possibility of simultaneous work at several wavelengths [1], a comparatively light and rapid replacement of irradiators and, therefore, wave band, especially if we apply the removable cabins/compartments, placed at the apex/vertex of basic mirror and other advantages.

The international conference conducted in 1966 on the design of

large full-turn antennas in London showed that the interest, exhibited to the parabolic antennas, not only does not weaken, but, on the contrary, it continues to increase. At the same time parabolic antennas require for their creation both the use/application of large engineering and serious scientific investigations, connected with questions of the measurement of the surface of mirror, the elastic properties of the framework of mirror and its suspension, shading/blanketing of aperture by the constructions/designs, carrier the system of irradiation, etc. One of the most difficult problems with which we encounter during the creation of large parabolic antennas, is the guarantee of high mechanical rigidity of mirror.

The deformations of the reflecting surface of antenna in essence are caused by three reasons: by the effect of dead loads, loads due to wind and heating temperature by solar radiation. For the parabolic antennas of high rigidity and, therefore, relatively greater weight loads due to wind (at operational wind velocity $v_{в.к} \approx 6$-12 m/s) comprise the order 10o/o dead loads [2]. Thermal deformations, as shown in [3], can be partially or completely removed, the same relates also to loads due to wind. However, deformations from the dead weight under the conditions of the gravitational field of the Earth are nonremovable. Therefore principal part of the problem of the guarantee of high mechanical rigidity of parabolic antenna is the guarantee of low deformations from the effect of dead weight.

The difficulty of the problem of the guarantee of high rigidity of mirror lies in the fact that the mirror must rotate around the horizontal axis and its elastic deformations must be lowest possible at any angles of elevation of mirror, i.e., in any position of mirror in the space. In connection with this it is necessary to focus attention on the following fact. For technological reasons the installation of skin/sheathing of mirror, its alignment and finishing are produced in the horizontal position of the plane of the aperture of mirror.

Page 37.

Thus, in this position the form of the reflecting surface of mirror in the best way corresponds to calculated form[1].

FOOTNOTE [1]. In this position the form of mirror corresponds to calculated form with the precision/accuracy of measurements and finishing, i.e., with the precision/accuracy of the technological errors of manufacture. ENDFOOTNOTE.

Let us name/call this best form of the mirror of technological. This form of mirror does not depend on elastic deformations, caused

by the effect of dead weight, and therefore it is obtained without taking into account the latter. But these deformations, compensated by the finishing of surface, are located as in the concealed/latent form. If in the horizontal position of mirror was removed gravitational force, then deformations would be revealed, but in the opposite direction.

The same occurs during the rotation of mirror around the horizontal axis. In the vertical position of the plane of the aperture of mirror the direction of the force of gravity became parallel to the plane of aperture, whereas in the normal (to the plane of the aperture) direction the force of gravity in this position of mirror is absent. In this case is created such state of mirror which is equal to loading by its symmetric loadings of opposite direction. Furthermore, mirror by the load forces of dead weight, directed in parallel to the plane of aperture, and the picture of deformations is more complicated. The forces, normal to the plane of aperture, create symmetrical deformations, while the forces, parallel to the plane of aperture, skew-symmetric deformations.

In the present work is examined the method of determining symmetrical elastic deformations of mirror from the forces of dead weight.

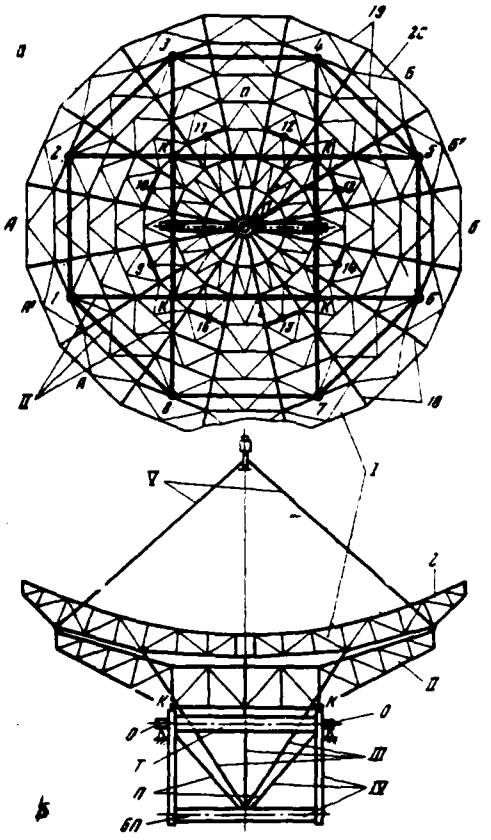

Fig. 1. The structure diagram of parabolic reflector on the multiple-support suspension. a) plan/layout; b) side view along the plane of the rotations of mirror around the horizontal axis.

Page 38.

1. The structure diagram of parabolic reflector on the

multiple-support suspension.

Fig. 1 depicts the structure diagram of parabolic reflector on the multiple-support suspension: on it it is marked: I - mirror; II - intermediate eight-support construction/design; III - Nine-rod pyramid with the central rod; IV - unit of the sectors of rotation; V - Eight-rod pyramid, carrier the system of irradiator; O - supporting/reference pins, BP - beam/gully of counterweight; P - half struts; T - horizontal axis; 1, 2, ..., 8 - eight basic supports of mirror, formed by eight-support intermediate construction/design; 9, 10, ..., 16, 17 - auxiliary supports, formed by the nine-rod pyramid which by its apex/vertex rests on the beam/gully of counterweight; letters K designated four units of intermediate construction/design, by which it is connected with the sectors of rotation. These units are arranged/located radiately relative to the center of mirror. The load-bearing frame of mirror is radiate three-dimensional frame, which encompasses radial, chord load-bearing elements and half struts in the lower panels, designated by 18, 19 and 20 respectively.

Fig. 2 depicts intermediate eight-support construction/design with the sectors of rotation in three projections. Into the structure diagram of intermediate construction/design they enter: 1-4, 8-5, 2-7, 3-6 - main beams; 1-8, 4-5, 2-3, 5-7 - end farms/trusses; 1-2, 3-4, 5-6, 7-8 - struts; K-9 - half struts; 10-10 -

connection/communication. Letters K designated the reference points of intermediate construction/design, i.e., the units, which connect it with the sectors of rotation.

Two sectors of rotation, connected with the beam/gully of counterweight, by the duct/tube/pipe of horizontal axis and by the communication system, which connects of the rim of sectors it is similar to squirrel wheel, is formed the rigid joint, capable of transferring the bending and torsional moments, applied between the supporting pins/journals. Intermediate eight-support construction/design, nine-rod pyramid and unit of the sectors of rotation are the system of the multiple-support suspension of parabolic reflector.

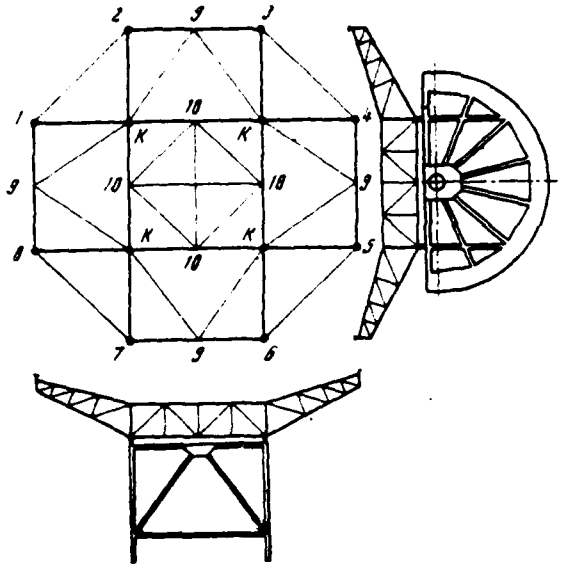

Fig. 2. The structure diagram of intermediate eight-support construction/design and unit of the sectors of rotation.

Page 39.

In this case the supporting structure contains 17 supports, arranged/located radiately relative to the center of mirror.

In the horizontal position of the plane of the aperture of mirror eight (1-8) basic supports, formed by intermediate supporting structure, have identical rigidity as a result of the symmetry of construction/design and load. All radial load-bearing elements are arranged/located equally relative to supports and, therefore, they

possess identical rigidity. Eight auxiliary (9—16) supports, formed by the side rods of nine-rod pyramid, also possess the identical rigidity of the first and second groups of supports, and also support 17, formed by central rod, then all supports will be identical rigidity and their displacements/movements will not affect the form of mirror.

In this case the discussion deals with the displacements/movements, parallel to the geometric (optical) axis of mirror, i.e., perpendicular to the plane of aperture. Besides vertical components, all reference points, eliminating central, will have even and the horizontal components of the displacements/movements which in the first approximation, it is possible not to consider, since, in the first place, the rigidity of mirror in the radial directions many times more than rigidity in the transverse direction, i.e., along the normal to the plane of aperture; in the second place, the distortion of the profile/airfoil of mirror they are only insignificant portion of the radial displacements, especially in the middle part.

2. Selection of basic system.

The calculation of parabolic reflector to the rigidity is reduced to two basic cases: a) calculation for the symmetric loadings

when are determined the symmetrical deformations corresponding to loads; b) calculation for the skew-symmetric loads when are determined skew-symmetric deformations.

In the present work we will examine the case of the symmetric loading of mirror, which corresponds to the horizontal position of the plane of aperture. In this case as a result of the symmetry the constructions/designs and the load of effort/force in all half struts, except those which match up the supporting units, are equal to zero.

Let us examine, for example, unit n (see Fig. 1). Efforts/forces in the half struts, which are adequate/approach unit n, as a result of the symmetry must be identical in the value and with respect to sign and, therefore, give component, normal to the chord element/cell. However, since chord element/cell cannot receive the efforts/forces, perpendicular to it, efforts/forces in the half struts prove to be equal to zero. Efforts/forces in all appropriate (symmetrical) elements/cells are identical. Therefore it suffices to produce the calculation only one one fourth of the mirror, which consists of two adjacent diametric load-bearing elements, mutually-intersecting in the center of mirror, and adjacent them chord and other load-bearing elements. The part of the mirror indicated, designated (see Fig. 1) by letters A-A'-A and B-B'-B, is

depicted in Fig. 3, where V - rods of the pyramid, carrier the system of irradiator; 2 - rods of nine-rod pyramid; 1, 9, 17, 13 and 5 - support of mirror. Entire mirror consists of four such parts, and each of them has five supports. Fig. 4 depicts in isometry the part of the load-bearing frame of mirror, which switches on two basic supports 5 and 6.

As it was already said, with the symmetric loading work only those half struts in the lower panels which match up the supporting units (for example, to units 1, 9, 13, and 5, Fig. 3).

Page 40.

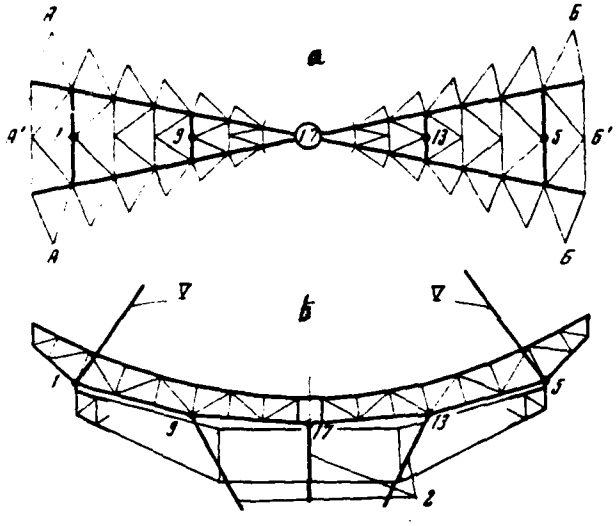

Fig. 3. Structure diagram of isolation/liberation of 1/4 parts of mirror with basic and auxiliary supports. a) plan/layout; b) side view.

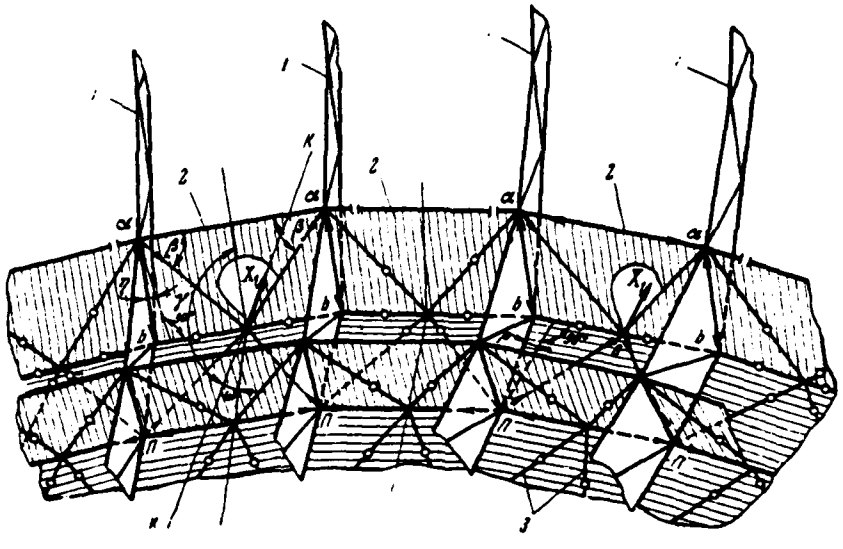

Fig. 4. Basic system of mirror (isometry). 1 - radial load-bearing elements; 2 - chord elements/cells; 3 - half struts in the lower panels; K-K - radial direction of effort/force X_1.

Page 41.

As far as chord (circular) load-bearing elements are concerned, in the principle on the symmetric loadings work all chord elements/cells, although in the central region of the mirror where its surface differs little from the horizontal plane, deformations and, consequently, also efforts/forces in the chord elements/cells are low, and for simplification in the calculation it is possible not to consider them. Then for the chosen part of the mirror for the basis it would be possible to accept the system, depicted in Fig. 5.

Two basic (outer) supports, which imitate intermediate construction/design, are resilient mountings. Three auxiliary supports are formed by three rods of the nine-rod pyramid whose apex/vertex (0) is fastened also to the resilient mounting (beam/gully of counterweight).

As the excess unknowns are accepted: the force of thrust, which appears from the effect of the intermediate supporting structure X_1; efforts/forces in the rods of pyramid X_2 and X_3; efforts/forces in

the chord elements/cells (circular efforts/forces) X_1, X_2, ..., X_{13}. Is here given the special case, when a number of excess unknowns is equal to 13. In large parabolic reflectors a number of chord elements/cells and, consequently, also the number of excess unknowns can be considerably greater. Since with an increase in the number of unknowns strongly grows/rises not only volume of calculating work[1], but also number of possible errors, then it is advisable as far as possible to decrease a number of unknowns with the substantiated simplification in the design diagram and basic system.

FOOTNOTE [1]. The volume of calculating work grows/rises proportional approximately/exemplarily to the square of a number of unknowns. ENDFOOTNOTE.

Basic requirement for the structure diagram of the multiple-support suspension of mirror lies in the fact that the vertical components of the displacements/movements of all its supports would be identical. Consequently, the lateral deformations of the load-bearing frame of mirror are possible only in the flights/spans between the supports and on the arms.

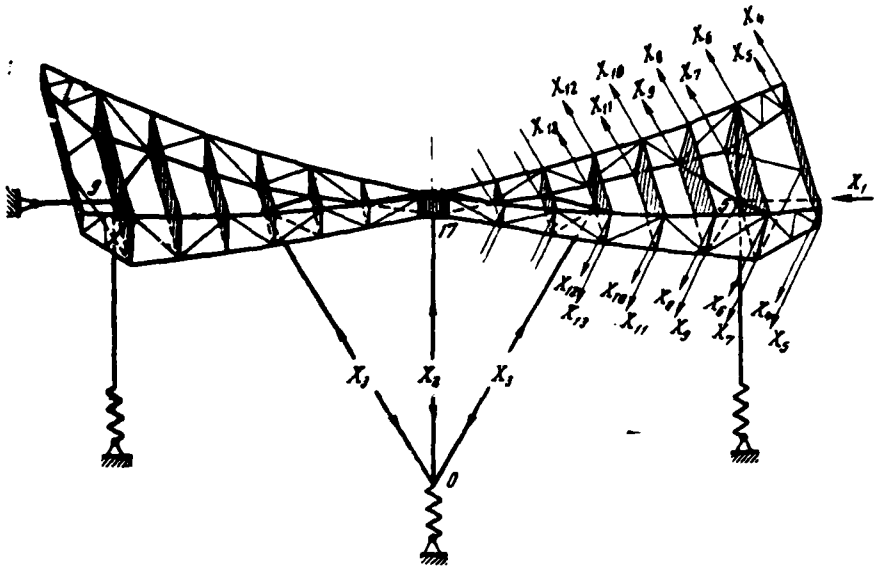

Fig. 5. Basic system for the chosen part of the mirror.

Page 42.

The lateral deformations of arms, generally speaking, can cause the considerable stretch deformations of chord elements/cells, for example the elements/cells of outer ring. However, transverse deformations in the flights/spans cause the insignificant stretch deformations of chord (circular) elements/cells, especially in the average/mean flights/spans.

Taking into account this fact, basic system for the mirror can be substantially simplified. Fig. 6 depicts the simplified basic

system for the mirror. On the side view is shown the power articulation of the chosen part of the mirror with the intermediate supporting structure and the beam/gully of counterweight. This system switches on altogether only five excess unknowns: X_1, ..., X_5, where X_1 - force of thrust (effect of intermediate construction/design), X_2 and X_3 - efforts/forces in the rods of pyramid, X_4 and X_5 - efforts/forces in the chord elements/cells of outer ring. Fig. 6b the dead weight of chosen one fourth of mirror ($^1/_4 G_{зерк}$) conditionally shows in the form of distributed load at the length of the projection of diametric elements/cells. P and Q - concentrated load on the beam/gully from the counterweight (P) and the weights of the rods of pyramid (Q). The dead weight of the beam/gully of counterweight is depicted in the form of evenly distributed load q. One of the special features/peculiarities of the structure diagram of mirror and its suspension in question is the fact that this diagram consists of three clearly divisible power packs: the load-bearing frame of mirror with the nine-rod pyramid, intermediate eight-support construction/design and sector of rotation with the beam/gully of counterweight. In accordance with this and the design diagram, and basic system were divided into three parts: for the chosen section of mirror (Fig. 5 and 6); for the intermediate construction/design (Fig. 7 and 8); for the beam/gully of counterweight (Fig. 9).

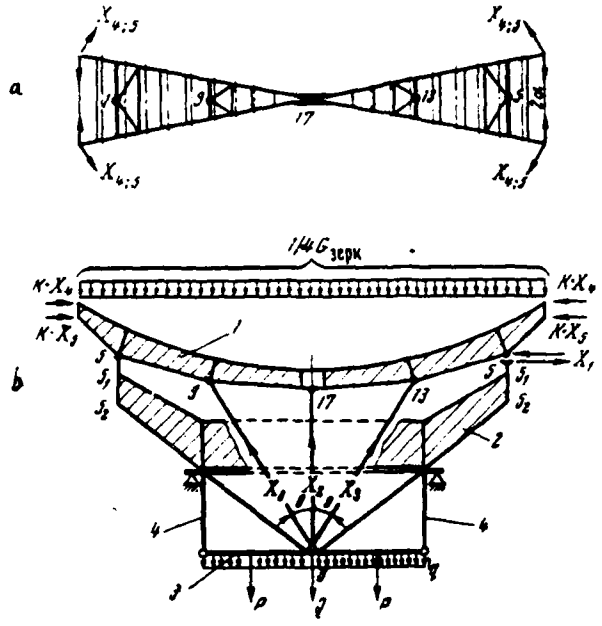

Fig. 6. Simplified basic system for the chosen part of the mirror. a) plan/layout; b) side view; K=2sinα; 1 - mirror; 2 - intermediate supporting structure; 3 - beam/gully of counterweight; 4 - load-bearing elements of the sectors of rotation (spoke).

Page 43.

Fig. 7 depicts the basic system for the intermediate supporting structure (in the plan/layout), which contains one excess unknown.

Fig. 8 presents (in isometry) one fourth of the intermediate supporting structure, which corresponds to half of the part of the

mirror depicted in Fig. 5, i.e., by two adjacent radial farms/trusses with the adjacent chord elements/cells and the half struts.

Fig. 9 depicts basic system for the unit of the sectors of rotation with the beam/gully of counterweight which also contains one excess unknown.

Thus, entire system of mirror and its suspension contains seven excess unknowns, but it is divided into three independent systems, two of which contain only on one unknown.

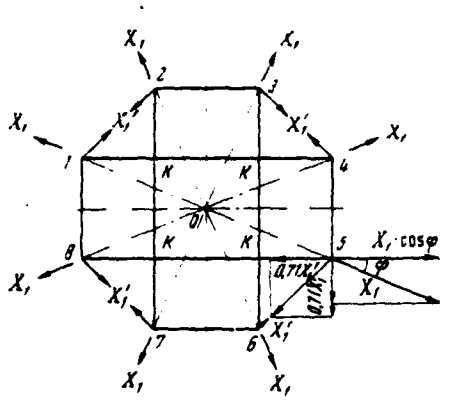

Fig. 7.

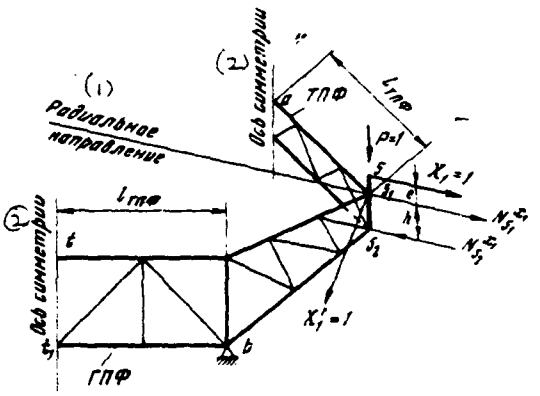

Fig. 8.

Fig. 7. Basic system for intermediate construction/design.

Fig. 8. Basic system for chosen part of intermediate construction/design. TPF - end semitruss; GPF - main semitruss.

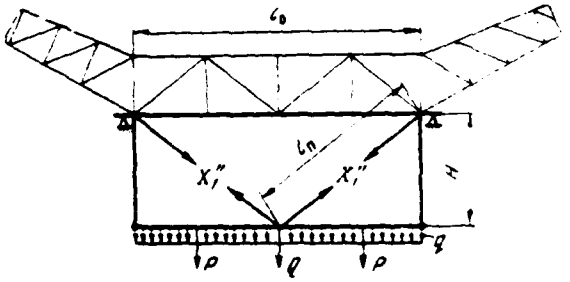

Fig. 9. Basic system for unit of sectors with beam/gully of counterweight.

Page 44.

3. Static computation of mirror and its suspension according to the separated diagram.

It was previously noted that the diagram of mirror in question on the multi-support suspension (17-support) structurally/constructionally consists of three assemblies: mirror with the nine-rod pyramid, intermediate eight-support construction/design and sectors of rotation with the beam/gully of counterweight.

Static computation according to the expanded diagram lies in the fact that independently are calculated the chosen part of the mirror along the basic system (Fig. 6), intermediate supporting structure along the basic system (Fig. 7 and 8) and assembly of the sectors of rotation with the beam/gully of counterweight (Fig. 9). In this case the system of mirror contains five excess unknowns, and systems for the intermediate construction/design and for the sectors have, as to already be said, only on one unknown.

The determination of unknowns for the systems of intermediate construction/design and sectors is not of interest and by us it is not examined. However, system for the mirror contains some special features/peculiarities, and its examination is of known interest. The fact is that the displacements/movements in the basic system for the mirror depend on the elasticity of intermediate construction/design and sectors of rotation.

The system of canonical equations for the basic system of mirror and nine-rod pyramid let us register as follows:

$$\begin{aligned}
\delta_{11}X_1+\delta_{12}X_2+\delta_{13}X_3+\cdots+\delta_{15}X_5+\Delta_{1p}&=-X_1\delta'_{11}-X_2\delta'_{12}-X_3\delta'_{13}-\Delta'_{1p},\\
\delta_{21}X_1+\delta_{22}X_2+\delta_{23}X_3+\cdots+\delta_{25}X_5+\Delta_{2p}&=-X_1\delta'_{21}-X_2(\delta'_{22}+\delta''_{22})-\\
&\quad-X_3(\delta'_{23}+\delta''_{23})-\Delta'_{2p}-\Delta''_{2p},\\
\delta_{31}X_1+\delta_{32}X_2+\delta_{33}X_3+\cdots+\delta_{35}X_5+\Delta_{3p}&=-X_1\delta_{31}-X_2(\delta'_{32}+\delta''_{32})-\\
&\quad-X_3(\delta'_{33}+\delta''_{33})-\Delta'_{3p}-\Delta''_{3p},\qquad(1)\\
\delta_{41}X_1+\delta_{42}X_2+\delta_{43}X_3+\cdots+\delta_{45}X_5+\Delta_{4p}&=0,\\
\delta_{51}X_1+\delta_{52}X_2+\delta_{53}X_3+\cdots+\delta_{55}X_5+\Delta_{5p}&=0.
\end{aligned}$$

Page 45.

In the general case (without taking into account of torsion and temperature effects) the coefficients with the unknowns and the absolute terms of the right sides of the equations are determined by known formulas [4]:

$$\begin{aligned}
\delta_{ii}&=\frac{1}{E}\left(\sum\overline{N}_i^2\frac{l}{F}\right)+\frac{1}{E}\int\overline{M}_i^2\frac{dx}{I}+\frac{\mu}{G}\int\overline{Q}_i^2\frac{dx}{F},\\
\delta_{ik}&=\frac{1}{E}\left(\sum\overline{N}_i\overline{N}_k\frac{l}{F}\right)+\frac{1}{E}\int\overline{M}_i\overline{M}_k\frac{dx}{I}+\frac{\mu}{G}\int\overline{Q}_i\overline{Q}_k\frac{dx}{F},\\
\Delta_{ip}&=\frac{1}{E}\left(\sum\overline{N}_i\overline{N}_p\frac{l}{F}\right)+\frac{1}{E}\int\overline{M}_i\overline{M}_p\frac{dx}{I}+\frac{\mu}{G}\int\overline{Q}_i\overline{Q}_p\frac{dx}{F},
\end{aligned}$$

where the first terms - displacement/movement due to the deformations of the rod elements of system, the second and third terms - displacement/movement respectively due to the bending deformations and the shearing strains in the girder elements of system. The right sides of the system of equations (1) are the effect of intermediate construction/design and sectors of rotation with the beam/gully of counterweight and are determined by the relationships/ratios

$$E\delta_{11}' = \left(\sum \overline{X}_1 N_{\Sigma x_1} \frac{l}{E}\right)_{\text{ст.п.к}} + \frac{1}{I}\int \overline{M}_1^2 dx - \frac{\mu k}{F_{\text{ст}}}\int \overline{Q}_1^2 dx.$$

where the first term - displacement/movement in direction X_1 due to the deformations of the cruxes of intermediate construction/design, the second and third terms - displacement/movement in the same direction due to the bending strains and shift/shear in beam-strut $5\text{-}5_2$ (see Fig. 8), the generatrix the basic reference point of mirror; $\overline{X}_1$ and $N_{\Sigma x_1}$ - effort/force in the rod elements of intermediate construction/design from effect $\overline{X}_1=1$ in the basic system and respectively total efforts/forces in the same elements/cells taking into account effort/force $\overline{X}_1'$ in the strut; $\overline{M}_1$ and $\overline{Q}_1$ - bending moment and transverse force in beam- strut from effect $X_1=1$; l and F - length and the cross-sectional area of rods; I, $F_{\text{ст}}$ and μ - moment of inertia, cross-sectional area and the coefficient of structural section; k=E/G; E and G - moduli of elasticity of the first and second kind.

$$E\delta_{12}' = \left(\sum \overline{X}_1 N_{\Sigma x_1} \frac{l}{F}\right)_{\text{ст.п к}},$$

$$E\delta_{13}' = 2\delta_{12}' \cos\theta,$$

where $N_{\Sigma x_1}$ - total efforts/forces in the rod elements of intermediate construction/design from effect $X_2=1$ taking into account effort/force X'_1 in the strut.

Since efforts/forces in the girder element/cell $5\text{-}5_2$ from effect $\overline{X}_2=1$ and $\overline{X}_3=1$ are equal to zero, then the terms, which contain integrals, are absent.

$$E\Delta'_{1p} = \left(\sum \overline{N}_1 N_{\Sigma p} \frac{l}{F}\right)_{\text{ст.п.к}} + \int \overline{M}_1 M_{\Sigma p} \frac{dx}{I} + \mu k \int \overline{Q}_1 Q_{\Sigma p} \frac{dx}{F_{\text{ст}}}.$$

Here $N_{\Sigma p}$ - effort/force in the rod elements of intermediate construction/design from the effect of load (the dead weight of system) taking into account effort/force in the strut; $M_{\Sigma p}$ and $Q_{\Sigma p}$ - bending moment and transverse force in the girder element/cell $5\text{-}5_2$ taking into account effort/force in strut X_1 (see Fig. 7 and 8).

$$E\delta'_{22} = \left(\sum \overline{N}_2 N_{\Sigma x_2} \frac{l}{F}\right)_{\text{ст.п.к}} + \left(\sum \overline{N}_2 N_{\Sigma x_2} \frac{l}{F}\right)_{\text{ст. сект}} + \int \overline{M}_2 M_{\Sigma x_2} \frac{dx}{I} + \mu k \int \overline{Q}_2 Q_{\Sigma x_2} \frac{dx}{F_{\text{ст}}},$$

where the second term - displacement/movement due to the deformations of the rod elements/cells of the unit of sectors from effect $X_2=1$ taking into account effort/force in half struts X'_1; two latter term - displacement/movement due to the deformations of the beam/gully of counterweight, moreover $M_{\Sigma x_2}$ and $Q_{\Sigma x_2}$ - bending moment and transverse force in the beam/gully from effect $X_2=1$ taking into account

effort/force in half struts X'$_1$'.

$$\delta'_{23} = 2\delta'_{22}\cos\theta,$$

$$E\Delta'_{2p} = \sum \bar{N}_2 N_{\Sigma p} \frac{l}{F}_{\text{ст п.к}} - \sum \bar{N}_2 N_{\Sigma p} \frac{l}{F}_{\text{ст. сект}} -$$
$$- \int \bar{M}_2 M_{\Sigma p} \frac{dx}{I} - \mu k \int \bar{Q}_2 Q_{\Sigma p} \frac{dx}{F_{\text{ст. б.5-5}_2}} -$$
$$- \int \bar{M}_2 M_{\Sigma p} \frac{dx}{I} - \mu k \int \bar{Q}_2 Q_{\Sigma p} \frac{dx}{F_{\text{ст. б п.в}}},$$

where the first two members - displacement/movement due to the deformations of the rod elements of intermediate structure and unit of the sectors of rotation; latter/last two members - displacement/movement due to the bending strains and shift of the respectively girder elements of intermediate structure (beam/gully 5-5$_2$) and unit of sectors (beam/gully of counterweight) from the effect of load (inherent weight of system); $N_{\Sigma p}$, $M_{\Sigma p}$ and $Q_{\Sigma p}$ - corresponding power factors, undertaken taking into account efforts/forces in struts X'$_1$ and half struts X'$_1$'.

$$\delta'_{33} = 4\delta'_{22}\cos^2\theta,$$
$$\Delta'_{3p} = 2\Delta'_{2p}\cos\theta.$$

Page 46.

Concerning δ'_{21}, δ'_{31}, δ'_{32}, they, as is known, are equal to respectively δ'_{12}, δ'_{13} and δ'_{23}.

System of equations (1) can be registered also in other form, after transferring all terms of equations from right to left and giving the similar terms:

$$
\begin{aligned}
&(\delta_{11}+\delta'_{11})X_1-(\delta_{12}+\delta'_{12})X_2+(\delta_{13}+\delta'_{13})X_{13}+\cdots+\delta_{15}X_{15}+(\Delta_{1p}+\Delta'_{1p})=0,\\
&(\delta_{21}+\delta'_{21})X_1+(\delta_{22}+\delta'_{22}+\delta''_{22})X_2-(\delta_{23}+\delta'_{23}+\delta''_{23})X_3+\cdots\\
&\qquad\qquad\cdots\delta_{25}X_5+(\Delta_{2p}+\Delta'_{2p})=0;\\
&(\delta_{31}+\delta'_{31})X_1+(\delta_{32}+\delta'_{3.})X_2+(\delta_{33}+\delta'_{33})X_3+\cdots+\delta_{35}X_5+(\Delta_{3p}+\Delta'_{3p})=0,\\
&\delta_{41}X_1+\delta_{12}X_2+\delta_{43}X_3+\cdots+\delta_{45}X_5+\Delta_{4p}=0,\\
&\delta_{51}X_1+\delta_{52}X_2+\delta_{53}X_3+\cdots+\delta_{55}X_5+\Delta_{5p}=0.
\end{aligned}
\qquad (2)
$$

The recording of system of equations (2) reflects only that (formal) fact that the sum of displacements/movements over directions 1, 2, ..., 5 from the effects of all power factors is equal to zero, i.e., construction/design is continuous. However, recording (2) will be necessary by us subsequently in order to show the identity of coefficients and absolute terms, obtained in the separated diagram, with the coefficients and the absolute terms which we will deduce subsequently in the examination of the method of static computation of mirror and its suspension as single system.

4. Static computation of mirror and its suspension as single system.

The system: mirror, intermediate eight-support construction/design, nine-rod pyramid and the unit of the sectors of rotation with the beam/gully of the counterweight (see Fig. 6-9) - it contains seven excess unknowns: X_1, X_2, ..., X_5, X'_1 and $X'_1{}'$. After designating X'_1 and $X'_1{}'$ respectively through X_6 and X_7, let us write the system of canonical equations for seven unknowns:

$$
\begin{aligned}
&\bar{\delta}_{11}X_1 + \bar{\delta}_{12}X_2 + \bar{\delta}_{13}X_3 + \bar{\delta}_{14}X_4 + \bar{\delta}_{15}X_5 + \bar{\delta}_{16}X_6 + \bar{\delta}_{17}X_7 + \bar{\Delta}_{1p} = 0,\\
&\bar{\delta}_{21}X_1 + \bar{\delta}_{22}X_2 + \bar{\delta}_{23}X_3 + \bar{\delta}_{24}X_4 + \bar{\delta}_{25}X_5 + \bar{\delta}_{26}X_6 + \bar{\delta}_{27}X_7 + \bar{\Delta}_{2p} = 0,\\
&\bar{\delta}_{31}X_1 + \bar{\delta}_{32}X_2 + \bar{\delta}_{33}X_3 + \bar{\delta}_{34}X_4 + \bar{\delta}_{35}X_5 + \bar{\delta}_{36}X_6 + \bar{\delta}_{37}X_7 + \bar{\Delta}_{3p} = 0,\\
&\bar{\delta}_{41}X_1 + \bar{\delta}_{42}X_2 + \bar{\delta}_{43}X_3 + \bar{\delta}_{44}X_4 + \bar{\delta}_{45}X_5 + \bar{\delta}_{46}X_6 + \bar{\delta}_{47}X_7 + \bar{\Delta}_{4p} = 0,\\
&\bar{\delta}_{51}X_1 + \bar{\delta}_{52}X_2 + \bar{\delta}_{53}X_3 + \bar{\delta}_{54}X_4 + \bar{\delta}_{55}X_5 + \bar{\delta}_{56}X_6 + \bar{\delta}_{57}X_7 + \bar{\Delta}_{5p} = 0,\\
&\bar{\delta}_{61}X_1 + \bar{\delta}_{62}X_2 + \bar{\delta}_{63}X_3 + \bar{\delta}_{64}X_4 + \bar{\delta}_{65}X_5 + \bar{\delta}_{66}X_6 + \bar{\delta}_{67}X_7 + \bar{\Delta}_{6p} = 0,\\
&\bar{\delta}_{71}X_1 + \bar{\delta}_{72}X_2 + \bar{\delta}_{73}X_3 + \bar{\delta}_{74}X_4 + \bar{\delta}_{75}X_5 + \bar{\delta}_{76}X_6 + \bar{\delta}_{77}X_7 + \bar{\Delta}_{7p} = 0. \qquad (3)
\end{aligned}
$$

Page 47.

Here coefficient with the unknowns and absolute terms, generally speaking, are different from the coefficients and the absolute terms of system (1) and therefore they are noted by hyphens.

Coefficients and absolute terms of system (3) can be expressed through the coefficients and the absolute terms of system (1) as follows:

$$\bar{\delta}_{ii} = 2\left(\sum \bar{X}_i^2 \frac{l}{EF}\right)_{\text{р.ф}} + \left(\sum \bar{X}_i^2 \frac{l}{EF}\right)_{\text{ст.д.к}} + \int \bar{M}_i^2 \frac{dx}{EI} + \mu \int \bar{Q}^2 \frac{dx}{GF_{\text{ст}}}, \qquad (4)$$

where the first term - displacement/movement due to the deformation of the rods of two adjacent radial farms/trusses of the mirror (see Fig. 5 and 6), and also the rods of nine-rod pyramid; the second term - displacement/movement due to the deformation of the cruxes of intermediate construction/design, latter/last two members - displacement/movement due to the deformation of the girder elements

of intermediate construction/design. But

$$2\left(\sum \bar{X}_1^2 \frac{l}{EF}\right)_{\text{р.ф}} = \delta_{11}, \tag{5}$$

$$\left(\sum \bar{X}_1^2 \frac{l}{EF}\right)_{\text{ст.п.к}} + \int \bar{M}_1^2 \frac{dx}{EI} + \mu \int \bar{Q}_1^2 \frac{dx}{EF_{\text{ст}}} = \delta'_{11} + \frac{\bar{\delta}_{16}^2}{\bar{\delta}_{66}}. \tag{6}$$

Equality (6) can be demonstrated as follows. Let us represent the displacement of the point of 5 intermediate constructions/designs (see Fig. 8) in direction X_1 as

$$\delta'_{11} = \left(\sum \bar{X}_1^2 \frac{l}{EF}\right)_{\text{ст.п.к}} + \int \bar{M}_1^2 \frac{dx}{EI} + \mu \int \bar{Q}_1^2 \frac{dx}{GF_{\text{ст}}} - \left[\left(\sum \bar{X}_1 \bar{X}'_1 \frac{l}{EF}\right)_{\text{ст.п.к}}\right] X'_1. \tag{7}$$

Here the first three members - displacement of point 5 without taking into account the effect of the strut of intermediate construction/design; the binomial in the brackets, multiplied by X'_1 (effort/force in the strut), the displacement of point 5 from effect X'_1.

Effort/force in the strut, in turn, is determined from the basic system for the intermediate construction/design (Fig. 7 and 8) by the Maxwell-Moore formula [4]

$$X'_1 = \frac{-\Delta_{1p}^{\text{п.к}}}{\delta_{11}^{\text{п.к}}} = \frac{\left(\sum \bar{X}_1 \bar{X}'_1 \frac{l}{EF}\right)_{\text{ст.п.к}}}{\left[\sum (\bar{X}'_1)^2 \frac{l}{EF}\right]_{\text{ст.п.к}}}. \tag{8}$$

But

$$\left(\sum \bar{X}_1 \bar{X}'_1 \frac{l}{EF}\right)_{\text{ст.п.к}} = \left(\sum \bar{X}_1 \bar{X}_6 \frac{l}{EF}\right)_{\text{ст.п.к}} = \bar{\delta}_{16} \tag{9}$$

and

$$\left[\sum (\bar{X}'_1)^2 \frac{l}{EF}\right]_{\text{ст.п.к}} = \bar{\delta}_{66}.$$

Consequently, $\bar{X}_1=\bar{\delta}_{1s}/\bar{\delta}_{ss}$.

Substituting the value of X'_1 from (9) in (7) taking into account (8), we will obtain

$$\delta'_{11}=\left(\sum \bar{X}_1^2\frac{l}{EF}\right)_{\text{ст.п.к}}+\int \bar{M}_1^2\frac{dx}{EI}+\mu\int \bar{Q}_1^2\frac{dx}{GF_{\text{ст}}}-\frac{\bar{\delta}_{1s}^2}{\bar{\delta}_{ss}}$$

or

$$\left(\sum \bar{X}_1^2\frac{l}{EF}\right)_{\text{ст.п.к}}+\int \bar{M}_1^2\frac{dx}{EI}+\mu\int \bar{Q}_1^2\frac{dx}{GF_{\text{ст}}}=\delta'_{11}+\frac{\bar{\delta}_{1s}^2}{\bar{\delta}_{ss}}.$$

Page 48.

From equalities (4)-(6) we obtain

$$\bar{\delta}_{11}=\delta_{11}+\delta'_{11}+\frac{\bar{\delta}_{1s}^2}{\bar{\delta}_{ss}}. \tag{10}$$

It is analogous

$$\bar{\delta}_{12}=2\left(\sum \bar{X}_1\bar{X}_2\frac{l}{EF}\right)_{\text{р.ф}}+\left(\sum \bar{X}_1\bar{X}_2\frac{l}{EF}\right)_{\text{ст.п.к}}, \tag{11}$$

where

$$2\left(\sum \bar{X}_1\bar{X}_2\frac{l}{EF}\right)_{\text{р.ф}}=\delta_{12} \tag{12}$$

and

$$\delta'_{12}=\left(\sum \bar{X}_1\bar{X}_2\frac{l}{EF}\right)_{\text{ст.п.к}}-\left(\sum \bar{X}_1\bar{X}'_1\frac{l}{EF}\right)_{\text{ст.п.к}}X'_1, \tag{13}$$

where

$$X'_1=\frac{\left(\sum \bar{X}_2\bar{X}'_1\frac{l}{EF}\right)_{\text{ст.п.к}}}{\left[\sum(\bar{X}'_1)^2\frac{l}{EF}\right]_{\text{ст.п.к}}}=\frac{\bar{\delta}_{1s}}{\bar{\delta}_{ss}}, \tag{14}$$

$$\left(\sum \bar{X}_1\bar{X}'_1\frac{l}{EF}\right)_{\text{ст.п.к}}=\bar{\delta}_{1s}. \tag{15}$$

Substituting the appropriate values from (14) and (15) in (13), we will obtain

$$\delta'_{12}=\left(\sum \bar{X}_1\bar{X}_2\frac{l}{EF}\right)_{\text{ст.п.к}}-\bar{\delta}_{1s}\frac{\bar{\delta}_{2s}}{\bar{\delta}_{ss}}. \tag{16}$$

Whence

$$\left(\sum \bar{N}_1 \bar{N}_2 \frac{l}{EF}\right)_{\text{ст.п.к}} = \delta'_{12} - \frac{\bar{\delta}_{16}\bar{\delta}_{26}}{\bar{\delta}_{66}}. \qquad (17)$$

Substituting (12) and (17) in (11), we will obtain

$$\bar{\delta}_{12} = \delta_{12} + \delta'_{12} + \frac{\bar{\delta}_{16}\bar{\delta}_{26}}{\bar{\delta}_{66}}. \qquad (18)$$

It is analogous

$$\bar{\delta}_{13} = \delta_{13} + \delta'_{13} + \frac{\bar{\delta}_{16}\bar{\delta}_{36}}{\bar{\delta}_{66}}, \qquad (19)$$

$$\bar{\delta}_{14} = \delta_{14}, \quad \bar{\delta}_{15} = \delta_{15}. \qquad (20)$$

Displacement from effect $X_1=1$, i.e., $(X'_1=1)$, in direction X_1 is equal to zero,

$$\delta_{17} = 0,$$

since efforts/forces in the elements of radial farms/trusses and intermediate construction/design from effect $X_1=1$ equal to zero and from effect $X_1=1$ of effort/force in the elements/cells of the unit of sectors are equal to zero.

It is analogous

$$\bar{\Delta}_{1p} = \Delta_{1p} + \Delta'_{1p} + \frac{\bar{\delta}_{16}\bar{\Delta}_{1p}}{\bar{\delta}_{66}}, \qquad (21)$$

$$\bar{\delta}_{21} = \bar{\delta}_{12} = \delta_{12} + \delta'_{12} + \frac{\bar{\delta}_{16}\bar{\delta}_{26}}{\bar{\delta}_{66}},$$

$$\delta_{22} = 2\left(\sum \bar{N}_2^2 \frac{l}{EF}\right)_{\text{р.ф}} + \left(\sum \bar{N}_2^2 \frac{l}{EF}\right)_{\text{ст.п.к}} + \left(\int \bar{M}_2^2 \frac{dx}{EI} + \mu \int \bar{Q}_2^2 \frac{dx}{GF_{\text{ст}}}\right)_{\text{б.п}}, \qquad (22)$$

where

$$2\left(\sum \bar{X}_2^2 \frac{l}{EF}\right)_{\text{р.ф.}} = \delta_{22\,\text{в}} \tag{23}$$

$$\left(\sum \bar{X}_2^2 \frac{l}{EF}\right)_{\text{ст.п.к}} = \delta'_{22} + \frac{\bar{\delta}_{26}^2}{\bar{\delta}_{66}}, \tag{24}$$

$$\left(\int \bar{M}_2^2 \frac{dx}{EI} + \mu \int \bar{Q}_2^2 \frac{dx}{GF_{\text{ст}}}\right)_{\text{б.п}} = \delta''_{22} + \frac{\bar{\delta}_{27}^2}{\bar{\delta}_{77}}. \tag{25}$$

Page 49.

Equations (24) and (25), the being displacements due to the deformations of intermediate construction/design and beam/gully of the counterweight of the sectors of rotation, can be expressed by the following relationship/ratio:

$$\delta'_{22} = \left(\sum \bar{X}_2^2 \frac{l}{EF}\right)_{\text{ст.п.к}} - \left(\sum \bar{X}_2 \bar{X}'_1 \frac{l}{EF}\right)_{\text{ст.п.к}} X'_1,$$

where

$$X'_1 = \frac{\left(\sum \bar{X}_2 \bar{X}'_1 \frac{l}{EF}\right)_{\text{ст.п.к}}}{\left[\sum (\bar{X}'_2)^2 \frac{l}{EF}\right]_{\text{ст.п.к}}} = \frac{\left(\sum \bar{X}_2 \bar{X}_6 \frac{l}{EF}\right)_{\text{ст.п.к}}}{\left(\sum \bar{X}_6^2 \frac{l}{EF}\right)_{\text{ст.п.к}}} = \frac{\bar{\delta}_{26}}{\bar{\delta}_{66}},$$

$$\delta'_{22} = \left(\sum \bar{X}_2^2 \frac{l}{EF}\right)_{\text{ст.п.к}} - \frac{\bar{\delta}_{26}^2}{\bar{\delta}_{66}};$$

whence

$$\left(\sum \bar{X}_2^2 \frac{l}{EF}\right)_{\text{ст.п.к}} = \delta'_{22} + \frac{\bar{\delta}_{26}^2}{\bar{\delta}_{66}}.$$

It is analogous for expression (25)

$$\delta''_{22} = \left(\int \frac{\bar{M}_2^2}{EI} dx + \mu \int \frac{\bar{Q}_2^2}{GF} dx\right)_{\text{б.п}} - \left(\int \frac{\bar{M}_2 \bar{M}''_1}{EI} dx + \mu \int \frac{\bar{Q}_2 \bar{Q}''_1}{GE} dx\right)_{\text{б.п}} X''_1, \tag{26}$$

where

$$X'' = \frac{\left(\int \frac{\bar{M}_2 \bar{M}''_1}{EI} dx + \mu \int \frac{\bar{Q}_2 \bar{Q}''_1}{GF} dx\right)_{\text{б.п}}}{\left(\int (\bar{M}''_1)^2 \frac{dx}{EI} + \mu \int \frac{\bar{Q}_2 \bar{Q}''_1}{GF} dx\right)_{\text{б.п}}} = \frac{\bar{\delta}_{27}}{\bar{\delta}_{77}}. \tag{27}$$

From (26) and (27)

$$\delta_{22}^{''} = \left(\int \frac{\overline{M}_2^2}{EI}\,dx + \mu\int \frac{\overline{Q}_2^2}{GF}\,dx\right)_{6.n} - \frac{\overline{\delta}_{27}^2}{\overline{\delta}_{77}};$$

whence

$$\left(\int \frac{\overline{M}_2^2}{EI}\,dx + \mu\int \frac{\overline{Q}_2^2}{GF}\,dx\right)_{6.n} = \delta_{22}^{''} + \frac{\overline{\delta}_{27}^2}{\overline{\delta}_{77}}.$$

Substituting the appropriate values from (23)-(25) in (22), we will obtain

$$\overline{\delta}_{22} = \delta_{22} + \delta_{22}^{'} + \frac{\overline{\delta}_{26}^2}{\overline{\delta}_{66}} + \delta_{22}^{''} + \frac{\overline{\delta}_{27}^2}{\overline{\delta}_{77}}. \tag{28}$$

Page 50.

It is analogous

$$\overline{\delta}_{23} = \delta_{23} + \delta_{23}^{''} + \frac{\overline{\delta}_{26}\overline{\delta}_{36}}{\overline{\delta}_{66}} + \delta_{23}^{'} + \frac{\overline{\delta}_{27}\overline{\delta}_{37}}{\overline{\delta}_{77}}, \tag{29}$$

$$\overline{\Delta}_{2p} = \Delta_{2p} + \Delta_{2p}^{'} + \frac{\overline{\delta}_{26}}{\overline{\delta}_{66}}\overline{\Delta}_{6p} + \Delta_{2p}^{'} + \frac{\overline{\delta}_{27}}{\overline{\delta}_{77}}\overline{\Delta}_{7p}, \tag{30}$$

$$\left.\begin{aligned} \overline{\delta}_{31} &= \overline{\delta}_{13}, \quad \overline{\delta}_{32} = \overline{\delta}_{23}, \\ \overline{\delta}_{33} &= \delta_{33} + \delta_{33}^{'} + \frac{\overline{\delta}_{36}^2}{\overline{\delta}_{66}} + \frac{\overline{\delta}_{37}^2}{\overline{\delta}_{77}} + \delta_{33}^{''}, \end{aligned}\right\} \tag{31}$$

$$\overline{\Delta}_{3p} = \Delta_{3p} + \Delta_{3p}^{'} + \frac{\overline{\delta}_{36}}{\overline{\delta}_{66}}\overline{\Delta}_{6p} + \Delta_{3p}^{''} + \frac{\overline{\delta}_{37}}{\overline{\delta}_{77}}\Delta_{7p}. \tag{32}$$

Let us note that

$$\overline{\delta}_{46} = \overline{\delta}_{47} = \overline{\delta}_{56} = \overline{\delta}_{57} = 0,$$

since from effect $X_6=1$ and $X_7=1$ effort/force in the elements of intermediate construction/design and in the beam/gully of

counterweight they are equal to zero, also, from effect $\bar{X}_4=1$ and $\bar{X}_7=1$ efforts/forces in the elements/cells of radial forms are equal to zero.

Further, $\bar{\delta}_{4,7}=\bar{\delta}_{7,4}=0$, since efforts/forces in equivalent components of system from effect $X_4=1$ and $X_7=1$ are equal to zero.

Thus, system of equations (3) takes the form

$$\begin{aligned}
&\bar{\delta}_{11}X_1+\bar{\delta}_{12}X_2+\bar{\delta}_{13}X_3+\bar{\delta}_{14}X_4+\bar{\delta}_{15}X_5+\bar{\delta}_{16}X_6+0+\bar{\Delta}_{1p}=0,\\
&\bar{\delta}_{21}X_1+\bar{\delta}_{22}X_2+\bar{\delta}_{23}X_3+\bar{\delta}_{24}X_4+\bar{\delta}_{25}X_5+\bar{\delta}_{26}X_6+\bar{\delta}_{27}X_7+\bar{\Delta}_{2p}=0,\\
&\bar{\delta}_{31}X_1+\bar{\delta}_{32}X_2+\bar{\delta}_{33}X_3+\bar{\delta}_{34}X_4+\bar{\delta}_{35}X_5+\bar{\delta}_{36}X_6+\bar{\delta}_{37}X_7+\bar{\Delta}_{3p}=0,\\
&\bar{\delta}_{41}X_1+\bar{\delta}_{42}X_2+\bar{\delta}_{43}X_3+\bar{\delta}_{44}X_4+\bar{\delta}_{45}X_5+0+0+\bar{\Delta}_{4p}=0,\\
&\bar{\delta}_{51}X_1+\bar{\delta}_{52}X_2+\bar{\delta}_{53}X_3+\bar{\delta}_{54}X_4+\bar{\delta}_{55}X_5+0+0+\bar{\Delta}_{5p}=0;\\
&\bar{\delta}_{61}X_1+\bar{\delta}_{62}X_2+\bar{\delta}_{63}X_3+0+0+\bar{\delta}_{66}X_6+0+\bar{\Delta}_{6p}=0,\\
&0+\bar{\delta}_{72}X_2+\bar{\delta}_{73}X_3+0+0+0+\bar{\delta}_{77}X_7+\bar{\Delta}_{7p}=0.
\end{aligned}\tag{33}$$

From (33) it is evident that the obtained system of seven equations with seven unknowns can be converted into the system of five equations with five unknowns.

Using system (33), is expressed X_4 and X_7 through X_1, X_2 and X_3:

$$X_6=\frac{\bar{\delta}_{61}X_1+\bar{\delta}_{62}X_2+\bar{\delta}_{63}X_3+\bar{\Delta}_{6p}}{\bar{\delta}_{66}},$$

$$X_7=\frac{\bar{\delta}_{72}X_2+\bar{\delta}_{73}X_3+\bar{\Delta}_{7p}}{\bar{\delta}_{77}}.$$

Page 51.

Substituting the value of X_4 and X_7 into the first three

equations of system (33) and after leading similar terms, we will obtain the system of five equations with five unknowns:

$$\begin{aligned}
&\bar{\delta}_{11}X_1 + \bar{\delta}_{12}X_2 + \bar{\delta}_{13}X_3 + \bar{\delta}_{14}X_4 + \bar{\delta}_{15}X_5 + \bar{\Delta}_{1p} = 0,\\
&\bar{\delta}_{21}X_1 + \bar{\delta}_{22}X_2 + \bar{\delta}_{23}X_3 + \bar{\delta}_{24}X_4 + \bar{\delta}_{25}X_5 + \bar{\Delta}_{2p} = 0,\\
&\bar{\delta}_{31}X_1 + \bar{\delta}_{32}X_2 + \bar{\delta}_{33}X_3 + \bar{\delta}_{34}X_4 + \bar{\delta}_{35}X_5 + \bar{\Delta}_{3p} = 0,\\
&\bar{\delta}_{41}X_1 + \bar{\delta}_{42}X_2 + \bar{\delta}_{43}X_3 + \bar{\delta}_{44}X_4 + \bar{\delta}_{45}X_5 + \bar{\Delta}_{4p} = 0,\\
&\bar{\delta}_{51}X_1 + \bar{\delta}_{52}X_2 + \bar{\delta}_{53}X_3 + \bar{\delta}_{54}X_4 + \bar{\delta}_{55}X_5 + \bar{\Delta}_{5p} = 0,
\end{aligned} \tag{34}$$

where

$$\begin{aligned}
&\bar{\bar{\delta}}_{11} = \bar{\delta}_{11} - \frac{\bar{\delta}_{16}^2}{\bar{\delta}_{66}}, \quad \bar{\bar{\delta}}_{12} = \bar{\delta}_{12} - \frac{\bar{\delta}_{16}\bar{\delta}_{26}}{\bar{\delta}_{66}},\\
&\bar{\bar{\delta}}_{13} = \bar{\delta}_{13} - \frac{\bar{\delta}_{16}\bar{\delta}_{36}}{\bar{\delta}_{66}}, \quad \bar{\bar{\Delta}}_{1p} = \bar{\Delta}_{1p} - \frac{\bar{\delta}_{16}}{\bar{\delta}_{66}}\bar{\Delta}_{6p},\\
&\bar{\bar{\delta}}_{22} = \bar{\delta}_{22} - \frac{\bar{\delta}_{26}^2}{\bar{\delta}_{66}} - \frac{\bar{\delta}_{27}^2}{\bar{\delta}_{77}},\\
&\bar{\bar{\delta}}_{23} = \bar{\delta}_{23} - \frac{\bar{\delta}_{26}\bar{\delta}_{36}}{\bar{\delta}_{66}} - \frac{\bar{\delta}_{27}\bar{\delta}_{37}}{\bar{\delta}_{77}},\\
&\bar{\bar{\Delta}}_{2p} = \bar{\Delta}_{2p} - \frac{\bar{\delta}_{26}}{\bar{\delta}_{66}}\bar{\Delta}_{6p} - \frac{\bar{\delta}_{27}}{\bar{\delta}_{77}}\bar{\Delta}_{7p},\\
&\bar{\bar{\delta}}_{33} = \bar{\delta}_{33} - \frac{\bar{\delta}_{36}^2}{\bar{\delta}_{66}} - \frac{\bar{\delta}_{37}^2}{\bar{\delta}_{77}},\\
&\bar{\bar{\Delta}}_{3p} = \bar{\Delta}_{3p} - \frac{\bar{\delta}_{36}}{\bar{\delta}_{66}}\bar{\Delta}_{6p} - \frac{\bar{\delta}_{37}}{\bar{\delta}_{77}}\bar{\Delta}_{7p}.
\end{aligned} \tag{35}$$

Substituting in (35) values $\bar{\delta}_{11}$, $\bar{\delta}_{12}$ ... $\bar{\delta}_{1k}$, $\bar{\Delta}_{1k}$ from (10), (18), (19), (21), (28)-(32), we will obtain

$$\bar{\delta}_{11} = \delta_{11} + \delta'_{11} + \frac{\bar{\delta}_{16}^2}{\bar{\delta}_{66}} - \frac{\bar{\delta}_{16}^2}{\bar{\delta}_{66}} = \delta_{11} + \delta'_{11},$$

$$\bar{\delta}_{12} = \delta_{12} + \delta'_{12} + \frac{\bar{\delta}_{16}\bar{\delta}_{26}}{\bar{\delta}_{66}} - \frac{\bar{\delta}_{16}\bar{\delta}_{26}}{\bar{\delta}_{66}} = \delta_{12} + \delta'_{12},$$

$$\bar{\delta}_{13} = \delta_{13} + \delta'_{13} + \frac{\bar{\delta}_{16}\bar{\delta}_{36}}{\bar{\delta}_{66}} - \frac{\bar{\delta}_{16}\bar{\delta}_{36}}{\bar{\delta}_{66}} = \delta_{13} + \delta'_{13},$$

$$\bar{\Delta}_{1p} = \Delta_{1p} \Delta'_{1p} + \frac{\bar{\delta}_{16}\bar{\Delta}_{6p}}{\bar{\delta}_{66}} - \frac{\bar{\delta}_{16}\bar{\Delta}_{6p}}{\bar{\delta}_{66}} = \Delta_{1p} + \Delta'_{1p}, \qquad (36)$$

$$\bar{\delta}_{22} = \delta_{22} + \delta'_{22} + \frac{\bar{\delta}_{26}^2}{\bar{\delta}_{66}} + \delta''_{22} + \frac{\bar{\delta}_{27}^2}{\bar{\delta}_{77}} - \frac{\bar{\delta}_{26}^2}{\bar{\delta}_{66}} - \frac{\bar{\delta}_{27}^2}{\bar{\delta}_{77}} = \delta_{22} + \delta'_{22} + \delta''_{22},$$

$$\bar{\delta}_{23} = \delta_{23} + \delta'_{23} + \frac{\bar{\delta}_{26}\bar{\delta}_{36}}{\bar{\delta}_{66}} + \delta''_{23} + \frac{\bar{\delta}_{27}\bar{\delta}_{37}}{\bar{\delta}_{77}} - \frac{\bar{\delta}_{26}\bar{\delta}_{36}}{\bar{\delta}_{66}} - \frac{\bar{\delta}_{27}\bar{\delta}_{37}}{\bar{\delta}_{77}} = \delta_{23} + \delta'_{23} + \delta''_{23},$$

$$\bar{\delta}_{33} = \delta_{33} + \delta'_{33} + \frac{\bar{\delta}_{36}^2}{\bar{\delta}_{66}} + \frac{\bar{\delta}_{37}^2}{\bar{\delta}_{77}} + \delta''_{33} - \frac{\bar{\delta}_{36}^2}{\bar{\delta}_{66}} - \frac{\bar{\delta}_{37}^2}{\bar{\delta}_{77}} = \delta_{33} + \delta'_{33} + \delta''_{33},$$

$$\bar{\Delta}_{2p} = \Delta_{2p} + \Delta'_{2p} + \frac{\bar{\delta}_{26}}{\bar{\delta}_{66}}\bar{\Delta}_{6p} + \Delta''_{2p} + \frac{\bar{\delta}_{27}}{\bar{\delta}_{77}}\bar{\Delta}_{7p} - \frac{\bar{\delta}_{26}\bar{\Delta}_{6p}}{\bar{\delta}_{66}} - \frac{\bar{\delta}_{27}}{\bar{\delta}_{77}}\bar{\Delta}_{7p} = \Delta_{2p} + \Delta'_{2p} + \Delta''_{2p},$$

$$\bar{\Delta}_{3p} = \Delta_{3p} + \Delta'_{3p} + \frac{\bar{\delta}_{36}}{\bar{\delta}_{66}}\bar{\Delta}_{6p} + \Delta''_{3p} + \frac{\bar{\delta}_{37}}{\bar{\delta}_{77}}\bar{\Delta}_{7p} - \frac{\bar{\delta}_{36}}{\bar{\delta}_{66}}\bar{\Delta}_{6p} - \frac{\bar{\delta}_{37}}{\bar{\delta}_{77}}\bar{\Delta}_{7p} = \Delta_{3p} + \Delta'_{3p} + \Delta''_{3p}.$$

Page 52.

The obtained coefficients and absolute terms coincide in accordance with coefficients and absolute terms of system of equations (1).

Consequently, our system: mirror, intermediate supporting structure and unit of the sectors of rotation, that contains seven

excess unknowns, it is possible to solve in by the aid of system of equations with five unknowns and two equations, which contain on one unknown.

After the determination of excess unknowns further static computation is produced in the usual way.

1). Are located calculated (total) efforts/forces in all elements of system through the formulas

$$\begin{aligned} N_{\text{расч}} &= N_{\Sigma} = \sum_{i=1}^{i=6} \overline{X}_i X_i + N_p, \\ M_{\text{расч}} &= M_{\Sigma} = \Sigma \overline{M}_i X_i + M_p, \\ Q_{\text{расч}} &= Q_{\Sigma} = \Sigma \overline{Q}_i X_i + Q_p, \end{aligned} \tag{37}$$

where the first terms - total efforts/forces in the rod elements of the systems, which bend moments/torques and transverse forces in the girder elements of system from effect X_1, X_2, ..., X_6; second terms N_p, M_p and Q_p - effort/force in rod elements, bending moments and transverse forces respectively in the girder elements/cells from the effect of load (the dead weight of system).

2). Is produced the static and kinematic checking of the calculated efforts/forces, where the criterion of the correctness of the solution of problem are equality to zero sums of the internal and external forces, which function on any unit of system, and equality

to zero displacements in any section/cut of the load-bearing structural element (continuity condition of construction/design).

3). Are determined the vertical components of the displacements of eight basic and nine auxiliary mirror supports. If the vertical components of basic and auxiliary supports are identical, then are determined displacements in the span and cantilever sections of mirror. If the vertical components of the displacements of supports are dissimilar, then by intensification or weakening of the sections/cuts of the half struts of the beam/gully of counterweight and rods of nine-rod pyramid we attain the identity of the displacements indicated. As are shown the calculations of the diagram in question, it suffices to produce 6-8 conversions with respect to the variable sections/cuts in order to obtain satisfactory result.

Displacements are determined by the usual method:

$$\delta_i = \frac{1}{E} \Sigma \overline{N}_i N_\Sigma \frac{l}{F} + \frac{1}{E} \int \overline{M}_i M_\Sigma \frac{dx}{I} + \frac{\mu}{G} \int \overline{Q}_i Q_\Sigma \frac{dx}{F_{cr}}, \qquad (38)$$

where the first term - displacement due to the deformations of the rod elements of system, and two latter - displacement due to the bending strains and shift of the girder elements of system; $\overline{N}_i$, $\overline{M}_i$ and $\overline{Q}_i$ - effort/force in the rod elements/cells and the respectively bending moments and transverse forces in the girder elements of system from the unit load, applied at point and in the direction of

tne unknown displacement; N_Σ, M_Σ and Q_Σ - calculated efforts/forces, which bend moments/torques and transverse forces in equivalent components.

Page 53.

For the basic and auxiliary supports of mirror, besides central support, are even horizontal components of displacements. To them correspond some further vertical (or normal to the profile/airfoil mirrors) displacements which distort the reflecting surface of mirror.

Let us consider the possible extents of these further movements. From Fig. 10 it is evident that to further horizontal displacement Δx corresponds the transverse displacement, i.e., the distortion of the profile/airfoil of mirror Δy, equal to

$$\Delta y = \Delta x \operatorname{tg} \varphi,$$

where tg φ=y'. For the parabola of the mirror

$$y = \frac{x^2}{4F}, \quad y' = \frac{x}{2F},$$

where F - focal length. Usually F=(0.33-0.53) $D_{зерк}$, where $D_{зерк}$ - diameter of mirror.

By accepting F=0.43 $D_{зерк}$ and determining displacements at the points of auxiliary and basic supports, we will obtain

a) a radius of the location of auxiliary supports approximately/exemplarily $0{,}2D_{\text{зерк}}$:

$$y'_{\text{всп. оп}} = \frac{0{,}2D_{\text{зерк}}}{4 \cdot 0{,}4D_{\text{зерк}}} = 0{,}12,$$

$$\Delta y_{\text{всп. оп}} = 0{,}12\Delta x,$$

i.e., the distortion of the profile/airfoil of mirror due to the horizontal displacements of auxiliary supports is only about 12o/o of the horizontal displacement;

b) a radius of the location of basic supports approximately/exemplarily $0{,}4D_{\text{зерк}}$:

$$y'_{\text{осн. оп}} \approx 0{,}24,$$

$$\Delta y_{\text{осн. оп}} = 0{,}24\Delta x.$$

i.e., the distortion of the profile/airfoil of mirror due to the horizontal displacements of basic supports composes approximately/exemplarily 24o/o of the horizontal displacement.

The extents of most horizontal movements of supports also prove to be insignificant to the form of the fact that the hardness of mirror in the radial directions, i.e., in the planes, parallel to the plane of its aperture, several times higher than hardness in the transverse direction.

As are shown calculations [5], the horizontal displacements of auxiliary reference points are approximately 10o/o of the vertical displacements, and the horizontal displacements of basic reference points - about 25o/o of the corresponding vertical displacements.

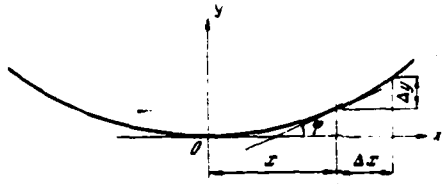

Fig. 10. Diagram of the profile/airfoil of the reflecting surface of mirror.

Page 54.

Thus, the horizontal displacements of supports do not affect substantially the distortion of the profile/airfoil of mirror, and in the first approximation, it is possible not to consider them.

REFERENCES

1. И. В. Вавилова, Г. Н. Галимов, П. Д. Калачев, А. М. Карачун, А. Д. Кузьмин, Б. Н. Лосовский, А. Е. Саломонович. Вопросы радиоэлектроники, серия общетехн., № 1, 14 (1964).
2. П. Д. Калачев. Труды ФИАН, 28, 51 (1965).
3. Ю. Л. Шахбазян. Изв. ГАО, 23, вып. 3, № 172, 180 (1964).
4. И. М. Рабинович. Курс строительной механики стержневых систем, ч. 2. Госстройиздат, 1940.
5. П. Д. Калачев, В. П. Назаров, В. Я. Чашников, А. А. Парщиков. Труды ФИАН, 47, 61 (1969).

Page 55.

EVALUATION OF THE RIGIDITY OF THE CANTILEVER SUSPENSION OF A PARABOLIC REFLECTOR.

P. D. Kalachev.

Method of the suspension of parabolic full-turn mirror (parabolic antenna) on a supporting-rotary device/equipment - one of the most important factors, which are determining its mechanical rigidity. Is most promising, in our opinion, multiple-support suspension with the radiate location of supports in the radiate (cyclic) structure diagram of the framework/body of mirror itself. In the frequent case the radiate diagram of suspension - this is suspension for the central bushing of the framework/body of mirror.

True, the suspension of mirror for central bushing, being radiate, is not multiple-support. This diagram is called cantilever. The simplest in structural/design sense, cantilever suspension has the essential shortcoming: the basic load-bearing elements of the framework/body of mirror - radial elements/cells - they work as socle

girders and, therefore, they are subjected to large strains.

Fig. 1 depicts the diagram of cantilever suspension, similar to the schematic of the suspension of the mirror of the Australian radiotelescope, arranged/located near Sydney [1]. Strictly speaking, this diagram can be named radiate (cyclic) in such a case, when the diameter of central bushing "is equal to zero".

Virtually this indicates the following: so that the bushing it would be possible to consider absolutely rigid, it must have low not only relative, but also absolute sizes/dimensions.

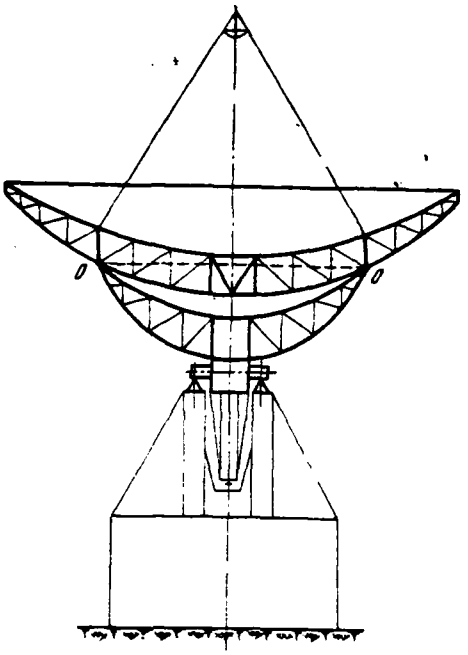

Fig. 1. Diagram of suspension of mirror for central bushing (cantilever suspension).

Page 56.

In Fig. 1 it is evident that the central bushing of mirror has two supporting pins/journals, and therefore saggings/deflections (vertical displacements/movements) at different points of its contour/outline (in the plan/layout) are dissimilar: the further from the supporting pins/journals, the greater these saggings/deflections. Saggings/deflections are maximum at two points, arranged/located on

the diameter, perpendicular to the line of supporting pins/journals. However, the rigidity of central bushing can be increased substantially, applying to it the also multiple-support fastening, in particular four-legged, since it structurally/constructionally easily is accomplished/realized by means of two sectors. Two sectors of rotation with two supporting pins/journals provide four supports of identical rigidity on central bushing, which raises its its own rigidity almost by an order.

For the evaluation of the acceptable absolute size/dimension of central bushing with the assigned magnitude of its inherent strain let us examine the dependence of amounts of deflection of bushing from its sizes/dimensions.

Fig. 2a depicts the diagram of the central bushing, carried out in the form of right dioctahedron, connected with internal radial elements/cells - edges/fins. Fig. 2b gives the diagram of the sectors of rotation with the horizontal axis and the supporting pins/journals. The diametric edges/fins, equally arranged/located relative to supports, are designated one and the same by numerals; near of 1-1, distant 2-2. In Fig. 2b it is evident that four supporting units in the sectors of rotation possess identical rigidity relative to supporting pins/journals. This is the easiest method of the transformation of two supports on the supporting

pins/journals into four identical supports on the central bushing. But in this case we do not obtain the complete radial symmetry of the supporting/reference attachment (suspension) of bushing. For the complete radial symmetry the necessary minimum number of supports is equal to eight, through every two adjacent edges/fins.

With eight-support radiate attachment of central bushing a question about its own rigidity drops off, since it does not affect the distortion of the form of mirror[1].

FOOTNOTE [1]. Certainly, central bushing must possess sufficient rigidity as usual metal structure. ENDFOOTNOTE.

But, since the eight-support attachment of bushing requires the complication of construction/design, in this work we will be restricted to the examination of the rigidity of the central bushing on four supports.

Let us examine the maximum saggings/deflections of the bushing, subjected to the effect of dead weight, in the vertical position of its centerline (see Fig. 2a). Saggings/deflections will be maximum at points C, arranged/located symmetrically between supports[2].

FOOTNOTE [2]. The sagging/deflection of the central point of bushing on

the centerline us does not interest although it can be *even* more than at point C. ENDFOOTNOTE.

As a result of the symmetry of construction/design and load central bushing is twice statically indeterminable.

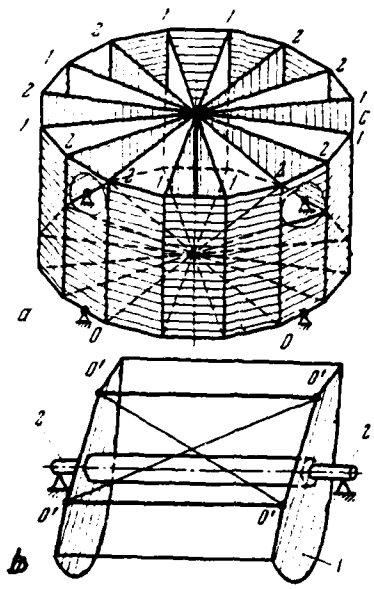

Fig. 2. Structure diagram of central bushing of parabolic reflector (a) and schematic of unit of sectors of rotation with supporting pins/journals (b).

1 - sectors of rotation; 2 - supporting pins/journals; 1-1, 2-2 - diametric elements/cells - edge/fin; 0 - supporting units of the central bushing: 0' - reciprocal supporting points of attachment of central bushing in the sectors of rotation.

Page 57.

It suffices to find efforts/forces and strains in the elements/cells

of bushing, entering $^1/_4$ its part, since in its all other appropriate elements/cells efforts/forces and strain are repeated.

Fig. 3a depicts basic system for $^1/_4$ part of the central bushing. Supporting/reference rods (connections/communications) K replace the effect of the rejected/thrown part of the bushing. The low part of the wall O-O-Sh-Sh is distant, and introduced two hinge joints Sh. The excess unknown X_1 is the transverse force of interaction of two mutually intersecting diametric edges/fins 1-1 and 2-2; the excess unknown X_2 - the bending moment of interaction of the rejected/thrown part of the bushing. Let us note that as a result of symmetry the rotation of the sections/cuts of the ring of the bushing above the supports, and also at points C (in the middles between the adjacent supports) is equal to zero. The bending moment in ring X_2 remains constant as a result of symmetry [2]; the bending moments from other loads on the ring are distributed on it as in the rectilinear flat/plane beam/gully. Therefore for the ring of basis there will be the system, depicted in Fig. 3b. Here q [kgf/cm] - the evenly distributed dead load of ring; P [kg] - concentrated load from the weight of edge/fin; X_1 and X_2 - effect on the ring of excess unknowns. Fig. 3c, d shows basic systems for diametral elements/cells of bushing (edges/fins). Here g [kgf/cm] - the evenly distributed load from the natural weight of edge/fin; m_1 and m_2 - bending moments in radial elements/cells 1 and 2 respectively, that appear from the

bending moments/torques in the ring, caused by load q and P; m_{X_1} - bending moment in radial element/cell 2 from effect X_1 on the circular beam/gully; m_{X_2} - bending moments in the radial elements/cells from effect X_2.

The bending moments m_1, m_2, m_{X_1} and m_{X_2} appear in the radial elements/cells as a result of the fact that the circular beam/gully is located not in one plane, but it has breaks in the points of intersection with the radial elements/cells[1].

FOOTNOTE [1]. The bending moments, which affect in the ring, in the point of rupture of circular beam/gully (intersection with the radial element/cell) are decomposed/expanded on two components, which affect in planes of radial elements/cells and new direction of circular element/cell. ENDFOOTNOTE.

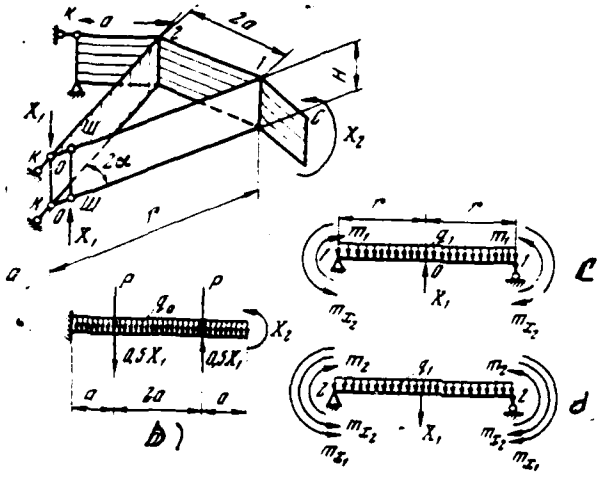

Fig. 3. Basic system for part of central bushing.

Page 58.

The bending moments indicated are determined by the following relationships/ratios:

$$\begin{aligned} m_1 &= 2m_{k_1}\sin\alpha, \\ m_2 &= 2m_{k_2}\sin\alpha; \end{aligned} \qquad (1)$$

$$\begin{aligned} m_{x_1} &= 2aX_1\sin\alpha, \\ m_{x_2} &= 2X_2\sin\alpha, \end{aligned} \qquad (2)$$

where $m_{k_1} = 0.5g_0a^2$ - bending moment from the load in the ring in section/cut 1; $m_{k_2} = 4.5\,g_0a^2 - 2aP$ - bending moment from the load in the ring in section/cut 2; aX_1 - bending moment in the ring from X_1 in section/cut 2.

Substituting the value m_{k_1} and m_{k_2} with $X_1=1$ and $X_2=1$ in (1) and (2), we get

$$\begin{aligned} m_1 &= g_0 a^2 \sin\alpha, \\ m_2 &= (9g_0 a^2 + 4aP)\sin\alpha, \\ m_{x_1} &= 2a\sin\alpha, \\ m_{x_2} &= 2\sin\alpha. \end{aligned} \qquad (3)$$

For simplicity of considerations the circular and radial elements/cells of central bushing we accept as the simple flat/plane beams/gullies of rectangular cross section (Fig. 4). The moment of the inertia of the cross section of this beam/gully relative to axis/axle Z-Z is expressed by the relationship/ratio

$$I = \frac{tH^3}{12}. \qquad (4)$$

The structurally/constructionally cross section of beams/gullies is made by more advantageous from the point of view of an increase in the flexural rigidity, since cross-sectional area evenly is not distributed on the height/altitude of section/cut, but the considerable part of it is concentrated at the upper and bottom edges of beam/gully (forming its belts/zones), which considerably increases the moment of inertia I. Therefore, accepting the cross section of beam/gully on Fig. 4, we understate I.

It is expressed values a, H, t, g_0 and P through the value of a radius of bushing r under the condition so that the value of breaking

stress in the beam/gully, considered as plate, with an increase in the sizes/dimensions of panels a and H would remain approximately/exemplarily constant.

Breaking stress for the compressed plate is expressed by formula [3]

$$\sigma_{кр} = k\frac{\pi^2 D}{H^2 t}. \qquad (5)$$

Here $D = \frac{Et^3}{12(1-\mu^2)}$ - flexural rigidity of plate; E [kgf/cm²] - Young's modulus; $\mu \sim 0.3$ - Poisson ratio (for steel). Substituting the value of D in (5), we will obtain

$$\sigma_{кр} = \frac{k\pi^2 E}{12(1-\mu^2)}\frac{t^3}{H^3} = k_1\frac{t^3}{H^3}. \qquad (6)$$

For $\sigma_{кр} = \text{const}$ must be retained the condition

$$t/H = \text{const}.$$

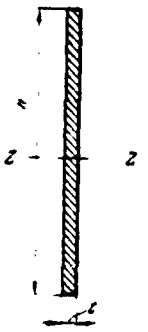

Fig. 4. Diagram of cross section of element/cell of bushing.

Page 59.

Since from the requirements of high rigidity the elements/cells of bushing work with the low stresses/voltages, then let us accept value $\sigma_{кр} \approx 1200$ kgf/cm² (in this case each face of ring and edge/fin is divided/marked off on four panels by local edges/fins so that in each panel is retained the relation of sides, equal to a/H). In this case the thickness of beam/gully can be expressed by relationship/ratio t=0.004 r. We further accept H=1.5 r. For the dioctahedral bushing α=11°15', sin $\alpha \sim$0.195 and $a = r \sin \alpha \approx 0{,}195r$. Cross-sectional area of the element/cell of ring F_0=Ht=0.006 r². Moment of the inertia of the cross section of the element/cell of the ring

$$I_0 = \frac{tH^3}{12} = \frac{0{,}004r(1{,}5r)^3}{12} = 112{,}50 \cdot 10^{-5} r^4.$$

The weight per unit length

$$g_0 = F_0\gamma = 0{,}006\, r^2\gamma.$$

For steel specific gravity/weight $\gamma=0.00785$ kgf/cm^3 and

$$g_0 = 4{,}72\ 10^{-6}\ r^2.$$

For concentrated load (weight of edge/fin)[1]

$$P = 0{,}5\ rg_0 = 2{,}36 \cdot 10^{-6}\ r^3.$$

FOOTNOTE [1]. For the radial elements/cells - edges/fins we accept section/cut two times less than for the circular beam/gully. ENDFOOTNOTE.

Now bending moments (3) will be written as follows:

$$\begin{aligned} m_1 &= 0{,}35 \cdot 10^{-6}\ r^4, \\ m_2 &= 6{,}740 \cdot 10^{-6}\ r^4, \\ m_{x_1} &= 0{,}076\ r, \\ m_{x_2} &= 0{,}39. \end{aligned} \tag{7}$$

Excess unknowns we determine by the solution of system of equations

$$\begin{aligned} \delta_{11}X_1 + \delta_{12}X_2 + \Delta_{1p} &= 0, \\ \delta_{21}X_1 + \delta_{22}X_2 + \Delta_{2p} &= 0, \end{aligned} \tag{8}$$

where the coefficients with the unknowns and absolute terms are determined by the Maxwell-Moore formulas [4]

$$\delta_{11} = \frac{1}{E}\int \frac{M_1^2}{I}\,dx + \frac{1}{G}\mu\int \frac{Q_1^2}{F}\,dx,$$
$$\delta_{22} = \frac{1}{E}\int \frac{M_2^2}{I}\,dx + \frac{1}{G}\mu\int \frac{Q_2^2}{F}\,dx,$$
$$\delta_{12} = \frac{1}{E}\int \frac{M_1 M_2}{I}\,dx + \frac{1}{G}\mu\int \frac{Q_1 Q_2}{F}\,dx, \qquad (9)$$
$$\Delta_{1p} = \frac{1}{E}\int \frac{M_1 M_p}{I}\,dx + \frac{1}{G}\mu\int \frac{Q_1 Q_p}{F}\,dx,$$
$$\Delta_{2p} = \frac{1}{E}\int \frac{M_2 M_p}{I}\,dx + \frac{1}{G}\mu\int \frac{Q_2 Q_p}{F}\,dx,$$

where M_1, M_2, Q_1 and Q_2 - bending moments and transverse forces in the elements/cells of bushing from the effect of the unit values of unknowns; M_p and Q_p - bending moment and transverse force in the elements/cells of bushing from the effect of load; E and G - moduli of elasticity of the first and second kind; F - sectional area element/cell (beams/gullies); μ - coefficient of section/cut.

Page 60.

After integration (9), carried out by the method of Vereshchagin (by multiplication of diagrams/curves) [4], we will obtain the following values of coefficients and free terms:

$$E\delta_{11} = 887{,}5\ r^{-1},$$
$$E\delta_{22} = 1235\ r^{-3},$$
$$E\delta_{12} = 120{,}5\ r^{-2}, \qquad (10)$$
$$E\Delta_{1p} = 0{,}00923\ r^{2},$$
$$E\Delta_{2p} = -0{,}035\ r.$$

Solving system of equations (8) taking into account (10), we

will obtain

$$X_1 = -14{,}46 \cdot 10^{-6}\ r^3,$$
$$X_2 = +30{,}20 \cdot 10^{-6}\ r^4. \qquad (11)$$

Maximum sagging/deflection at point C (see Fig. 3a), found from formula [4]

$$\delta_C = \frac{1}{EI}\int M_C M_\Sigma dx + \frac{\mu}{GF}\int Q_C Q_\Sigma dx, \qquad (12)$$

where M_C and Q_C - bending moment and transverse force in the elements/cells of bushing from the unit power, applied at point C; M_Σ and Q_Σ - calculated the bending moment and transverse force (from the total effect of load and X_1 and X_2), it is expressed by the following relationship/ratio:

$$\delta_C = 50 \cdot 10^{-10}\ r^3. \qquad (13)$$

From (13) it is evident that the maximum sagging/deflection of bushing in the middle between the adjacent supports is proportional to the square of its radius. In this case the weight of bushing grows/rises proportional to the cube of its radius and is determined by the relationship/ratio

$$G_{\text{ц.вт}} = 67{,}4 \cdot 10^{-5}\ r^3. \qquad (14)$$

In formulas (13) and (14) r is given in cm, while δ_C and $G_{\text{ц.вт}}$ - respectively in cm and kgf.

Thus despite the fact that the moment of the inertia of the elements/cells of bushing grows/rises proportional to the fourth degree of its radius

$$I_0 = 112{,}50 \cdot 10^{-6} r^4, \qquad (15)$$

the saggings/deflections of bushing rapidly increase with an increase in its sizes/dimensions (13). Fig. 5 gives the graph/diagram of dependence δ_c and $G_{\text{ц.вт}}$ on r bushing. In the figure it is evident that the maximum sagging/deflection on the rim of central bushing only from the effect of its dead weight with r=300 cm (D=600 cm) is equal to 0.0045 mm.

Let us assume that the diameter of bushing composes 10o/o of the diameter of the mirror, and the dead weight of mirror (tentative) is determined by relationship/ratio [5]

$$G_{\text{зерк}} = 28D^{2,5}. \qquad (16)$$

Then concentrated load on the circular element/cell of the bushing (see Fig. 3) is equal to

$$P_1 = P + \frac{1}{16} G_{\text{зерк}} = P + \frac{28}{16} D^{2,5}, \qquad (17)$$

and maximum sagging/deflection on its rim

$$\delta_C \approx \left(\frac{16P_1}{G_{\text{ц. вт}}} \delta_C\right). \qquad (18)$$

With r=300 cm P=0.5 g, r=637 kg, $G_{п.ст}$=18140kg (Fig. 5),

$D_{зерк} = 10 \cdot 2r = 6000\,\text{cm} = 60$ m, $G_{зерк} = 28 \cdot D^{2,5} = 28 \cdot 60^{2,5} = 780000$ kgf.

← Supplying these values in (17) and (18), we will obtain

$$(\delta_C)_1 = \frac{16}{18\,140}\,\delta\left(637 + \frac{1}{16} \cdot 780\,000\right) \approx 43{,}4\,\delta_1.$$

With δ_1=0.0045 mm $(\delta_C)_1 \approx 0{,}2$ mm.

If the central bushing of mirror was double-seat, then maximum sagging/deflection on its rim (in the middle between the supports) was approximately/exemplarily eight times more, i.e., $\delta'_1 \sim 8 \cdot 0.2 = 1.6$ mm.

On the basis of that presented we come to the conclusion that for large parabolic reflectors, intended for the work on waves 1-2 cm, the distortion of the form of mirror in the central (most important) part due to the nonuniform strains of central only reaches noticeable value, if bushing has the large absolute sizes/dimensions (more than 5 m) and it is fastened to two supports.

In view of the fact that the size/dimension of central bushing substantially affects the rigidity of the suspension of mirror, the

use/application of its four-legged fastening is very desirable, since it makes it possible to increase the size/dimension of bushing with the simultaneous increase of its rigidity in comparison with the rigidity of double-seat bushing.

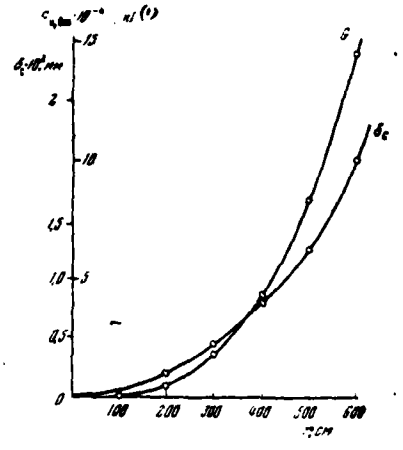

Fig. 5. Graph/diagrams of dependence of maximum sagging/deflection on rim of bushing δ_c and weight of bushing $G_{\text{п.вт}}$ on radius r.

Key: (1). kgf.

REFERENCES

1. E. G. Bowen, H. C. Minnett. Proc. IRE Australia, 24, N 2 (1963).
2. П. Д. Калачев. Труды ФИАН, 28, 183 (1965).
3. Энциклопедический справочник машиностроения, т. 1, кн. 2. М., 1947.
4. И. М. Рабинович. Курс строительной механики стержневых систем, ч. 2. Госстройиздат, 1940.
5. Б. А. Гарф. Использование солнечной энергии, вып. 1. Изд-во АН СССР, 1957, стр. 62.

CALCULATED ELASTIC DEFORMATIONS OF A 7.5-METER MODEL OF PARABOLIC REFLECTOR.

P. D. Kalachev, V. P. Nazarov, V. Ya. Chashnikov, A. A. Parshchikov.

Introduction.

Recently noticeably was increased specialists' interest in the radiotelescopes with a fully revolving parabolic optical-type antennas [1].

FOOTNOTE [1]. This is borne out by conferences in London and Munich in 1966. ENDFOOTNOTE.

This is explained by the fact that the antennas indicated have the known advantages on which in this article we consider it possible not to stop. One of the most important problems which it is necessary to solve during the creation of large/coarse parabolic full-turn mirrors

with the large permission/resolution, is the guarantee of high mechanical rigidity of mirror in any attitude of it. The basic difficulty of this guarantee exactly consists in the fact that the mirror changes its attitude [1, 2].

The calculation of parabolic reflectors of radiotelescopes is produced in essence in two load cases: static computation of mirror to the rigidity in the case of acting the operating loads and static computation of mirror on the strength in the case of acting the hurricane wind. The dynamic calculation of mirror to the action of inertial forces usually is not produced, since speeds and accelerations during the rotations of mirror are insignificant.

Operating loads on the mirror are dead loads of construction/design and loads due to wind. For the mirrors of high rigidity and, therefore, with the large dead weight weight loads comprise order 100-200 kg to 1 m^2 of the area of the aperture of mirror. Loads due to wind at operational wind velocity, taken to 8-12 m/s, comprise order 8-16 kgf/m^2. During the calculation for loads due to wind with the hurricane wind the speed of the latter takes as the equal to 40-50 m/s.

The task of the first calculated case consists of the determination of elastic deformations of mirror and this selection of

the sections/cuts of the load-bearing structural elements its (in the prescribed/assigned structure diagram), which would ensure the minimum values of elastic deformations. Selected from this condition sections/cuts of load-bearing elements, as a rule, provide the strength of mirror for the second case of calculation, i.e., under the effect of loads from the hurricane wind.

Page 63.

Simplest analysis of parabolic reflector as structure, and also experiment of planning telescopes with full-turn parabolic reflectors show that by a simple increase in the sections/cuts of the load-bearing elements of the framework/body of mirror it is impossible to achieve the considerable increase of its rigidity, although within known limits increase of the sections/cuts of the basic carriers (radial elements/cells) gives noticeable gain [3]. Radical resolution of this problem is the decrease of the "calculated" lengths of load-bearing elements, i.e., the decrease of the cantilever and span sections of mirror. This can be achieved/reached by an increase in the number of supports of mirror.

In the present work is given static computation of the model of full-turn parabolic reflector with a diameter of 7.5 m on the multiple-support suspension. The results of this calculation show

that the rigidity of mirror on a 17-supporting/reference suspension almost by an order higher than rigidity of mirror on common double-seat suspension [1]. The general view of a 7.5-meter model fully revolving parabolic antenna is shown in Fig. 1.

In the first case (static computation of mirror to the rigidity) the calculation is produced on two diagrams, which correspond to two basic concepts of the loading of the mirror: the symmetric loading of mirror and skew-symmetric loading. Will be here examined the balanced network of the loading of mirror for the first calculated case.

Since interests mirror with the high mechanical rigidity, basic design loads will be dead loads of construction/design. Consequently, symmetric loading corresponds to the horizontal position of the plane of the aperture of mirror. Fig. 2 depicts the structure diagram of mirror and its suspension in the separated form in isometry. The internal struts m-m and I-n of intermediate construction/design with the symmetric loading do not work and therefore they are depicted as thin lines. In the structure diagram of mirror (Fig. 2a) the half struts in the lower panels which do not work on the symmetric loadings, are not shown. In order not to darken drawing, elements/cells k-k and c-t, which raise the rigidity of the unit of sectors to the bend and torsion, they are depicted as conditionally thin lines.

AD-A118 963 FOREIGN TECHNOLOGY DIV WRIGHT-PATTERSON AFB OH F/G 3/2
RADIO-ASTRONOMICAL INSTRUMENTS OBSERVATIONS (SELECTED ARTICLES)--ETC(U)
AUG 82 L I MATVEYENKO, G S MISEZHNIKOV
UNCLASSIFIED FTD-ID(RS)T-0564-82 NL

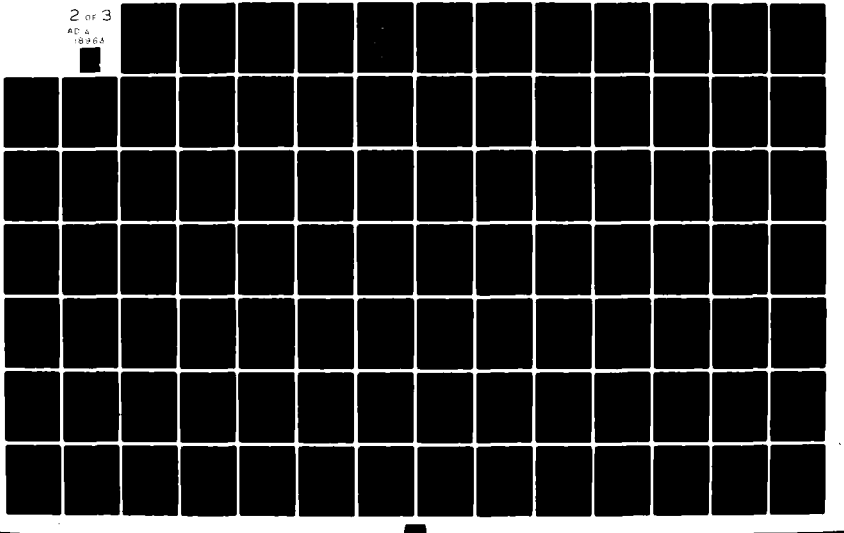

As a result of the symmetry of construction/design and load of effort/force in all same-type load-bearing elements, i.e., the elements/cells, arranged/located radially symmetrical relative to the center of mirror, they will be respectively identical. Taking into account the conditions of symmetry, for the basic system for the mirror we accept its 1/4 part, limited by two adjacent mutually intersecting diametric load-bearing elements/cells (farms/trusses) and entering this part of the mirror chord elements and half struts which match up the supporting units. For the basic system for the intermediate construction/design we accept also its 1/4 part, which switches on main beam (for example, 8-5), end semitrusses 5-m and 8-m. Into basic system for the unit of the sectors of rotation enter: struts N-T (spoke), the beam/gully of the counterweight I-I and horizontal axis 27-27. The systems indicated are depicted in Fig. 3 as conditionally combined.

Conditionality here lies in the fact that in actuality the single load-bearing flat/plane element, arranged/located along the diagonal of intermediate construction/design, there does not exist, but in view of the symmetry all load-bearing elements, as it was already said both the mirrors and intermediate construction/design they work respectively equally. Therefore it is possible to consider

that two reference points 1 and 5 are formed by one main beam of intermediate construction/design (for example, 8-5 together with its reinforcing elements/cells: by braces 6-5 and 7-8 and by end semitrusses 5-m and 8-m), although in actuality, as it is represented in Fig. 3, into the diagram enter semitrusses 1-4 and 5-8, 1-m and 5-m.

Page 64.

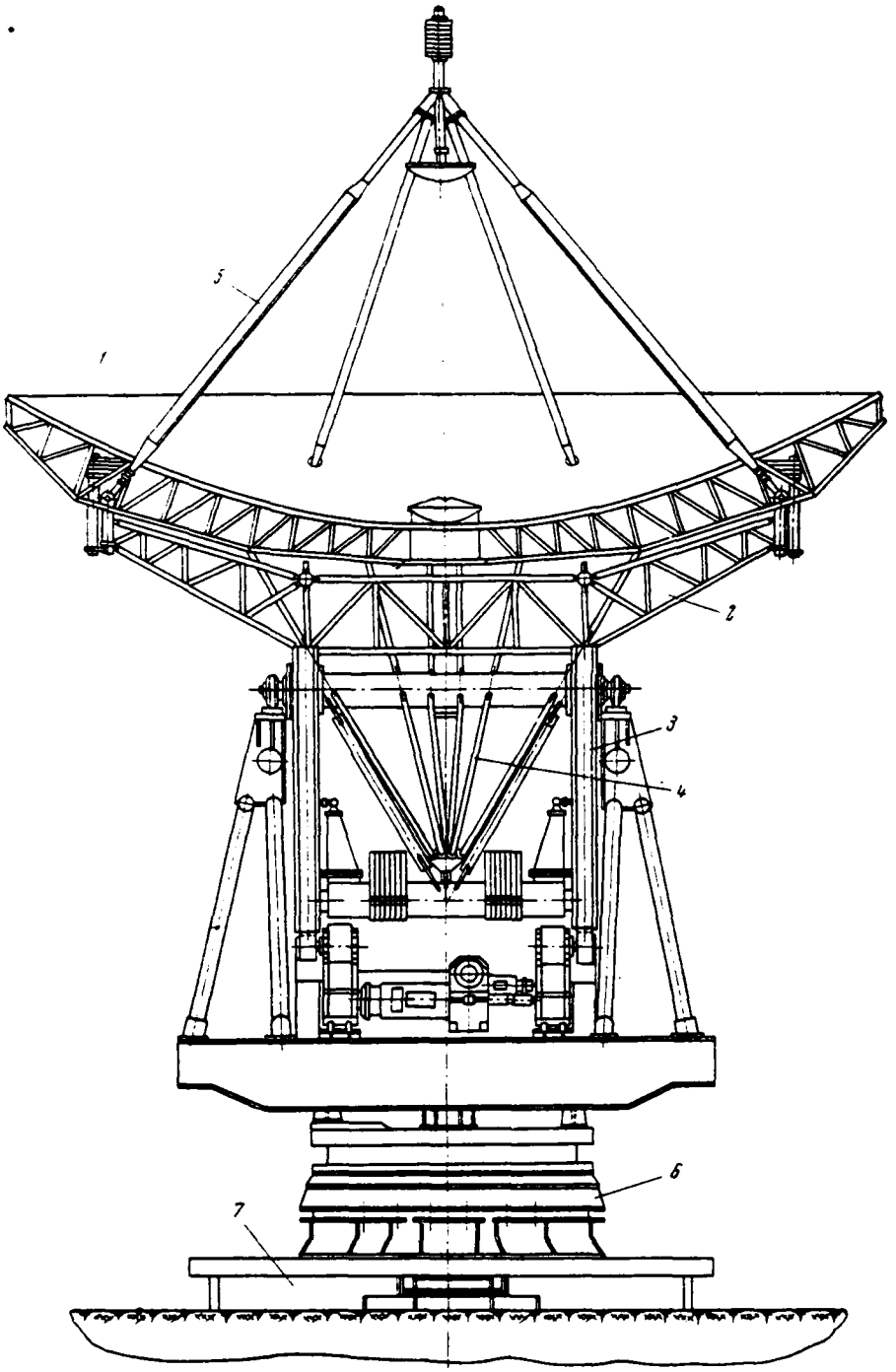

Fig. 1.

Fig. 1. General view of model of radiotelescope with 7.5-meter parabolic reflector on multiple-support suspension. 1 - parabolic reflector; 2 - intermediate eight-support construction/design; 3 - unit of the sectors of rotation; 4 - nine-rod pyramid; 5 - eight-rod pyramid, which carries irradiator; 6 - supporting-rotary device; 7 - foundation.

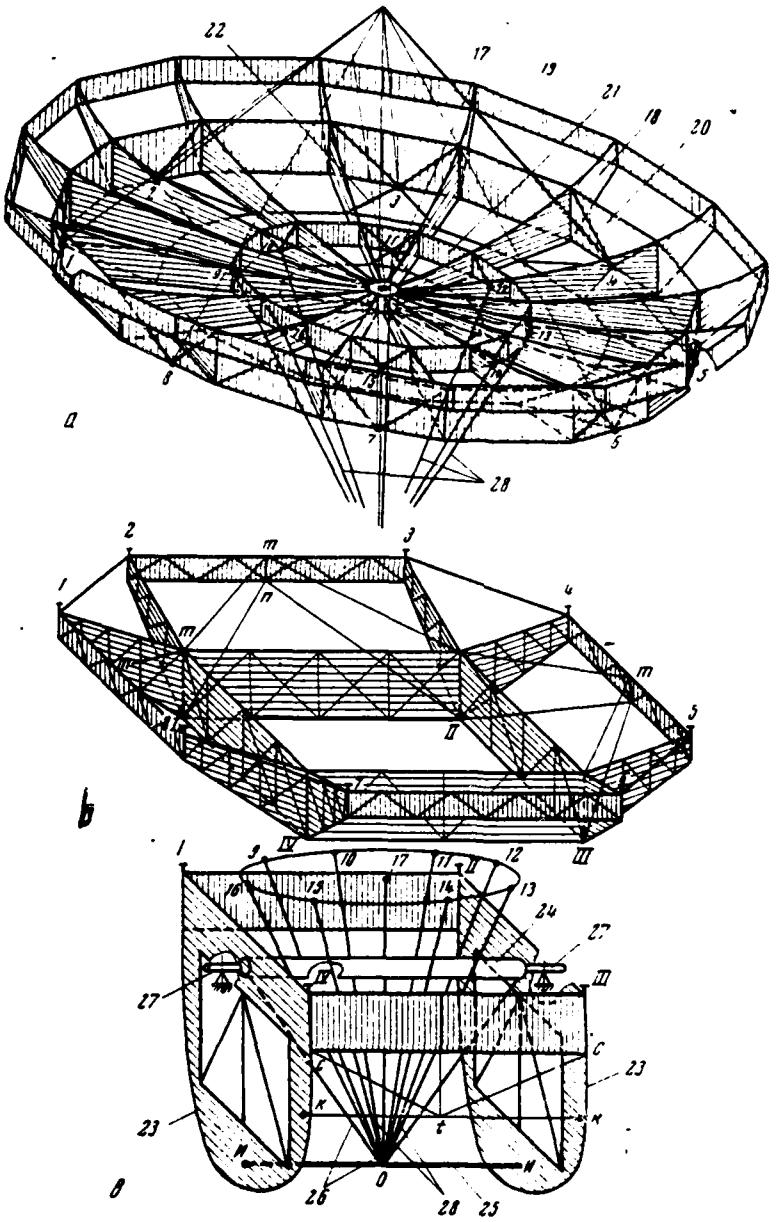

Fig. 2. Power (separated) diagram of mirror and its suspension in

separated form. a) mirror; b) intermediate eight-support construction/design; c) the unit of the sectors of rotation. I, II, III, IV - reference points of intermediate construction/design in the sectors of rotation; 1, 2, ..., 8 - basic reference points of mirror, formed by intermediate construction/design; 9, 10, ..., 17 - auxiliary reference points of mirror, formed by nine-rod pyramid with the central rod; 18 - radial load-bearing elements; 19, 20, 21 - chord (circular) load-bearing elements; 22 - half struts in the lower panels of framework/body; 23 - sectors of rotation; 24 - horizontal axis; 25 - beam/gully of counterweight; 26 - half struts; 27 - supporting pins/journals; 28 - nine-rod pyramid.

Page 66.

As the excess unknowns they are accepted: X_1 - force of thrust between the framework/body of mirror and the intermediate construction/design; X_2 and X_3 - efforts/forces, which affect in the rods of nine-rod pyramid; X_4 and X_5 - efforts/forces, which affect in the external chord (circular) element/cell respectively in the upper and lower belts/zones; X_6 - effort/force in the braces of the intermediate construction/design (see Fig. 3); X_7 - effort/force in the half struts of the unit of sectors (Fig. 4).

Let us note that the system: mirror, intermediate

construction/design, the unit of the sectors of rotation - seemingly naturally it is dismembered to three independent units. Thus, efforts/forces in the elements/cells of the unit of the sectors of rotation from effect $X_7=1$ (Fig. 4) are determined independent of mirror and intermediate construction/design, and efforts/forces in the elements of intermediate construction/design from effect $X_6=1$ are determined independent of mirror and unit of the sectors (see Fig. 2, 3).

The system of canonical equations, which links the excess unknowns X_1, ..., X_7, takes the form

$$\begin{aligned}
&\delta_{11}X_1+\delta_{12}X_2+\delta_{13}X_3+\ldots+\delta_{17}X_7+\Delta_{1p}=0,\\
&\delta_{21}X_1+\delta_{22}X_2+\delta_{23}X_3+\ldots+\delta_{27}X_7+\Delta_{2p}=0,\\
&\delta_{31}X_1+\delta_{32}X_2+\delta_{33}X_3+\ldots+\delta_{37}X_7+\Delta_{3p}=0,\\
&\ldots\ldots\ldots\ldots\ldots\ldots\ldots\ldots\ldots\\
&\ldots\ldots\ldots\ldots\ldots\ldots\ldots\ldots\ldots\\
&\delta_{71}X_1+\delta_{72}X_2+\delta_{73}X_3+\ldots+\delta_{77}X_7+\Delta_{7p}=0.
\end{aligned} \qquad (1)$$

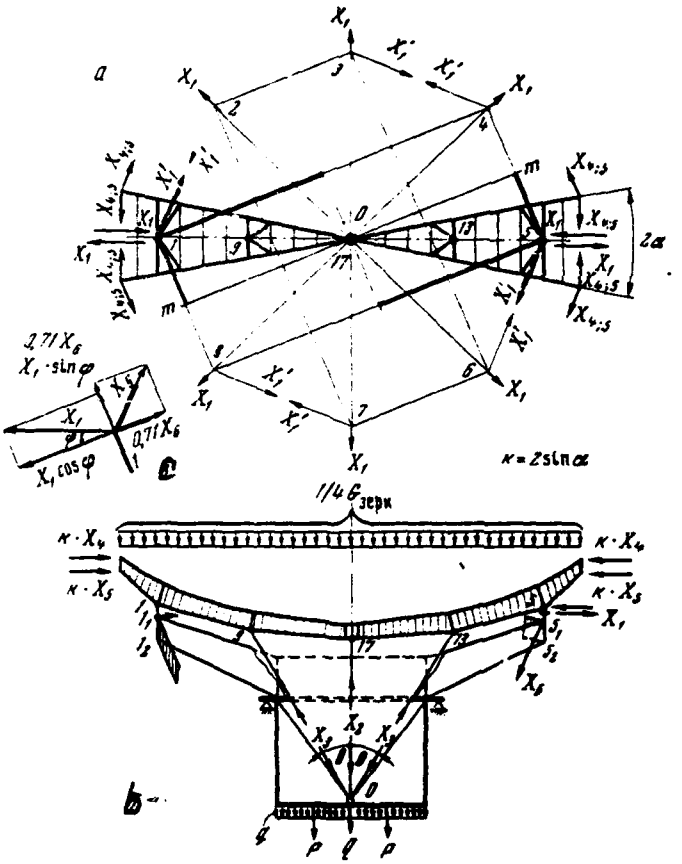

Fig. 3. Basic system of chosen part of mirror, intermediate supporting structure and unit of sectors. a) plan view; b) side view; c) the carrying out of unit 1.

Coefficients and absolute terms of equations (1) are determined by the known Maxwell-Moore formulas:

$$\delta_{ii} = \Sigma \overline{X}_i^2 \frac{l}{EF} + \int \overline{M}_i^2 \frac{dx}{EI} + \mu \int \overline{Q}_i^2 \frac{dx}{GE_{ст}},$$
$$\delta_{ik} = \Sigma \overline{X}_i \overline{X}_k \frac{l}{EF} + \int \overline{M}_i \overline{M}_k \frac{dx}{EI} + \mu \int \overline{Q}_i \overline{Q}_k \frac{dx}{GF_{ст}}, \qquad (2)$$
$$\Delta_{ip} = \Sigma \overline{X}_i N_p \frac{l}{EF} + \int \overline{M}_i M_p \frac{dx}{EI} + \mu \int \overline{Q}_i Q_p \frac{dx}{GF_{ст}},$$

where the first terms - displacement/movement due to the strains of rod elements/cells, the second and the third - displacement/movement due to the bending strains and shift/shear in the girder elements/cells respectively.

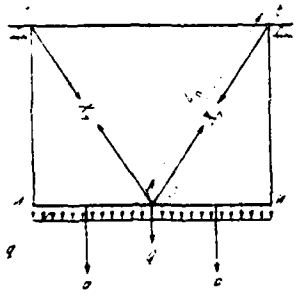

Fig. 4.

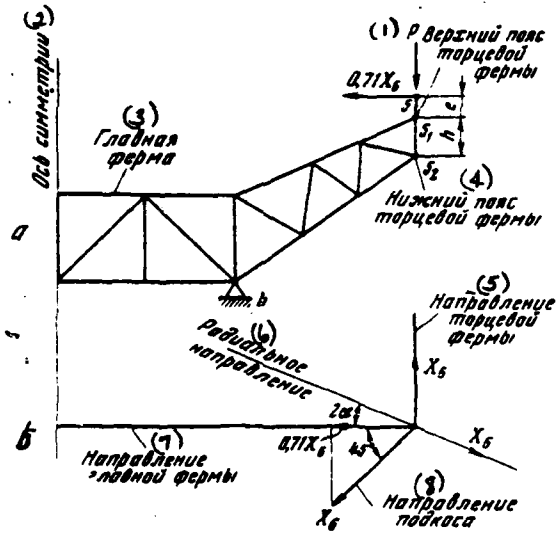

Fig. 5.

Fig. 4. Basic system for unit of sectors ($l_п$ — length of half strut).

Fig. 5. Main semitruss of intermediate supporting structure. a) side view; b) plan view; $P = \frac{1}{4}(G_{\text{ферм}} + G_{\text{облуч}})$

Key: (1). Upper belt/zone end farm/truss. (2). Axis of symmetry. (3). Main beam. (4). Lower belt/zone of end farm/truss. (5). Direction of end truss. (6). Radial direction. (7). Direction of main farm/truss. (8). Direction of brace.

Page 68.

In our case, coefficients and free terms of operations (1) are determined by the following relationships:

$$\delta_{11} = \left(\sum \bar{X}_1^2 \frac{l}{EF}\right)_{\text{пояс}} + \left(\sum \bar{X}_1^2 \frac{l}{EF}\right)_{\text{п.к}} + \int \bar{M}_1^2 \frac{dx}{ET_{\text{б.оп}}} + \mu \int \bar{Q}_1^2 \frac{dx}{GF_{\text{б.оп}}},$$

$$\delta_{12} = \left(\sum \bar{X}_1 \bar{X}_2 \frac{l}{EF}\right)_{\frac{1}{4}\text{ зерк}} - \left(\sum \bar{X}_1 \bar{X}_2 \frac{l}{EF}\right)_{\frac{1}{4}\text{ п.к}},$$

$$\delta_{13} = \left(\sum \bar{X}_1 \bar{X}_3 \frac{l}{EF}\right)_{\frac{1}{8}\text{ зерк}} + \left(\sum \bar{X}_1 \bar{X}_3 \frac{l}{EF}\right)_{\frac{1}{8}\text{ п.к}},$$

$$\delta_{14} = \left(\sum \bar{X}_1 \bar{X}_4 \frac{l}{EF}\right)_{\frac{1}{4}\text{ зерк}},$$

$$\delta_{15} = \left(\sum \bar{X}_1 \bar{X}_5 \frac{l}{EF}\right)_{\frac{1}{8}\text{ зерк}},$$

$$\delta_{16} = \left(\sum \bar{X}_1 \bar{X}_6 \frac{l}{EF}\right)_{\frac{1}{8}\text{ п.к}},$$

$$\delta_{17} = 0, \qquad \delta_{21} = \delta_{12}, \tag{3}$$

$$\delta_{22} = \left(\sum \bar{X}_2^2 \frac{l}{EF}\right)_{\frac{1}{4}\text{ зерк}} + \left(\sum \bar{X}_2^2 \frac{l}{EF}\right)_{\frac{1}{4}\text{ п.к}} + \left(\sum \bar{X}_2^2 \frac{l_{\text{ск}}}{EF'_{\text{ск}}}\right)_{\frac{1}{2}\text{ у.сек}} + \bar{X}_2^2 \frac{l'_{\text{ст.п}}}{EF_{\text{ст.п}}} + \int \bar{M}_2^2 \frac{dx}{EI'_{\text{б.п.в}}} + \mu \int \bar{Q}_2^2 \frac{dx}{GF'_{\text{б.п.в}}},$$

$$\delta_{23} = \left(\sum \bar{X}_2 \bar{X}_3 \frac{l}{EF}\right)_{\frac{1}{8}\text{ зерк}} + \left(\sum \bar{X}_2 \bar{X}_3 \frac{l}{EF}\right)_{\frac{1}{8}\text{ п.к}} + \left(\sum \bar{X}_2 \bar{X}_3 \frac{l_{\text{ск}}}{EF'_{\text{ск}}}\right)_{\frac{1}{2}\text{ у.сек}} + \int \bar{M}_2 \bar{M}_3 \frac{dx}{EI'_{\text{б.п.в}}} + \mu \int \bar{Q}_2 \bar{Q}_3 \frac{dx}{GF'_{\text{б.п.в}}},$$

$$\delta_{24} = \left(\sum \bar{X}_2 \bar{X}_4 \frac{l}{EF}\right)_{\frac{1}{8}\text{ зерк}},$$

$$\delta_{25} = \left(\sum \bar{X}_2 \bar{X}_5 \frac{l}{EF}\right)_{\frac{1}{8}\text{ зерк}},$$

$$\delta_{26} = \left(\sum \bar{X}_2 \bar{X}_6 \frac{l}{EF}\right)_{\frac{1}{8}\text{ п.к}},$$

$$\delta_{27} = \left(\sum \bar{X}_2 \bar{X}_7 \frac{l_{\text{ск}}}{EF'_{\text{ск}}}\right)_{\frac{1}{2}\text{ у.сек}} + \bar{M}_2 \bar{M}_7 \frac{dx}{EI'_{\text{б.п.в}}} + \mu \int \bar{Q}_2 \bar{Q}_7 \frac{dx}{GF'_{\text{б.п.в}}},$$

$$\delta_{31} = \delta_{13}, \quad \delta_{32} = \delta_{23},$$

$$\delta_{33} = \left(\sum \bar{X}_3^2 \frac{l}{EF}\right)_{\frac{1}{8}\text{ зерк}} + \left(\sum \bar{X}_3^2 \frac{l}{EF}\right)_{\frac{1}{8}\text{ п.к}} + \left(\sum \bar{X}_3^2 \frac{l_{\text{ск}}}{EF'_{\text{ск}}}\right)_{\frac{1}{8}\text{ у.сек}} + \int \bar{M}_3^2 \frac{dx}{EI'_{\text{б.п.в}}} + \mu \int \bar{Q}_3^2 \frac{dx}{GF'_{\text{б.п.в}}} + \bar{X}_3^2 \frac{l_{\text{ст.п}}}{EF_{\text{ст.п}}},$$

$$\delta_{34} = \left(\sum \bar{X}_3 \bar{X}_4 \frac{l}{EF}\right)_{\frac{1}{8}\text{ зерк}},$$

$$\delta_{35} = \left(\sum \bar{X}_3 \bar{X}_5 \frac{l}{EF}\right)_{\frac{1}{8}\text{ зерк}},$$

$$\delta_{36} = \left(\sum \bar{X}_3 \bar{X}_6 \frac{l}{EF}\right)_{\frac{1}{8}\text{ п.к}},$$

$$\delta_{37} = \left(\sum \bar{X}_3 \bar{X}_7 \frac{l_{\text{ск}}}{EF'_{\text{ск}}}\right)_{\frac{1}{2}\text{ у.сек}} + \int \bar{M}_3 \bar{M}_7 \frac{dx}{EI'_{\text{б.п.в}}} + \mu \int \bar{Q}_3 \bar{Q}_7 \frac{dx}{GF'_{\text{б.п.в}}},$$

$$\delta_{41} = \delta_{14}, \quad \delta_{42} = \delta_{24}, \quad \delta_{43} = \delta_{34},$$

Page 69.

$$\delta_{44} = \left(\sum \bar{X}_4^2 \frac{l}{EF}\right)_{\frac{1}{8}\text{ зерк}} + \bar{X}_4^2 \frac{l_{\text{н. к}}}{F_{\text{н. к}}},$$

$$\delta_{45} = \left(\sum \bar{X}_4 \bar{X}_5 \frac{l}{EF}\right)_{\frac{1}{8}\text{ зерк}},$$

$$\delta_{46} = 0, \quad \delta_{47} = 0,$$

$$\delta_{51} = \delta_{15}, \quad \delta_{52} = \delta_{25}, \quad \delta_{53} = \delta_{35}, \quad \delta_{54} = \delta_{45},$$

$$\delta_{55} = \left(\sum \bar{X}_5^2 \frac{l}{EF}\right)_{\frac{1}{8}\text{ зерк}} + \bar{X}_5^2 \frac{l_{\text{н. к}}}{F_{\text{н. к}}},$$

$$\delta_{56} = 0, \quad \delta_{57} = 0,$$

$$\delta_{61} = \delta_{16}, \quad \delta_{62} = \delta_{26}, \quad \delta_{63} = \delta_{36}, \quad \delta_{64} = \delta_{46}, \quad \delta_{65} = \delta_{56},$$

$$\delta_{66} = \left(\sum \bar{X}_6^2 \frac{l}{EF}\right)_{\frac{1}{8}\text{ п. к}} + \bar{X}_6^2 \frac{l_p}{EF_p},$$

$$\delta_{71} = \delta_{17}, \quad \delta_{72} = \delta_{27}, \quad \delta_{73} = \delta_{37}, \quad \delta_{74} = \delta_{47},$$

$$\delta_{75} = \delta_{57}, \quad \delta_{76} = \delta_{67},$$

$$\delta_{77} = \left(\sum \bar{X}_1^2 \frac{l_{\text{ск}}}{EF_{\text{ск}}}\right)_{\frac{1}{2}\text{ у. сек}} + \bar{X}_7^2 \frac{l_{\text{п. р}}}{EF_{\text{п. р}}} + \int \bar{M}_7^2 \frac{dx}{EI_{\text{б. п в}}} + \mu \int \bar{Q}_7^2 \frac{dx}{GF_{\text{б. в. п}}},$$

$$\Delta_{1p} = \left(\sum \bar{X}_1 N_p \frac{l}{EF}\right)_{\frac{1}{8}\text{ зерк}} \left(\sum \bar{X}_1 N_p \frac{l}{EF}\right)_{\frac{1}{3}\text{ п. к}} + \int \bar{M}_1 M_p \frac{dx}{EI_{\text{б. оп}}} + \mu \int \bar{Q}_1 Q_p \frac{dx}{GF_{\text{ст. оп}}},$$

$$\Delta_{2p} = \left(\sum \bar{X}_2 N_p \frac{l}{EF}\right)_{\frac{1}{8}\text{ зерк}} + \left(\sum \bar{X}_2 N_p \frac{l}{EI}\right)_{\frac{1}{8}\text{ п. к}} + \left(\sum \bar{X}_2 N_p \frac{l_{\text{ск}}}{EF_{\text{ск}}}\right)_{\frac{1}{2}\text{ у сек}} + \int \bar{M}_2 M_p \frac{dx}{EI_{\text{б. п. в}}} + \mu \int \bar{Q}_2 Q_p \frac{dx}{GF_{\text{б. п. в}}},$$

$$\Delta_{3p} = \left(\sum \bar{X}_3 N_p \frac{l}{EF}\right)_{\frac{1}{8}\text{ зерк}} + \left(\sum \bar{X}_3 N_p \frac{l}{EF}\right)_{\frac{1}{8}\text{ п. к}} + \left(\sum \bar{X}_3 N_p \frac{l_{\text{ск}}}{EF_{\text{ск}}}\right)_{\frac{1}{2}\text{ у сек}} + \int \bar{M}_3 M_p \frac{dx}{EI_{\text{б. п. в}}} + \mu \int \bar{Q}_3 Q_p \frac{dx}{GF_{\text{б. п в}}},$$

$$\Delta_{4p} = \left(\sum \bar{X}_4 N_p \frac{l}{EF}\right)_{\frac{1}{8}\text{ зерк}}, \qquad \Delta_{5p} = \left(\sum \bar{X}_5 N_p \frac{l}{EF}\right)_{\frac{1}{8}\text{ зерк}},$$

$$\Delta_{6p} = \left(\sum \bar{X}_6 N_p \frac{l}{EF}\right)_{\frac{1}{8}\text{ п. к}};$$

$$\Delta_{7p} = \left(\sum \bar{X}_7 N_p \frac{l_{\text{ск}}}{EF_{\text{ск}}}\right)_{\frac{1}{2}\text{ у сек}} + \int \bar{M}_7 M_p \frac{dx}{EI_{\text{б. п. в}}} + \mu \int \bar{Q}_7 Q_p \frac{dx}{GF_{\text{б. п. в}}}.$$

Page 70.

Here $\overline{X}_1$, $\overline{X}_2$, ..., $\overline{X}_7$ - effort/force in the rod elements of system from the effect of the unit values of the unknowns X_1, X_2, ..., X_7; N_p — effort/force in the same elements/cells from the effect of load (the dead weight of construction/design); $\overline{M}_{1,2,\ldots,7}$ and $\overline{Q}_{1,2,\ldots,7}$ — the bending moments and the transverse forces, which appear in the girder elements of system from the effect of the unit values of the unknowns X_1, X_2, ..., X_7; M_p and Q_p — the bending moments and the transverse forces, which appear in the same girder elements of system from the effect of load (the dead weight of construction/design); l and F - length and the cross-sectional area of the rod elements/cells: E and G - moduli of elasticity of the material of the construction/design of the first and second kind; $I'_{б.оп}$ and $F'_{б.оп}$ — the moment of inertia and the cross-sectional area of the beam/gully of support (strut);

$$I'_{б.п.в} = \frac{1}{4} I_{б.п.в}, \quad F'_{б.п.в} = \frac{1}{4} F_{б.п.в},$$ where $I_{б.п.в}$ and $F_{б.п.в}$

-moment of inertia and the cross-sectional area of the beam/gully of the counterweight (are here considered only 1/4 structural sections with respect to 1/4 parts of the mirror and intermediate construction/design, entering the calculation). Integration is produced on half of the length of the beam/gully of counterweight with respect so that subsequently into the calculation only half from

1/4 parts of the mirror and intermediate construction/design (1/8 mirror and of 1/8 intermediate structure).

The members of form $\left(\sum X_i^2 \frac{l}{EF}\right)_{\frac{1}{8}\text{sepк}}$, $\left(\sum X_i X_k \frac{l}{EF}\right)_{\frac{1}{8}\text{sepк}}$ and $\left(\sum X_i N_p \frac{l}{EF}\right)_{\frac{1}{8}\text{sepк}}$ are displacements/movements due to the strain of the rod elements/cells entering the part of the framework/body of mirror, namely two adjacent radial farms/trusses and the adjacent them chord farms/trusses and half struts in the lower panels. Members of form $\left(\sum X_i^2 \frac{l}{EF}\right)_{\frac{1}{8}\text{п.к}}$, $\left(\sum X_i X_k \frac{l}{EF}\right)_{\frac{1}{8}\text{п.к}}$ and $\left(\sum X_i N_p \frac{l}{EF}\right)_{\frac{1}{8}\text{п.к}}$ displacement/movement due to the strain of the rod elements/cells, entering 1/8 part of the intermediate eight-support construction/design, namely - main semitruss, end semitruss and half of the length of strut (1-2 or 3-4 in Fig. 2 and 3) [1].

FOOTNOTE [1]. Half struts 1-n and m-m (Fig. 2) on the symmetric loadings do not work. ENDFOOTNOTE.

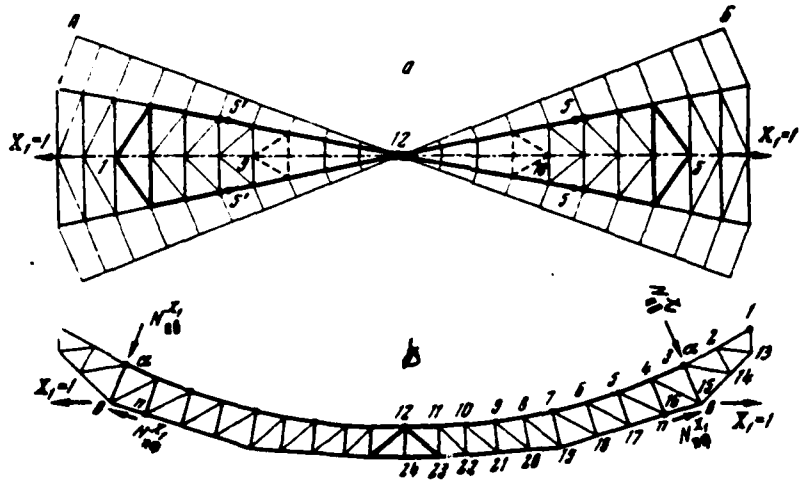

Fig. 6. Chosen part of mirror with two adjacent mutually intersecting diametric farms/trusses. a) plan view; b) side view.

Page 71.

The rod elements/cells of the unit of the sectors of rotation are the elements/cells, which lie at the vertical plane, which passes through the supporting pins/journals (duct/tube/pipe 27-27 it serves as the horizontal rotational axis, strut (spoke) T-I and the beam/gully of the counterweight I-I). The structure diagram of the unit of the sectors of rotation with the symmetric loading is depicted in Fig. 4.

Loads on the unit of the sectors of rotation, i.e., to the rod elements/cells T-T, I-I, O-O and to the beam/gully of the

counterweight I-I, they are: the dead weight of the beam/gully of counterweight - distributed load of the constant intensity q, weight of the cargos of counterweight P and weight of the part of the nine-rod pyramid, which falls to its apex/vertex Q. We repeat, that for effective length T-T, I-T and beam/gully of the counterweight I-I is accepted half of their geometric length, and for the calculated cross-sectional area - 1/4 part of the cross-sectional area of equivalent component respectively of the designed part of the mirror and intermediate construction/design.

The chosen part of the mirror (see Fig. 3 and 6) - two adjacent mutually intersecting diametric farms/trusses with the adjacent them chord elements/cells and the half struts in the lower panels - are three-dimensional frame.

Fig. 7 depicts one supporting unit of mirror, connected with the chord supporting farm/truss aa-bb and half struts 5-n with the radial trusses into three-dimensional frame.

Decomposing/expanding the vertical bearing pressure R to the components, which affect on the rods 5-a, 5-n, a-a and b-b, we convert/transfer to the flat/plane radial farms/trusses. Thus we enter with effort/force $X_1=1$.

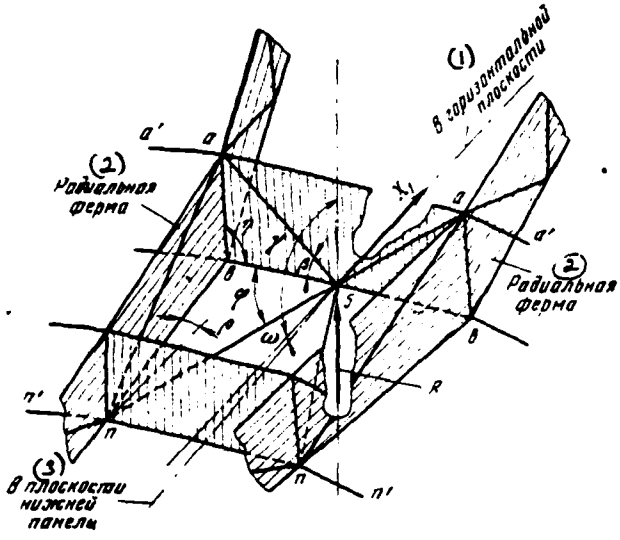

Fig. 7. Diagram of one of basic supporting units of mirror.

Key: (1). In the horizontal plane. (2). Radial farm/truss. (3). In plane of lower panel.

Page 72.

Efforts/forces in the rods 5-a, 5-n, a-a and b-b from R and X=1 are determined by the following relationships/ratios:

$$N^R_{5-a} = \frac{R}{2\sin\beta\,(\cos\gamma\,\mathrm{tg}\,\omega + \sin\gamma)},$$

$$N^R_{a-a} = \frac{R}{2}\,\frac{\mathrm{ctg}\,\eta + \mathrm{ctg}\,\beta}{\cos\gamma\,\mathrm{tg}\,\omega + \sin\gamma},$$

$$N^R_{a-b} = \frac{R}{2\sin\eta\,(\cos\gamma\,\mathrm{tg}\,\omega + \sin\gamma)},$$

$$N^{R}_{5-n} = \frac{R}{2\sin\varphi\,(\cos\omega\,\mathrm{tg}\,\gamma + \sin\omega)},$$

$$N^{R}_{n-n} = \frac{R\,(\mathrm{tg}\,\rho + \mathrm{ctg}\,\varphi)}{2\,(\cos\omega\,\mathrm{tg}\,\gamma + \sin\omega)},$$

$$N^{R}_{n\phi} = \frac{R}{2\cos\rho\,(\cos\omega\,\mathrm{tg}\,\gamma + \sin\omega)},$$

$$N^{X_1}_{5-a} = \frac{X_1}{2\sin 3\left(\frac{\sin\gamma}{\mathrm{tg}\,\omega} + \cos\gamma\right)}, \qquad (4)$$

$$N^{X_1}_{a-a} = \frac{X_1}{2\sin\eta\left(\frac{\sin\gamma}{\mathrm{tg}\,\omega} + \cos\gamma\right)},$$

$$N^{X_1}_{5-n} = \frac{X_1}{2\sin\varphi\left(\frac{\sin\omega}{\mathrm{tg}\,\gamma} + \cos\omega\right)}.$$

Analogous relationships/ratios are obtained for determining the efforts/forces in the appropriate rods of unit 13 (or 9 in Fig. 2 and 3) from efforts/forces $X_3=1$, which affect in the rods of the nine-rod pyramid O-13 taking into account angle θ. The diagram of the effect on the system of two adjacent diametric farms/trusses of efforts/forces $X_1=1$ is depicted in Fig. 6.

Formulas (4) are derived from the condition that the effect of the rods of the circular (chord) elements/cells a-a' and n-n' is considered by the duplication of the cross-sectional area of rods a-a and n-n. Numerical values of coefficients and absolute terms,

calculated according to formulas (3), were obtained equal to

$$\delta_{11} = +443{,}6\frac{1}{E},\ \delta_{12} = -409{,}9\frac{1}{E},\ \delta_{13} = -566{,}3\frac{1}{E},$$
$$\delta_{14} = +187{,}1\frac{1}{E},\ \delta_{15} = +153{,}4\frac{1}{E},\ \delta_{16} = -154{,}8\frac{1}{E},\ \delta_{17} = 0;$$
$$\delta_{22} = +1201{,}0\frac{1}{E},\ \delta_{23} = +1283{,}0\frac{1}{E},\ \delta_{24} = -594{,}8\frac{1}{E},$$
$$\delta_{25} = -473{,}8\frac{1}{E},\ \delta_{26} = +110{,}7\frac{1}{E},\ \delta_{27} = -122{,}9\frac{1}{E};$$
$$\delta_{33} = +1907{,}0\frac{1}{E},\ \delta_{34} = -696{,}8\frac{1}{E},\ \delta_{35} = -553{,}2\frac{1}{E},$$
$$\delta_{36} = +189{,}9\frac{1}{E},\ \delta_{37} = -210{,}8\frac{1}{E};$$
$$\delta_{44} = +660{,}8\frac{1}{E},\ \delta_{45} = +408{,}8\frac{1}{E},\ \delta_{46} = 0,\ \delta_{47} = 0;$$
$$\delta_{55} = +462{,}0\frac{1}{E},\ \delta_{56} = 0,\ \delta_{57} = 0;$$
$$\delta_{66} = +121{,}3\frac{1}{E},\ \delta_{67} = 0;$$
$$\delta_{77} = +452{,}3\frac{1}{E};$$
$$\Delta_{1p} = +187\,500\frac{1}{E},\ \Delta_{2p} = -266\,200\frac{1}{E},\ \Delta_{3p} = -367\,100\frac{1}{E},$$
$$\Delta_{4p} = +116\,300\frac{1}{E},\ \Delta_{5p} = -92\,360\frac{1}{E}.\quad \Delta_{6p} = -92\,200\frac{1}{E},$$
$$\Delta_{7p} = -28\,970\frac{1}{E}.$$

Page 73.

Solving system of equations (1), we obtain the following values of unknowns:

X_1=-95.24, X_2=+94.68, X_3=+9.64, X_4=+68.74, X_5=+6.71, X_6=+427.6, X_7=+126.9. The obtained numerical values of X_5=+6.71 kg and X_3=+9.64 kg show that the efforts/forces in the chord (circular) elements/cells are insignificant, what is the consequence of the low cross travels of the end points of the arms (saggings/deflections) of radial farms/trusses and justifies simplification in the design

diagram and basic system, obtained by the decrease of a number of the chord elements/cells considered (see Fig. 3, 6).

The total (calculated) values of efforts/forces in the rods of system are determined by the relationship/ratio

$$N_{\Sigma} = N_p + \Sigma \overline{X}_i X_i. \qquad (5)$$

Displacements/movements (saggings/deflections) were determined at six points of radial farm/truss (1, 3, 5, 7, 9 and 12) in the basic system (see Fig. 3 and 6), i.e., for the chosen part of the mirror, which has two supports (at points 1 and 5 or upon transfer to the flat/plane diametric farm/truss at points 3 and 16, designated also by letters a and n).

Were determined separately vertical and horizontal components of the displacements/movements indicated. In this case the vertical components of the displacement of basic reference points (1 and 5) took as equal to zero, since they appear as translational motion for the entire chosen part of the mirror as whole, without the distortion of form.

Vertical displacements were determined from the formulas

$$\delta_i^V = \left(\Sigma \overline{V}_i N_{\Sigma} \frac{l}{EF}\right)_{p.n.}, \qquad (6)$$

where $\overline{V}_i$ — effort/force in the rods of radial farm/truss from the

unit vertical force, applied at the point, at which searches for the displacement; N_i — calculated efforts/forces in the same rods. For determining the displacements at points 5, 7 and 9 chosen part of the mirror (see Fig. 6a) was charged by four unit power at points 5, 5 and 5, 5', and sum $\left(\Sigma \overline{N}_i N_i \frac{l}{EF}\right)_{1 \text{ p.}}$ was taken only for one radial farm/truss. For determining the displacement of central point (12) in it was applied the unit power and summation $\left(\Sigma \overline{N}_i N_i \frac{l}{EF}\right)_{4 \text{ (p. ф.)}}$ was produced on the entire chosen part of the mirror, i.e., on four radial farms/trusses.

The numerical values of the vertical components of displacements are equal to the following values (in mm):

$$\begin{aligned} &\delta_{12}^V = 0{,}0025, \quad \delta_5^V = 0{,}0185, \\ &\delta_9^V = 0{,}0094, \quad \delta_{5'}^V = 0{,}0028, \\ &\delta_7^V = -0{,}0001, \quad \delta_1^V = 0{,}0066. \end{aligned} \tag{7}$$

The horizontal components of displacement were determined at points 1, 3, 5 and 7 according to the formulas, analogous (6), where $\overline{N}_i$ is replaced and H_i — forces in rods from horizontal unit force.

Page 74.

Summation $\left(\Sigma H_i N_i \frac{l}{EF}\right)_{1 \text{ p.}}$ was produced on one radial farm/truss (Fig. 6b). The numerical values of the horizontal components of displacements proved to be equal (in mm):

$$\begin{aligned} \delta_{12}^{H} &= 0, & \delta_{5}^{H} &= 0{,}0105, \\ \delta_{9}^{H} &= \sim 0, & \delta_{3(4)}^{H} &= 0{,}0039, \\ \delta_{7}^{H} &= 0{,}0049, & \delta_{1}^{H} &= 0{,}0053. \end{aligned} \tag{8}$$

As can be seen from (7), the values of the vertical components of displacements at the points in question were obtained different (although in the principle it would be possible to achieve their equality), since the variation of these values was accomplished/realized due to a change in the sections/cuts of certain limited number of elements/cells, namely: the rods of pyramid O-13 and O-17 (see Fig. 3), the beam/gully of the counterweight I-I and the half struts O-t (see Fig. 4), braces 1-2, 3-4, 5-6 and so forth (see Fig. 3).

However, taking into account the horizontal components of the displacements indicated, the values of vertical components of corresponding points cannot be identical, but they must satisfy the condition for the arrangement of the displaced points on the initial parabolic curve, that forms mirror.

The extents of vertical movements must satisfy the following relationships/ratios (Fig. 8):

$$\delta_{a}^{V} = \delta_{12}^{V} - \Delta_{a}^{V}, \tag{9}$$

where

$$\Delta_a^V = \frac{\delta_a^H}{2F} X. \qquad (10)$$

In our case the paraboloid surface of mirror is determined by the equation of the generatrix of the parabola:

$$y = \frac{x^2}{4F}. \qquad (11)$$

where F=3.25 m and $y=x^2/13$.

From (9), (10) and (11) we have

$$\delta_a^V = \delta_{13}^V - \frac{\delta_a^H}{6,5} X. \qquad (12)$$

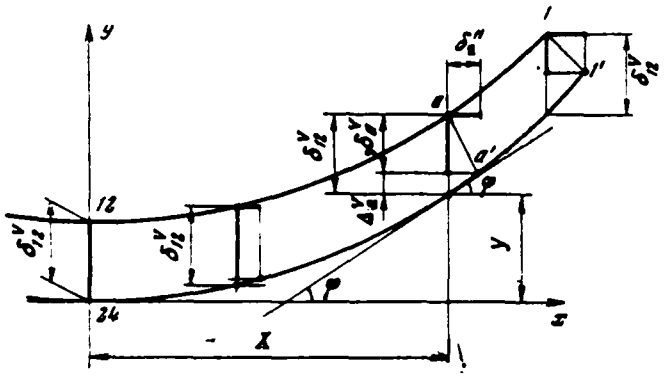

Fig. 8. Diagram of parallel shift of surface of mirror.

Page 75.

Substituting the value δ_i^H from (8) in (12) taking into account the distance of the point in question from the center of mirror X, we have the following equivalent values of vertical displacements (in mm)

$$\begin{aligned} {}_{э}\delta_1^V &= -0{,}00055, & {}_{э}\delta_7^V &= 0{,}00130, \\ {}_{э}\delta_3^V &= 0{,}00068, & {}_{э}\delta_9^V &= 0{,}00250, \\ {}_{э}\delta_5^V &= -0{,}00125, & {}_{э}\delta_{12}^V &= 0{,}00250. \end{aligned} \qquad (13)$$

The difference between the appropriate values of displacements over (7) and (13) is the distortion of the form of mirror. The maximum value of the difference indicated in our case occurs for point 5 and is $\Delta_э \approx 0{,}017$ mm.

The strains of parabolic reflectors, carried out on one structure diagram, with one and the same diagram of suspension and with the identical load factor, are proportional to the square [1] of the relation of their diameters [3].

FOOTNOTE [1]. Have in mind elastic deformations from the effect of dead weight. ENDFOOTNOTE.

Consequently, the maximum sagging/deflection, which distorts the form of mirror at point 1 (see Fig. 8), for the mirror with the diameter of 70 m will be equal to

$$(\Delta_s)_{\varnothing 70} = \Delta_s \left(\frac{70}{7{,}5}\right)^2 = 0{,}017 \cdot 9{,}32^2 = 1{,}50 \text{ мм}$$

However, taking into account, that the sagging/deflection at the same point of mirror in the vertical position is approximately/exemplarily two times more than sagging/deflection for the symmetric loading (horizontal position of mirror), it is possible to accept for the maximum value of the strain of mirror as the diameter of 70 m (on its edge) the value, equal to

$$(\Delta_1)^{\max}_{\varnothing 70} \approx 3 \text{ мм}.$$

If we accept the value of the rms value of the distortion of the form of mirror equal to

$$\frac{1}{2{,}6}(\Delta_1)^{\max}_{\varnothing 70} \approx 1{,}2 \text{ мм},$$

the 70-meter mirror on the multiple-support suspension can be used

for the work on wave 2 cm with good effectiveness [4], since the digression of the deformed surface of mirror from the calculated (as a result of elastic deformations) comprises

$$\Delta\delta = \frac{\lambda}{\frac{1}{2,6}(\Delta_1)^{\max}_{\varnothing 70}} = \frac{20}{1,2} \approx 16,5.$$

Besides strains, the precision/accuracy of the surface of mirror affect even the errors of its manufacture. Experiment of construction [5] of high-precision parabolic reflectors shows that the maximum errors of manufacture compose the value of the order

$$\Delta_{т.\,отб} = 1 \cdot 10^{-5} D_{зерк.}$$

Page 76.

For $D_{зерк} = 70$ м $\Delta_{т.отб} \approx 0,7$ mm. The mean square error of manufacture by approximately/exemplarily 0.3 mm. The mean square of the accumulated error

$$\Sigma_{\Delta_{ср.кв}} = \sqrt{1,2^2 - 0,3^2} \approx 1,25 \text{ мм}.$$

The obtained results according to the calculation of model are not optimum, since, in the first place, the overhangings length and flights/spans in the model are selected not optimally (it is necessary to somewhat decrease the overhanging length and the length of first extreme span); in the second place, factor of load K (see [3]) in the model it was obtained too great (about 4.5) and it it is possible to decrease to 3-3.5. These measures can raise the rigidity

of mirror approximately/exemplarily one and a half times.

REFERENCES

1. П. Д. Калачев, Труды ФИАН, 28, 183, (1965).
2. П. Д. Калачев, Труды ФИАН, 28, 204 (1965).
3. П. Д. Калачев, Труды ФИАН, 38, 72 (1967).
4. Г. З. Айзенберг, Антенны ультракоротких волн, Связьиздат, 1957.
5. П. Д. Калачев, А. Е. Саломонович, Труды ФИАН, 17, 13 (1963).

Page 77.

MULTIPLE-SUPPORT RADIATE SCHEMATICS OF THE SUSPENSION OF A PARABOLIC ANTENNA.

P. D. Kalachev.

One of the most important problems which it is necessary to solve during the creation of a large full-turn parabolic antenna (subsequently we will it call parabolic reflector or simply by mirror), is reaching/achievement of the high mechanical rigidity of mirror. An increase in the rigidity it is possible to attain by the use/application of a multiple-support suspension of mirror on supporting-rotary device [1, 2].

If we consider as the basic loads on parabolic reflector of dead load, then they will be in the general case the combination of symmetrical and skew-symmetric loads relative to horizontal axis. In the particular case these loads can be purely symmetrical (horizontal position of the plane of the aperture of mirror) or purely axisymmetric (the vertical position of the plane of the aperture of

mirror).

If we consider even and loads due to wind, but in this case to restrict operational wind velocity with the value of 10 m/s, then for mirrors with the high mechanical rigidity, whose dead weight of construction/design, which arrives to 1 m^2 of aperture, comprises order 100-200 kgf/m^2 (depending on the sizes/dimensions of mirror), distortion in the distribution of total loads (from the weight and the wind), introduced by loads due to wind, in the first approximation, it is possible not to consider, but to be restricted to a simple increase of weight loads on 8-12o/o.

The overwhelming majority of the constructions/designs of existing and projected/designed parabolic reflectors is carried out on radiate diagram [3, 4]. And this is completely justified both from the point of view of construction/design (same-type elements/cells)and from the point of view of simplification and, consequently, also increase in the precision/accuracy of calculation [5].

It would seem that the radiate diagram of the construction/design of mirror and symmetrical (skew-symmetric) load, naturally, require use/application and the radiate diagram of the suspension of mirror on a supporting-rotary device. However, in the

practice of the creation of full-turn parabolic reflectors are only unit (from many ten), carried out with the radiate suspension. As an example can serve the structure diagram of the mirror of the Australian radiotelescope, arranged/located near Sydney [3], and also the schematic of the mirror of radiotelescope of FIAN [6], working since 1951.

Page 78.

Usually the suspension of full-turn parabolic reflector is fulfilled according to the principle of simple beam, i.e., with the aid of two supporting pins/journals, arranged/located directly on the framework/body of mirror. This is explained by that fact that to mirror must be provided the rotations around the horizontal axis in limits of +-90° from the zenith. Meeting this requirement is striked into the known structural/design difficulties. Specifically, in view of these difficulties to the mirror of Australian radiotelescope [4] are provided rotations around the horizontal axis only in limits of 65°.

In the mentioned radiotelescopes of mirror they have the radiate suspension, called cantilever. The simplest in structural/design sense, cantilever suspension possesses that essential shortcoming, what basic load-bearing elements of the framework/body of mirror -

radial elements/cells, being cantilever, are subjected by large ones to lateral deformations, i.e., have large saggings/deflections. But the cantilever diagram of suspension has very important positive property. Being cyclic, this diagram possesses that property, that with the skew-symmetric loading the efforts/forces in the basic carriers (in the radial ones and the chord ones, and also in the struts of the panels, formed by chord and radial elements/cells) change according to cyclic law [7], namely:

$$N_{r_i} = 2P \sin (2i - 1) \varphi, \qquad (1)$$

where N_{r_i} - load on the i radial element/cell, which affects in the plane of this element/cell and applied at its cantilever end; P - external vertical load (part of the dead weight of mirror), applied at the same end of the radial element/cell; (2i-1) φ - angle between the plane of the i radial element/cell and the plane of the horizon/level. Since efforts/forces in the rods of radial load-bearing element (radial farm/truss) are proportional to load N_{r_i} effective on it therefore, they change according to the same law, as N_{r_i} i.e. cyclically. The cross travels (saggings/deflections) of the ends of the radial farms/trusses are also proportional to load and, it means to the sine of the angle between this radial element/cell and horizontal plane. From other side [7], distance of the ends of the arms of radial elements/cells from the horizontal axis h (intersection of the plane of the aperture of mirror with the plane of the horizon/level) they are proportional to the sine of the same angle:

$$h_i = 0{,}5\, D_{\text{зерк}} \sin (2i - 1) \varphi. \qquad (2)$$

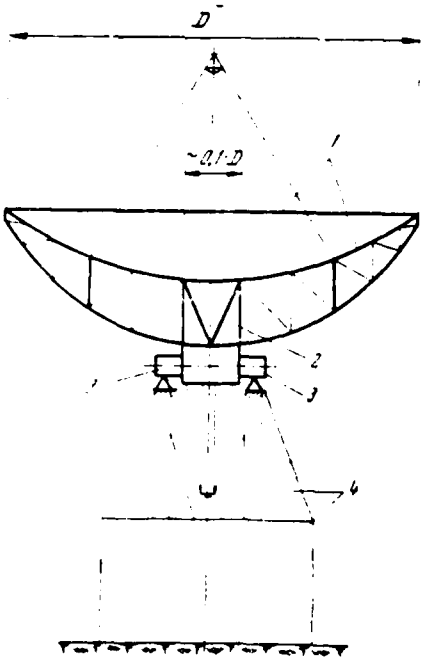

Fig. 1. The simple diagram of the multiple-support suspension of parabolic reflector (a special case) 1 - mirror; 2 - central bushing; 3 - supporting pins/journals; 4 - supporting-rotary device.

Page 79.

Thus, the sagging of the ends of the arms of radial elements/cells are proportional to their distances from the horizontal axis/axle indicated, and therefore in the strained state the plane of the aperture of mirror is not distorted. This property of the radiate structure diagram is expedient to utilize in the

diagrams of the multiple-support suspensions of parabolic reflector. Applying as the intermediate the supporting structure, constructed according to the radiate diagram, it is possible to ensure any required number of supports of mirror, arranged/located on one circle/circumference. In the previous diagrams a number of supports in one circle/circumference was limited by two. The cyclic properties of the radiate intermediate construction/design, used for the suspension of mirror, can be revealed, of course, only under specific conditions of its load by the weight of mirror.

Fig. 1 depicts the cantilever diagram of the suspension of a parabolic mirror, i.e., for the central bushing of framework/body. This diagram is a special case of the multiple-support cyclic diagram when all supports seemingly merged into one - central.

In the general case the multiple-support single-row suspension can be carried out with the aid of the intermediate radiate cyclic construction/design which, in turn, is hung for the central bushing.

A number of radial load-bearing structural elements intermediate is equal to a number of radial load-bearing elements of the framework/body of mirror. On each radial load-bearing element there is a support. Consequently, a number of supports is equal to a number of radial load-bearing elements. If the diagram of suspension does

not contain the central rod (central support), then in each diametric section/cut of mirror (on the load-bearing element) are furnished two supports. With the symmetric loading by dead weight the rigidity of mirror is determined by the rigidity of one diametric load-bearing element taking into account excess connections/communications, which are the chord elements/cells. In the first approximation, it suffices to consider only one such connection/communication, superimposed by external ring, and then the framework/body of mirror becomes once statically indeterminable, if the elements/cells (farms/trusses) of outer ring have comparatively small overall height.

Diametric load-bearing element can be considered as simple beam with two identical arms. For it, as is known, there is such most advantageous arrangement of supports during which the saggings/deflections of arms are equal to saggings/deflections in the flight/span. With the evenly distributed load and the permanent hardness along the length of beam/gully (diametric element/cell) the distance between the supports equally approximately/exemplarily

$0{,}56D_{отв}$.

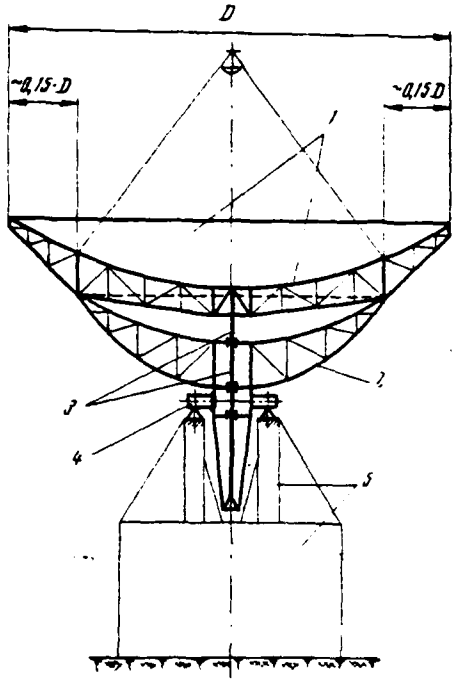

Fig. 2. The multiple-support diagram of the suspension of parabolic reflector with central supporting/reference rod 1 - mirror; 2 - intermediate multiple-support construction/design; 3 - central supporting/reference rod; 4 - supporting pins/journals; 5 - supporting-rotary device.

Page 80.

Upon consideration of that fact that the load to the ends of the arms grows/rises, the size/dimension of span part (distance between the supports) must be somewhat increased, and arms are respectively

reduced [8] and must comprise approximately/exemplarily $0{,}2D_{зерк}$.

If mirror is intended for the work on the waves of centimeter band (1-2 cm), then absolute overhanging length must be not more than 5 m. The maximum size of mirror in this case is equal to

$$D_{зерк}^{max} \approx \frac{5}{0{,}2} = 25 \text{ м}.$$

In order to increase the diameter of mirror without the decrease of effective area due to elastic deformations, it is necessary to increase a number of supports in the diametric section/cut of mirror.

Fig. 2 depicts the diagram of the multiple-support suspension of mirror with the radiate arrangement of supports with the central rod. With this suspension in each diametric section/cut (on power elements of framework/body) of mirror are contained three supports and each diametric element/cell works as tripod beam/gully (farm/truss).

The cross-sectional area of central rod is selected from the condition of the equality of the vertical displacements/movements of mirror at all reference points.

Accepting the again absolute size/dimension of arm equal to 5 m, we will obtain the maximum/overall diameter of the mirror whose

rigidity is equal to the rigidity of mirror with the suspension on the diagram in Fig. 1,

$$D_{верк} \approx \frac{5}{0,15} \approx 33 \text{ м}.$$

Further increase in the sizes/dimensions of mirror under the condition of retaining/preserving/maintaining its rigidity, i.e., without an increase in the absolute values of elastic deformations, is connected with the complication of diagram and construction/design of suspension.

Fig. 3 depicts the diagram of the multiple-support suspension of mirror with the two-layer radiate arrangement of supports and with the central supporting/reference rod. This suspension of mirror it is not possible to count completely cyclic, since the cyclic recurrence of rod (supporting/reference) pyramid is provided by the radial symmetry of mirror, and for retaining/preserving/maintaining the cyclic properties of the intermediate construction/design of this condition it is insufficient. Let us name/call the diagram of a mixed-cyclic in question.

A number of supporting/reference rods of rod pyramid is equal to a number of radial load-bearing elements of the framework/body of mirror; a number of radial elements of intermediate supporting structure is equal also to a number of radial load-bearing elements

of the framework/body of mirror.

The cross-sectional areas of rod pyramid, identical between themselves, are selected from the condition of the equality of the vertical displacements/movements of all supports of mirror. From the same conditions is selected the cross-sectional area of central supporting/reference rod taking into account elastic deformations of the beam/gully of counterweight, on which rests the apex/vertex of rod pyramid, and also taking into account the elasticity of the elements/cells of the sectors of rotation.

In the diagram in Fig. 3 in each diametric section/cut of mirror (on the load-bearing elements) are contained five supports. The values of arms comprise approximately/exemplarily $0{,}06D_{\text{зерк}}$. With the absolute size/dimension of arm 5 m the diameter of the reflector (under the condition of retaining/preserving/maintaining the same rigidity, as in the preceding/previous examples) proves to be equal to

$$D_{\text{зерк}} = \frac{5}{0{,}06} \approx 80 \text{ м}.$$

Page 81.

If a number of radial load-bearing elements of mirror is taken as equal to 16 (eight diametric elements/cells), then the total

number of supports of mirror will be equally 16·2+1=33.

In this diagram the construction/design becomes complicated not only by the fact that are introduced the new units (sectors of rotation, rod pyramid), but also fact that the rods of rod pyramid, being furnished in one plane with the radial load-bearing elements of intermediate supporting structure, naturally, they must not intersect, but pass one within another (for example, the rods of pyramid must be bifurcated in the vicinities of the load-bearing radial elements of intermediate supporting structure as this is conditionally shown in Fig. 3).

In the two-level multiple-support diagram of suspension in question, besides the condition for the identical vertical displacement/movement of all supports, must be observed one additional important condition - plane of the arrangement of the reference points, formed by rod pyramid, and plane the arrangements of the reference points, formed by intermediate supporting structure, being mutually parallel in the direction of mirror into the zenith, must remain mutual- parallel during the rotatior of mirror around the horizontal axis to the situation, when it becomes directed toward the horizon/level.

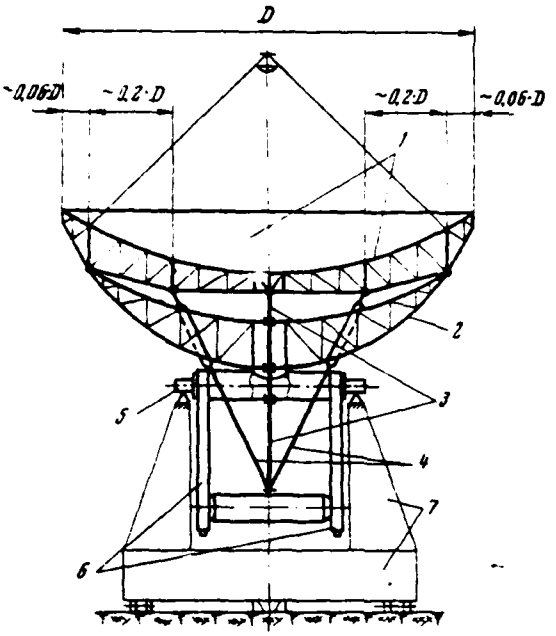

Fig. 3. The multiple-support two-level diagram of the suspension of parabolic reflector with central supporting/reference rod 1 - mirror; 2 · intermediate supporting structure; 3 - central supporting/reference rod; 4 - rod pyramid; 5 - supporting/reference pins/journals; 6 - unit of the sectors of rotation with the beam/gully of counterweight; 7 - supporting-rotary device.

Page 82.

As are shown calculations, the planes indicated do not remain, as a rule, mutually parallel[1], but they are easily led to the

position of mutual parallelism by the application/appendix of a comparatively small transverse force to the apex/vertex of the rod pyramid, which affects in the plane of the rotations of mirror around the horizontal axis.

FOOTNOTE [1]. In particular, it can seem that during the rotation of mirror around the horizontal axis the planes in question will remain mutually parallel. ENDFOOTNOTE.

This force can be obtained due to the torsional moment on the beam/gully of counterweight from the balance load, arranged/located eccentrically relative to this beam/gully.

In the diagrams (Fig. 2-3) examined the multiple-support suspension of mirror is accomplished/realized in such a way that the basic supporting units, which receive its weight in the vertical position of the plane of the aperture of mirror, are furnished far from the central bushing, in periphery, in consequence of which appears the need in intermediate rigid (and, consequently, heavy) supporting structure.

If we use support-rotary device with the large horizontal base, similar to the used rotary device in the English radiotelescope with 76-meter parabolic reflector[2] [9], then a multiple-support suspension

of mirror can be carried out without the use/application of intermediate supporting structure.

FOOTNOTE [2]. Shortcomings in such rotary devices is the increased moment of friction during the rotation along the azimuth and the increased moment of inertia, which requires the increased powers of homing/driving engines. ENDFOOTNOTE.

In this case the basic fastening of mirror is accomplished/realized for the central bushing of its framework/body.

Fig. 4 depicts the diagram of the multiple-support suspension of mirror with the radiate arrangement of supports and with the basic fastening of mirror for the central bushing. This diagram is cyclic. Since the weight of mirror (in the vertical position of aperture) is absorbed by horizontal duct/tube/pipe, then the latter must be by correspondingly reinforced in two planes. A number of supporting/reference rods of pyramid is equal to a number of radial load-bearing elements of the framework/body of mirror, and consequently, in each diametric section/cut of mirror (on the load-bearing elements) are contained three supports. The rigidity of mirror is compared with the rigidity of mirror with the suspension, carried out on the diagram in Fig. 2.

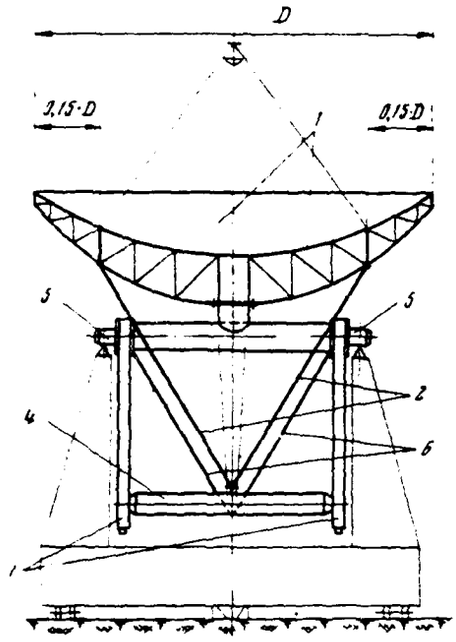

Fig. 4. The multiple-support diagram of the suspension of parabolic reflector without intermediate supporting structure 1 - mirror; 2 - rod pyramid; 3 - sectors of rotation; 4 - beam/gully of counterweight; 5 - supporting pins/journals; 6 - suspension of the beam/gully of counterweight.

Page 83.

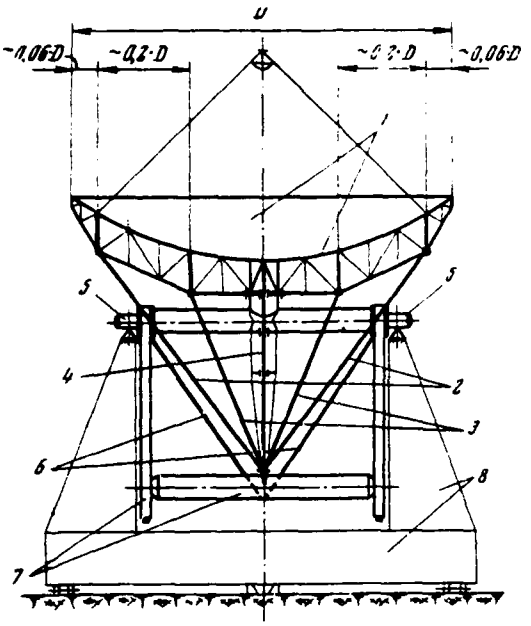

Fig. 5. Multiple-support two-level diagram of suspension of parabolic reflector without intermediate supporting structure. 1 - mirror; 2 - external rod pyramid; 3 - internal rod pyramid; 4 - central supporting/reference rod; 5 - supporting pins/journals; 6 - suspension of the beam/gully of counterweight; 7 - unit of the sectors of rotation with the beam/gully of counterweight; 8 - supporting-rotary device.

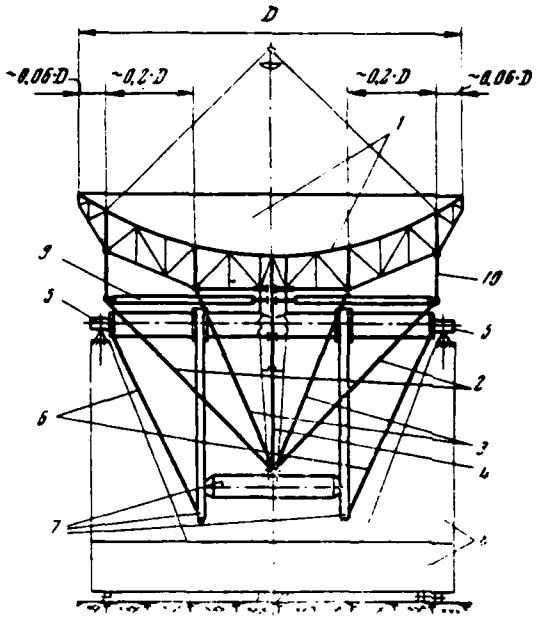

Fig. 6. Multiple-support double-row diagram of suspension of parabolic reflector with unloading radial rods.

Page 84.

Fig. 5 depict the diagram of the multiple-support suspension of mirror, its ensuring rigidity, compared with the rigidity of the mirror, depicted in Fig. 3. In this diagram in each diametric of the section/cut of mirror are contained five supports. Diagram is cyclic. The mutual parallelism of the planes of the arrangement of the reference points, formed by respectively external and internal rod

pyramids, is provided by the same method, that in the diagram, depicted in Fig. 3. A shortcoming in the diagram: comparatively high horizontal components of the bearing pressure of the rods of external rod pyramid cause large uncompensated deformations of mirror. In order to remove this shortcoming in the diagram, depicted in Fig. 6, it is used the unloading system, which consists of the radial rods, designated in Fig. 6 by numeral 9. The struts, arranged/located against each rod of external pyramid, are designated by numeral 10. Remaining designations in this figure are the same as in Fig. 5. A number of unloading rods is equal to a number of rods of each of the rod pyramids, and also to a number of radial elements/cells of the framework/body of mirror. The moved to the vertical plane symmetries sectors make it possible to somewhat decrease the horizontal dimensions of a supporting-rotary device.

In the latter/last three diagrams is absent intermediate supporting structure, but arose the new, very complicated and heavy unit: the large horizontal beam- duct/tube/pipe, which links the sectors of rotation and which receives gross weight of mirror in the vertical position of the plane of aperture. Horizontal duct/tube/pipe must have powerful/thick reinforcement at least in two planes: in the plane, parallel to the plane of the aperture of mirror, and in the vertical plane, passing through supporting/reference pins/journals.

It is at present difficult to express final judgment in favor of one of the diagrams, depicted in Fig. 3 and 6, since there is no sufficient data, based on static computations for the rigidity of the diagrams in question.

Fundamental, in our opinion, is the position, that the suspension of mirror must be multiple-support and cyclic in the cyclic schematic of the framework/body of mirror.

REFERENCES

1. Proc. IRE Australia, N 9, 519 (1959).
2. П. Д. Калачев. Труды ФИАН, 28, 51, (1965).
3. L. Mohr. Stahlbau, 1958, Jg. 27, H. 3, st. 62—69.
4. П. Д. Калачев, А. Е. Саломонович. Радиотехника и электроника, 4, вып. 3 (1961).
5. П. Д. Калачев. Труды ФИАН, 28, 183 (1965).
6. В. В. Виткевич. Труды 5-го космологического совещания по вопросам радиоастрономии. Изд-во АН СССР, 1956, стр. 14.
7. П. Д. Калачев. Труды ФИАН, 38, 60 (1967).
8. П. Д. Калачев. Труды ФИАН, 38, 72 (1967).
9. J. G. Bolton. Radio Telescopes. Univ. of Chicago Press, 1960.

STUDY OF VARIABLE TORQUE OF LOADS DUE TO WIND LOADS WHICH FUNCTION ON THE FULL-TURN ANTENNA AS RANDOM VARIABLES.

V. P. Nazarov, V. V. Dubarenko, D. G. Stepanov, A. I. Ukhov.

1. Formulation of the problem.

Experience of planning and operating powerful/thick radiotelescopes show that the basic factor, which impedes precise tracking of space objects, are the disturbances/perturbations, connected with the wind effects. Wind acts on guidance system through antenna, which is the aerodynamic filter, which converts energy of windstream. Wind velocity and moment/torque on the executive axis/axle are connected [1] with the relationship/ratio

$$M(t) = a(t)v^2(t), \qquad (1)$$

where M(t) - the instantaneous value of moment/torque from wind on the executive axis/axle, a(t) - the aerodynamic moment coefficient, v(t) - the instantaneous velocity of wind.

With the tracking of radiotelescope the space object the profile/airfoil of antenna relative to the velocity vector of wind is changed. In connection with this is changed aerodynamic moment coefficient, the process of its change in the general case carrying random character. Respectively, moment/torque M(t) is the random function of time, the determination of statistical characteristics of which composes the basic goal of present article.

In the antennas the devices/equipment, intended for accompanying the space objects, are applied two supporting structures - equatorial and horizontal. Are here examined only the devices/equipment with the horizontal suspension, which accompany object along its angle of elevation and azimuth.

Page 118.

2. Statistical characteristics of windstream.

Wind velocity never remains constant neither in the value nor in the direction. A change in the direction can be attributed due to the random character of a change in the aerodynamic coefficient. The instantaneous velocity of wind can be represented [1] by the following expression:

$$v(t) = v_0 + v_1(t). \qquad (2)$$

where v_0 - average/mean value of wind velocity, $v_1(t)$ - the instantaneous deflection of wind velocity from the average/mean value. Then moment/torque is defined as

$$M(t) = a(t)\ [v_0^2 + 2v_0v_1(t) + v_1^2(t)]. \qquad (3)$$

Adjoining and subtracting in the brackets of expression (3) value $\langle v^2_1(t)\rangle$ of the mean square of the fluctuations of wind velocity, we will obtain

$$M(t) = a(t)\ \{[v_0^2 + \langle v_1^2(t)\rangle] + 2v_0v_1(t) + [v_1^2(t) - \langle v_1^2(t)\rangle]\}. \qquad (4)$$

By the term $[v^2_1(t) - \langle v^2_1(t)\rangle]$ in expression (4) it is possible to disregard in view of its smallness. Then the fluctuations of moment/torque from faith/belief can be approximately represented as

$$M(t) \approx a(t)\ [v_0^2 + \langle v_1^2(t)\rangle + 2v_0v_1(t)]. \qquad (5)$$

Let us designate $v^2_0+\langle v^2_1(t)\rangle=\langle v^2\rangle$ the mean square of wind velocity. Then

$$M(t) = a(t)[\langle v^2\rangle + 2v_0v_1(t)]. \qquad (6)$$

From expression (6) it is evident that the process of the fluctuations of moment/torque on the actuating axis/axle is the combination of two random processes - the fluctuations of wind velocity and change in the aerodynamic coefficient. The statistical properties of the fluctuations of wind velocity are well studied and their characteristics are widely represented in aerodynamic and other literature.

Thus, on the basis [1-3] the correlation function of the

fluctuations of wind velocity approximately can be represented by the exponential curve of the form

$$R_{v_1 v_1}(\tau) = \langle v_1^2(t) \rangle e^{-\nu(\tau)}. \qquad (7)$$

The values of constants $\langle v^2_1(t) \rangle$ and ν_1 entering expression (7), they are determined by wind structure and they depend substantially on wind velocity, area relief and interval of observation, that lead to low-frequency oscillations/vibrations [3].

3. Statistical characteristics of aerodynamic moment coefficient.

The values of aerodynamic moment coefficient are determined by antenna position relative to the direction of windstream. In view of the complexity of the aerodynamic shape of antenna the calculation of coefficient of a presents considerable difficulties. In connection with this the dependence of aerodynamic moment coefficient on the bearing angles and place relative to the velocity vector of wind was determined experimentally - by the testing of model in wind tunnel of radiotelescope in wind tunnel [4].

Model was blown in its different positions, which correspond to the values of bearing angle (A) within the limits from 0 to 180° and angle of elevation (h) within the limits from 0 to 90°. The range of angles A and h indicated contains all positions which can occupy the antenna under the actual conditions, since it has a vertical plane of

symmetry. Thus, the antenna position with respect to the flow, which corresponds to the values of angles of A=30° and h=60°, is identical to the position in which angles A and h have values with respect to 330 and 60°. In this case the signs of some aerodynamic coefficients can be opposite.

Page 119.

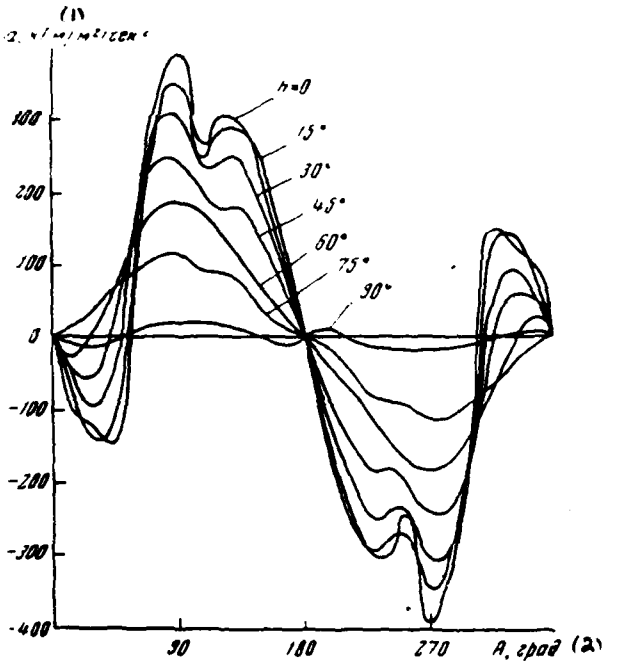

Fig. 1. Aerodynamic moment coefficient according to results of blasting.

Key: (1). kgm/m²/s². (2). deg.

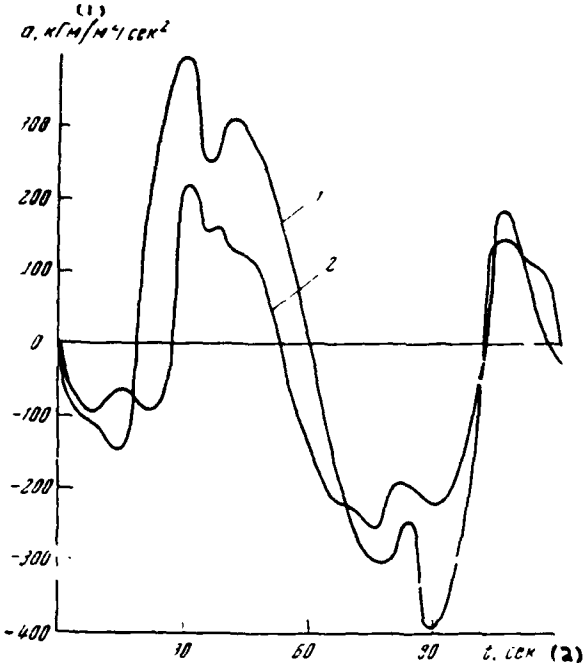

Fig. 2. Dependence of aerodynamic moment coefficient on time: 1 - according to results of blasting; 2 - according to results of full-scale tests ($\omega_A = 3$ deg/s, $n=0°$).

Key: (1). kgm/m²/s². (2). s.

Page 120.

Fig. 1 depicts the family of curves of a change in the aerodynamic coefficient from the angle of rotation in the azimuth (A) at the fixed/recorded angles of elevation h, obtained as a result of

the testing of model in wind tunnel of radiotelescope from a 32-meter parabolic antenna.

Fig. 2 for the comparison gives the curves of aerodynamic moment coefficient, constructed according to the results of blasting and full-scale tests of radiotelescope.

During the full-scale tests the aerodynamic moment coefficient was determined in the recording of the armature current of actuating motor of azimuth drive at the motion of antenna along the azimuth with a velocity of 3 deg/s from 0 to 360° and the angle of elevation h=0°. One of the recordings of armature current is represented in Fig. 3.

During the calculation of coefficient of a (curve 2, Fig. 2) were not considered the losses to the friction in the reducer and changes of the wind direction in the process of motion along the azimuth, nevertheless the character of a change in curves 1 and 2 (Fig. 2) coincides. Differences in curves 1 and 2 we link with the different conditions of the setting of experiments during the blasting and the full-scale tests.

Let us consider the methodology of obtaining the statistical characteristics of aerodynamic coefficient based on the example of

the analysis of data of the testing of model in wind tunnel of radiotelescope from a 32-meter parabolic antenna. Aerodynamic coefficient, is more accurate its mathematical model, has the series/row of special features/peculiarities.

1) $a=f(A,h)$,

but

$$A = f(t) = \{^{t}A(t)\}, \quad (8)$$
$$h = f(t) = \{^{t}h(t)\}, \quad (9)$$

i.e., in the general case random processes.

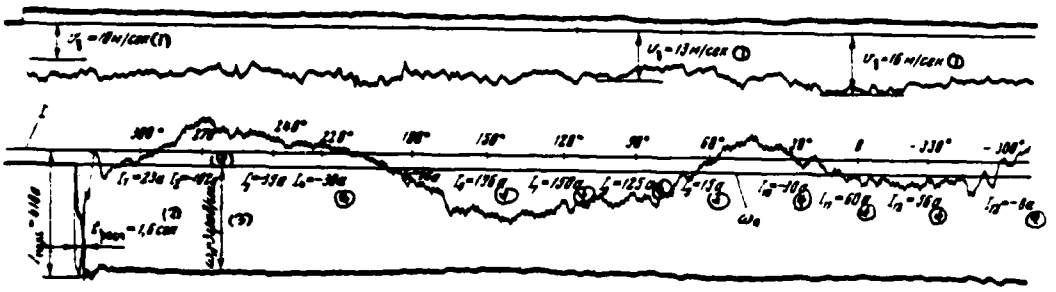

Fig. 3. Recording of the armature current of actuating motor during the motion of antenna along azimuth (n=0).

Key: (1). m/s. (2). s. (3). deg/s. (4). A.

Page 121.

Then a=f(A,h) is random process and can be represented by a set of functions of the time

$$\{{}^k a(t)\},\ 0 < t < {}^k T, \qquad (10)$$

where ${}^k T$ - time of the k realization of the random process of changing the aerodynamic moment coefficient. Index k is necessary in order to distinguish one realization of another.

2) At the moment of start the antenna position along the azimuth is equiprobable with respect to the sense of the vector of wind velocity, and position on the angle of elevation h=0°. It is thought that at the moment of the beginning of period of

communication (t=0) the object appears from behind the horizon/level.

3) The limited driving power of induction/guidance leads to limitation of maximum speeds and accelerations:

$$\begin{aligned} \omega_A(t) &\leqslant \Omega_A, \\ \omega_h(t) &\leqslant \Omega_h, \\ \varepsilon_A(t) &\leqslant \varepsilon_A, \\ \varepsilon_h(t) &\leqslant \varepsilon_h, \end{aligned} \qquad (11)$$

where $\omega_A(t), \omega_h(t), \varepsilon_A(t)$ and $\varepsilon_h(t)$ - instantaneous values of speeds and accelerations of antenna respectively on azimuth and angle of elevation; $\Omega_A, \Omega_h, \varepsilon_A$ and ε_h - amplitude values of the same speeds and accelerations.

Furthermore, the speed characteristics of antenna are limited by the length of period of communication T (time of the straight/direct visibility of object from the observation point). Processes $\{^k\omega_A(t)\}$ and $\{^k\omega_h(t)\}$ random, and for their characteristic it is necessary to know mathematical expectation and law of distribution relative to mathematical expectation or to have many realizations.

The limitation of velocities and accelerations leads to the appearance of "dead zones" for the telescopes with the horizontal suspension and, therefore, to breaks of connection/communication [5]. Subsequently the condition of continuous connection/communication we will consider necessary, i.e., the motion of artificial Earth

satellite (ISZ) in the "dead" for the telescope zone be examined will not be.

4) According to their designation/purpose the radiotelescopes serve: for the radio-astronomical observations, connection/communication with the distant space objects and ISZ.

In the first case the work of radiotelescope is characterized by slow (to several angular minutes per second) rates of change of the bearing angles and angle of elevation of antenna [5].

Examining the dynamics of the effects of windstream on guidance system [1], aerodynamic moment coefficient can be taken as equal to a constant value.

At the work of radiotelescope on ISZ with the heights/altitudes of the removal/distance of orbits from the surface of the Earth in several hundred kilometers of the velocity of the motion of antenna along the azimuth and the angle of elevation reach several degrees per second. This leads to considerable rates of change in the aerodynamic profile/airfoil of antenna. In connection with this the process of determining the statistical characteristics of a change in the aerodynamic moment coefficient leads to the complicated composite goal. For its solution will be required the special studies of the

trajectory motions of space objects and determination of their probabilistic characteristics. However, this exceeds the scope of present article.

It is obvious that the solution of the problem of determining the statistical properties of aerodynamic moment coefficient in the most general case when any tracked trajectory is equiprobable, is virtually inexpedient. Apparently, should be been bounded one trajectory or group of trajectories.

Page 122.

Let us consider the methodology of the determination of the correlation function of a change in the aerodynamic coefficient with the tracking of any trajectory from this group. For simplicity of considerations let us take trajectories with the circular ones, the orbits for which a change in azimuth and angle of elevation neglecting of the angular rate of rotation of the Earth they take the form (see the Appendix):

$$A(t) = \operatorname{arctg}\left[\frac{\omega_x}{\Omega_A}\operatorname{tg}(\omega_x t + x_0)\right],$$

$$h(t) = \operatorname{arctg}\frac{\sqrt{1-\frac{\omega_x}{\Omega_A}}\sin(\omega_x t + x_0) - \frac{R_3}{R_3+H}}{\sqrt{\cos^2(\omega_x t + x_0) + \left(\frac{\omega_x}{\Omega_A}\right)^2 \sin(\omega_x t + x_0)}}, \qquad (12)$$

where $\omega_x = \frac{\sqrt{g(R_3+H)}}{R_3+H} = \sqrt{\frac{g}{R_3+H}}$ - angular rotation speed of the

satellite around the Earth; R_3 - radius of the Earth; H - orbit altitude above the surface of the Earth.

Let us bound the group of orbits of ISZ by the range

$$H_1 < H_\xi < H_u. \qquad (13)$$

If now any trajectory with simultaneous satisfaction of conditions (11)-(13) is considered equiprobable, then, obviously, we will obtain a set of functions of the time

$$\{{}^\xi A(t)\} \text{ and } \{{}^\xi h(t)\}, \quad 0 < t < {}^\xi T. \qquad (14)$$

These sets characterize the motion of antenna. Here ξ - number of trajectory which takes all values from certain range of number scale axis from 1 to u, where u - number of the trajectories in question; ${}^\xi T$ - length of period of communication (time of straight/direct visibility of ISZ from the observation point). In other words, we have two finite sets of the analytically prescribed/assigned functions, each pair ${}^\xi A(t)$ and ${}^\xi h(t)$ characterizing the ξ-th trajectory of the ISZ. For all trajectories to the specific moment of time corresponds the specific value of azimuth and angle of elevation, and to these angles from the set of characteristics a (A, h) (see Fig. 1) - specific value of aerodynamic coefficient.

After decomposing the period of period of communication ${}^\xi T$ to the

equal time intervals, we find corresponding to the ends of these gaps/intervals of the value of coefficient of a, moreover for the reference point we accept any point on axis/axle A. Then, after changing reference point A for the same moments of time, we will obtain other values of coefficient of a. The curves of change a(t) will be different for the different wind directions at the moment of start. Wind direction we will assume/set by equiprobable for any azimuth at the moment of start.

If we take several points of reference point A, then each curve ${}^{\xi}a(t)$ can be considered as the realization of the random process of changing the aerodynamic coefficient, represented by the set of realization, that correspond to different wind directions in azimuth with the tracking of one concrete/specific/actual (ξ-th) trajectory of motion of the ISZ:

$$\{{}^{\xi}a(t)\}, \quad 0<t<{}^{\xi}T, \tag{15}$$

where ξ - number of the possible sense of the vector of wind velocity which takes all values from certain range of number scale axis from 1 to s, where s - number of possible wind directions.

Page 123.

Thus, for all trajectories of motion of ISZ

$$\{{}^{\xi}A(t)\}, \quad \{{}^{\xi}h(t)\}, \quad 0<t<{}^{\xi}T$$

the random process of changing the aerodynamic coefficient can be represented by a set of functions of time $\{^k a(t)\}$, $0 < t < {}^{\Sigma}T$ and it is described by its statistical characteristics.

The most general-purpose statistical characteristics for the random processes are their correlation functions. For random process $\{^k a(t)\}$ correlation function can be registered in the form

$$R_{aa}(t_1, t_2) = \langle {}^k a(t_1) {}^k a(t_2) \rangle \text{ av. read} = \lim_{N \to \infty} \frac{\sum_{k=1}^{N} {}^k a(t_1) {}^k a(t_2)}{N}. \qquad (16)$$

For each realization ${}^k a(t)$ with fixed/recorded k are taken values ${}^k a(t_1)$ and ${}^k a(t_2)$ and are multiplied. After this all similar products, obtained for different of realizations are summarized and are divided into a number of realizations. Result, thus, depends on the selection of the moments/torques of time t_1 and t_2.

Let us decompose set $\{^k a(t)\}$ into subsets $\{^{\Sigma} a(t)\}$, $0 < t < {}^{\Sigma}T$ such, that each of the realizations, entering this subset, has one and the same period of period of communication ${}^{\Sigma}T$. A number of such subsets is equal to a number of the trajectories u in question.

Let us consider one realization (recording) ${}^{\Sigma} a(t)$ of finite length ${}^{\Sigma}T$ of random process $\{^{\Sigma} a(t)\}$. Let us divide this recording into n of identical intervals by the points, equidistant from each

other, with the distance between them Δt and let us designate the obtained values of function at these points a_1, a_2, ..., a_n. Then the following formula gives approximate value of correlation function ${}^{\xi}R_{aa}(\tau)$ (in this case the beginning of the gap/interval of realization ${}^{\xi}T$ it is accepted for the origin of coordinates):

$$
\begin{aligned}
{}^{\xi}R_{aa}(\tau) \approx {}^{\xi}R_{aa}(\Delta tm) &= \frac{1}{{}^{\xi}T - \Delta tm} \int_0^{{}^{\xi}T-\Delta tm} {}^{\xi}a(t)\,{}^{\xi}a(t+\Delta tm)\,dt \approx \\
&\approx \frac{1}{{}^{\xi}T - \Delta tm} \sum_{i=1}^{i=n-m} {}^{\xi}a(t_i)\,{}^{\xi}a(t_i+\Delta tm)\,\Delta t, \qquad (17) \\
&\Delta t = \frac{{}^{\xi}T}{n}, \quad \tau = \Delta tm, \quad m = 0, 1, 2, \ldots, n.
\end{aligned}
$$

Then

$$
{}^{\xi}R_{aa}(m) \approx \frac{1}{n-m} \sum_{i=1}^{i=n-m} {}^{\xi}a_i\,{}^{\xi}a_{i+m}, \qquad (18)
$$

where

$$
{}^{\xi}a_i = {}^{\xi}a(t_i), \quad {}^{\xi}a_{i+m} = {}^{\xi}a(t_i + \Delta tm).
$$

In order to obtain ${}^{\xi}R_{aa}(m)$, it is necessary to compute n-m products a_1a_{1+m}, a_2a_{2+m}... according to formula (18), shifting/shearing each value on Δtm unity and multiplying initial values for the appropriate values, obtained after shift/shear. Further n-m products they store/add up and their sum is divided into a number of terms.

Page 124.

Let us register several of these sums:

$$
\begin{aligned}
n\,{}^{\xi}R_{aa}(0) &= a_1^2 + a_2^2 + \ldots + a_{n-1}^2 + a_n^2,\\
(n-1)\,{}^{\xi}R_{aa}(1) &= a_1a_2 + a_2a_3 + \ldots + a_{n-2}a_{n-1} + a_{n-1}a_n,\\
(n-1)\,{}^{\xi}R_{aa}(-1) &= a_1a_2 + a_2a_3 + \ldots + a_{n-2}a_{n-1} + a_{n-1}a_n,\\
(n-2)\,{}^{\xi}R_{aa}(2) &= a_1a_3 + a_2a_4 + \ldots + a_{n-3}a_{n-2} + a_{n-2}a_n, \qquad (19)\\
(n-2)\,{}^{\xi}R_{aa}(-2) &= a_1a_3 + a_2a_4 \ldots + a_{n-3}a_{n-2} + a_{n-2}a_n,\\
&\ldots\ldots\ldots\ldots\ldots\ldots\ldots\ldots\ldots\ldots\\
(n-m)\,{}^{\xi}R_{aa}(m) &= a_1a_{m+1} + a_2a_{m+2} + \ldots + a_{n-1}a_{n-(m+1)} + a_{n-m}a_n.
\end{aligned}
$$

From the examination of system of equations (19) it is possible to conclude that ${}^{\xi}R_{aa}(\tau)$ possesses the following two properties:

$$1)\quad {}^{\xi}R_{aa}(\tau) = {}^{\xi}R_{aa}(-\tau) \quad \text{for all} \quad m = 1, 2, 3, \ldots, n, \qquad (20)$$

i.e. the correlation function of a change in the aerodynamic moment coefficient - even function;

$$2)\qquad \sum_{i=1}^{n-m} (a_i \pm a_{i+m})^2 \geqslant 0,$$

but

$$\sum_{i=1}^{n-m} (a_i \pm a_{i+m})^2 = \sum_{i=1}^{n-m} a_i^2 \pm 2\sum_{i=1}^{n-m} a_i a_{i+m} + \sum_{i=1}^{n-m} a_{i+m}^2 =$$
$$= n\,{}^{\xi}R_{aa}(0) \pm (n-m)\,{}^{\xi}R_{aa}(m) + n\,{}^{\xi}R_{aa}(0).$$

Consequently,

$${}^{\xi}R_{aa}(0) \geqslant \left|\frac{n-m}{n}\,{}^{\xi}R_{aa}(m)\right|.$$

With $\Delta t \to 0$ and $n \to \infty$ for the final parameters of the correlation

Therefore $\lim\limits_{n\to\infty} \dfrac{n-m}{n} = 1.$

$${}^{\xi}R_{aa}(0) \geqslant |{}^{\xi}R_{aa}(\tau)|. \qquad (21)$$

From expression (21) it follows that the correlation function is symmetrical relative to point $\tau=0$. If we now suppose that a number of realizations ${}^{\xi}a(t)$ is equal to s and the duration of each exists ${}^{\xi}T$, then correlation function can be represented by the formula

$$ {}^{\xi}R_{aa}(m) = \frac{1}{s(n-m)} \sum_{\substack{i=1 \\ \xi=1}}^{\substack{i=n-m \\ \xi=s}} {}^{\xi}a_i {}^{\xi}a_{i+m}. \qquad (22) $$

Averaging on a set of realizations of random process $\{{}^{\xi}a(t)\}$, $0 < t < {}^{\xi}T$, we will further, producing obtain the general formula of the calculation of the correlation function of a change in the aerodynamic moment coefficient for the specific group of the trajectories of motion of the ISZ in the equiprobable wind direction along the azimuth at the moment of the beginning of period of communication (onset of an object from behind horizon/level t=0, h=0);

$$ R_{aa}(\tau) = \frac{1}{u} \sum_{\xi=1}^{\xi=u} {}^{\xi}R_{aa}(\tau), \qquad (23) $$

where u - number of the trajectories of motion of the ISZ in question.

Page 125.

4. Statistical characteristics of moment/torque on the executive

axis/axle of the guidance system of antenna.

Knowing the correlation functions of the random process of changing the aerodynamic moment coefficient and process of the fluctuations of wind velocity, let us determine the correlation function of the moment/torque, which functions on the executive axis/axle of antenna. On the basis of expression (6)

$$^{k}M(t) = {}^{k}a(t)[B + B^{k}v_1(t)], \qquad (24)$$

where $B=\langle v^2\rangle$ and $V=2v_0$.

Assuming/setting $\{^{k}a(t)\}$ and $\{^{k}v_1(t)\}$ by statistically independent variables, let us find correlation function $R_{MM}(\tau)$ of the total random process of disturbances/perturbations $\{^{k}M(t)\}$, applied to the executive axis/axle of the guidance system of the radiotelescope:

$$\begin{aligned} R_{MM}(\tau) &= \langle {}^{k}M(t)\,{}^{k}M(t+\tau)\rangle = \\ &= \langle \{{}^{k}a(t)[B + B^{k}v_1(t)]\}\{{}^{k}a(t+\tau)[B + B^{k}v_1(t+\tau)]\}\rangle = \\ &= \langle \{{}^{k}a(t)\,{}^{k}a(t+\tau)[B^2 + BB^{k}v_1(t) + BB^{k}v_1(t+\tau) + B^{2k}v_1(t+\tau)]\}\rangle. \end{aligned} \qquad (25)$$

Processes $\{^{k}a(t)\}$ and $\{^{k}v_1(t)\}$ are not mutually correlated; therefore their averaging on the set can be examined separately:

$$\begin{aligned} R_{MM}(\tau) = \langle {}^{k}a(t)\,{}^{k}a(t+\tau)\rangle \langle B^2 + BB^{k}v_1(t) + BB^{k}v_1(t+\tau) + \\ + B^{2k}v_1(t)\,{}^{k}v_1(t+\tau)\rangle, \\ \langle BB^{k}v_1(t)\rangle = \langle BB^{k}v_1(t+\tau)\rangle = 0. \end{aligned}$$

Since the mathematical expectation of the fluctuations of wind velocity relative to the average/mean value of wind velocity is equal to zero,

$$R_{MM}(\tau) = \langle {}^k a(t)^k a(t+\tau)\rangle \langle B^2 + B^2 {}^k v_1(t)^k v_1(t+\tau)\rangle,$$
$$\langle {}^k a(t)^k a(t+\tau)\rangle = R_{aa}(\tau),$$
$$\langle B^2 {}^k v_1(t)^k v_1(t+\tau)\rangle = R_{v_1 v_1}(\tau) B^2.$$

Then

$$R_{MM}(\tau) = R_{aa}(\tau)[B^2 + B^2 R_{v_1 v_1}(\tau)]. \qquad (26)$$

5. Example of calculation.

Let us consider an example of the calculation of the statistical characteristics of the random effects on the guidance system of radiotelescope according to the azimuth for three possible cases of moving the antenna:

1) antenna tracks trajectory of ISZ, a_1=a(t);

2) antenna revolves with the constant maximum speed along azimuth $\omega_A(t) = \Omega_A$ at the angle of elevation, equal to zero, a_2=a(t);

3) antenna position in the space is constant/invariable:

$$a_3 = a_{max} = \text{const.}$$

Page 126.

Let us designate the correlation functions of aerodynamic coefficient on the executive axis/axle for each of the

dismantled/selected cases respectively

$$R_{1\text{аа}}(\tau),\quad R_{1\text{мм}}(\tau),$$
$$R_{2\text{аа}}(\tau),\quad R_{2\text{мм}}(\tau),$$
$$R_{3\text{аа}}(\tau),\quad R_{3\text{мм}}(\tau).$$

Methodology examined above makes it possible to determine correlation functions $R_{1aa}(\tau)$ and $R_{2aa}(\tau)$.

Determination of $R_{1aa}(\tau)$. Calculation data: orbit of ISZ is circular; H=200 km; $\Omega_A = 3$ deg/s - the maximum speed of tracking along the azimuth at the point of the culmination (see Figs. 7 and 8); $R_з = 6{,}37\cdot 10^6$ м - radius of the Earth; $q = v^2/(R_3 - H)$ - free-fall acceleration; $v = \sqrt{g(R_3 - H)} = 8{,}04\cdot 10^3$ m/s - linear rotation speed of ISZ around the Earth; $\omega_з = v/R_3 = 0{,}07$ deg/s angular rotation speed of ISZ around the Earth; $\cos\varphi = \omega_з/\Omega_A = 0{,}023$ - cosine of the angle of inclination of the plane of orbit to the plane of the horizon in the observation point;

$$\alpha_0 = \arcsin\left[\frac{R_3}{R_3 + H}\frac{1}{\sqrt{1-\left(\frac{\omega_з}{\Omega_A}\right)^2}}\right] = 76°;$$

$$T = \frac{180° - 2\alpha}{\omega_з} = 400 \text{ — период сеанса связи. (1)}$$

$$A(t) = \operatorname{arctg}[0{,}0233\,\operatorname{tg}(0{,}07\,t + 76°)],$$

$$h(t) = \operatorname{arctg}\frac{\sin(0{,}07\,t + 76°) - 0{,}97}{\sqrt{\cos^2(0{,}07\,t + 76°) + 0{,}54\cdot 10^{-3}\sin(0{,}07\,t + 76°)}}; \quad (27)$$

$$\omega_A = \frac{dA(t)}{dt} = \frac{1{,}63\cdot 10^{-3}}{\cos^2(0{,}07\,t + 76°) + 0{,}54\cdot 10^{-3}\sin(0{,}07\,t + 76°)},$$

$$\omega_h = \frac{dh(t)}{dt} = \quad (28)$$

$$= 1{,}73\sqrt{\omega_A}\,\frac{\cos(0{,}07\,t + 76°) + 307\,\omega_A \sin(28° - 0{,}14\,t)[\sin(0{,}07\,t + 76°) - 0{,}97]}{1 + 613\,\omega_A[\sin(0{,}07\,t + 76°) - 0{,}97]^2}.$$

Key: (1). the period of period of communication.

$\omega_A(t), \omega_h(t)$

Graph A(t), h(t), on the basis of formulas (27), (28) they are given in Fig. 7 and 8. Correlation function $R_{1aa}(\tau)$ was computed according to (22):

$$R_{1aa}(m) \approx \frac{1}{8(40-m)} \sum_{\substack{i=0 \\ \xi=1}}^{\substack{\xi=8 \\ i=40-m}} {}^{\xi}a_i {}^{\xi}a_{i+m},$$

where $\tau = m\Delta t$ - parameter of correlation, $T = n\Delta t = 400$ s; $\Delta t = 10$ s; $n = 40$; $s = 8$ - number of possible wind directions at the moment of the beginning of the tracking (in the process of the tracking of antenna it was assumed that the wind direction remains constant/invariable).

Page 127.

In accordance with the graphs of the blasting (see Fig. 1)

when $\xi = 1$ $^1A = 0$,

when $\xi = 2$ $^2A = 45°$,

when $\xi = 3$ $^3A = 90°$,

. . . . . .

when $\xi = 8$ $^8A = 315°$.

The graph of correlation function $R_{1aa}(\tau)$ is represented in Fig. 4. Figure gives two analytical approximations of the function:

$$R_{1aa}(\tau) = D e^{-\mu(\tau)} \cos \beta\tau - R_0, \quad (29)$$

$$R_{1aa}(\tau) = D e^{-\mu(\tau)} (\cos \beta\tau + k \sin \beta_1 |\tau| - R_0), \quad (30)$$

where β - resonance frequency; μ - parameter of attenuation; R_0 - square of the average/mean value of aerodynamic moment coefficient in tracking process. Expression (30) gives better approximation/approach to to calculated curve I (see Fig. 4, curve 3), than (29); therefore for analytical approximation $R_{1aa}(\tau)$ we accept expression (30). After

the substitution of the numerical values

$$R_{1aa}(\tau) = -32{,}2\cdot 10^3 + 83{,}8\cdot 10^3\, e^{-0{,}048|\tau|}(\cos 0{,}044\,\tau + 0{,}1\sin 0{,}02\,|\tau|). \quad (31)$$

Determination $R_{2aa}(\tau)$. Data for the calculation: $\omega_A(t) = \Omega_A = 3$ deg/s, h(t)=0°.

Correlation function $R_{2aa}(\tau)$ was calculated according to (22):

$$R_{2aa}(m) = \frac{1}{n-m}\sum_{i=0}^{i=n-m} a_i a_{i+m},$$

where $\tau = m\Delta t$, $\Delta t = 1$ s, n=120 correspond to the complete revolution of antenna along the azimuth on 360°.

Computation $R_{2aa}(\tau)$ was produced in interval of T of one recording (realization) by a(t), obtained after replacement by the variable/alternating A on t in blasting/blowing diagram (see Fig. 2):

$$\frac{A}{\Omega_A} = t, \quad T = \frac{360°}{3\ \text{град/сек}} = 120\ \text{сек}.$$

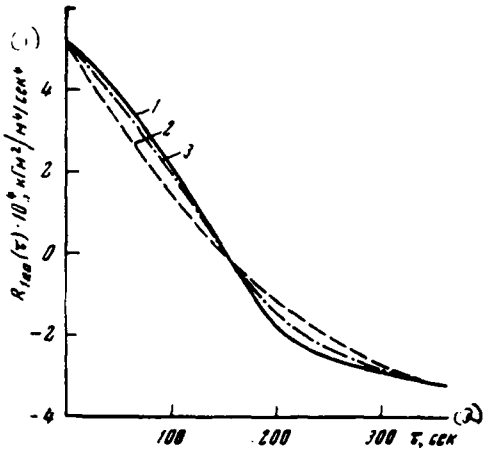

Fig. 4. Correlation function of aerodynamic moment coefficient and its analytical approximations with tracking ISZ. 1 - experimental curve; 2 - approximation according to (29); 3 - approximation according to (30).

Key: (1). kgm²/m⁴/s⁴. (2). s.

Page 128.

Graph $R_{2aa}(\tau)$ is represented in Fig. 5 (curve 1). Its two analytical approximations are given in the same figure:

$$R_{2aa}'(\tau) = D e^{-\mu|\tau|}\cos\beta\tau, \tag{32}$$

$$R_{2aa}(\tau) = D e^{-\mu|\tau|}\left[\cos\beta\tau + \frac{\mu}{\beta}\sin\beta|\tau|\right]. \tag{33}$$

Comparing the curves of the analytical approximation of

correlation function $R_{2aa}(\tau)$ with the experimental curve, we see that the first wave of experimental curve is approximated well by damped exponential-cosine function (32). At the end of the experimental curve are observed the random fluctuations around zero, which can be explained by the selection of the finite length of the recording of realization instead of by infinite and weak correlation in the high parameters of correlation τ:

$$R_{2aa}(\tau) = 4{,}95 \cdot 10^4 e^{-0.00316|\tau|} \cos 0{,}073\,\tau.$$

Correlation function $R_{3aa}(\tau) = a_{max}^2$. Let us assume $a_{max} = 400$ kg-m/(m/s)^2. The correlation function of the fluctuations of wind velocity takes form (7). The frequency band of the change in the spectral density of fluctuations is from 0.4 to 3 s^{-1} [1, 3]. For our goal we accept $\bar{\nu} = 1\ s^{-1}$. For average wind speed v_0=15 m/s, accordingly [1], the standard deviation from average wind speed composes 0.5 v_0, then

$$|\langle v_1^2 \rangle|^{1/2} = 0{,}5 \cdot 15 = 7{,}5 \text{ m/s}.$$

Respectively mean square of the fluctuations of wind velocity

$$\langle v_1^2(t) \rangle = 56{,}25 \ (м/сек)^2,$$

while

$$R_{v_1 v_1}(\tau) = 56{,}25\, e^{-|\tau|}.$$

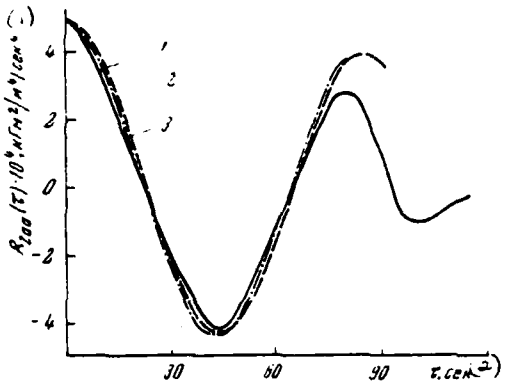

Fig. 5. Correlation function of aerodynamic coefficient and its analytical approximations during motion of antenna with $\omega_A = 3$ deg/s, n=0°. 1 - experimental curve; 2 - approximation according to (33); 3 - approximation according to (32).

Key: (1). kg-m²/m⁴/s⁴. (2). s.

Page 129.

On the basis (26), (30), (33) and (34) we determine the correlation functions of the moments/torques:

$$R_{1\,мм}(\tau) = -M_1^2 + D_1 e^{-\mu_1|\tau|}\cos\beta_1\tau + D_2 e^{-\mu_1|\tau|}\sin\beta_2|\tau| + D_3 e^{-\mu_2|\tau|}\cos\beta_1\tau + D_4 e^{-\mu_2|\tau|}\sin\beta_2|\tau| - D_5 e^{-\nu|\tau|},$$

$$R_{2мм}(\tau) = D_6 e^{-\mu_3|\tau|}\cos\beta_3\tau + D_7 e^{-\mu_4|\tau|}\cos\beta_3\tau,$$

$$R_{3\,мм}(\tau) = M_2^2 + D_8 e^{-\nu|\tau|},$$

where $M_1^2 = 25{,}4\cdot10^8$ $(кг.м)^2$, $\mu_1 = 0{,}0048$ $сек^{-1}$,

$M_2^2 = 126\cdot10^8$ $(кг.м)^2$, (1) $\mu_2 = 1{,}0048$ $сек^{-1}$, (2)
$D_1 = 66{,}2\cdot10^8$ $(кг.м)^2$, $\nu = 1$ $сек^{-1}$, (3)
$D_2 = 6{,}62\cdot10^8$ $(кг.м)^2$, $\mu_3 = 0{,}00314$ $сек^{-1}$, (4)
$D_3 = 42{,}4\cdot10^8$ $(кг.м)^2$, $\mu_4 = 1{,}00314$ $сек^{-1}$, (5)
$D_4 = 4{,}24\cdot10^8$ $(кг.м)^2$, $\beta_1 = 0{,}00437$ $сек^{-1}$, (6)
$D_5 = 16{,}3\cdot10^8$ $(кг.м)^2$, $\beta_2 = 0{,}021$ $сек^{-1}$, (7)
$D_6 = 39{,}1\cdot10^8$ $(кг.м)^2$, $\beta_3 = 0{,}073$ $сек^{-1}$. (8)
$D_7 = 25{,}1\cdot10^8$ $(кг.м)^2$, (9)

Key: (1). $(kg\text{-}m)^2$. (2). s^{-1}.

According to the known correlation functions let us determine the spectral densities of moment/torque on the executive axis/axle. For arbitrary random process $\{^k a(t)\}$ with $T\to\infty$ we have [2]

$$G_{aa}(f) = \lim_{T\to\infty}\int_{-\infty}^{\infty} e^{-j2\pi f\tau}\left[\frac{1}{2T}\int_{-T}^{T} R_{aa}(t_1 t+\tau)\,dt\right]d\tau. \qquad (35)$$

For correlation function $R_{1aa}(\tau)$ with the tracking by antenna ISZ, which moves along the stationary circular orbit, operation/process $\frac{1}{2T}\int_{-T}^{T} R_{aa}(t_1 t+\tau)\,dt$ was produced according to formula (23).

Correlation functions $R_{2aa}(\tau)$ and $R_{3aa}(\tau)$ correspond to stationary random processes. Consequently, formula (35) can be rewritten in the form

$$G_{aa}(f) = 2\int_{-\infty}^{\infty} R_{aa}(\tau)\,e^{-j2\pi f\tau}\,d\tau. \qquad (36)$$

If we utilize angular frequency ω [s^{-1}] instead of f(Hz), then expression (36) will take the form of the known relationship/ratio of Wiener-Khinchin

$$G_{aa}(\omega) = \frac{2}{\pi}\int_0^\infty R_{aa}(\tau)\cos\omega\tau\, d\tau. \qquad (37)$$

Let us note that G(f) is the doubled Fourier transform from $R_{aa}(\tau)$.

Thus, the general/common/total expression of the spectral density of the fluctuations of moment/torque on the executive axis/axle from the wind effect

$$G_{мм}(\omega) = \frac{2}{\pi}\int_0^\infty R_{мм}(\tau)\cos\omega\tau d\tau. \qquad (38)$$

Page 130.

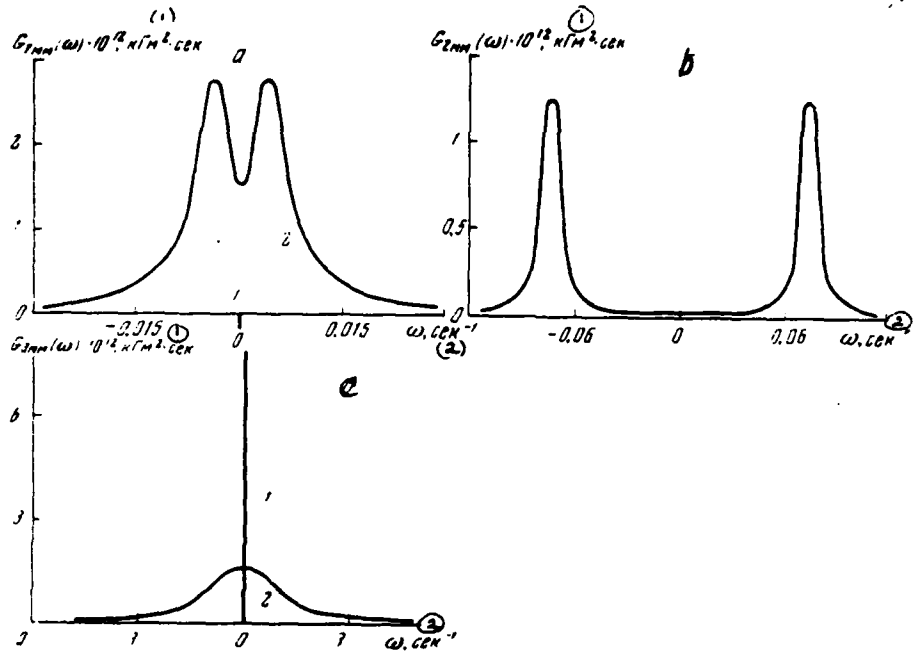

Fig. 6. Spectral densities of moment/torque on executive axis/axle of azimuth. a) with the tracking ISZ (1 - constant component, 2 - variable component); b) during the motion with $\omega_A = 3$ deg/s, n=0°; c) when $\omega_A = 0$, $\omega_n = 0$ and $= a_{max}$ (1 - constant component, 2 - variable component).

Key: (1). kg-m²/s. (2). s.

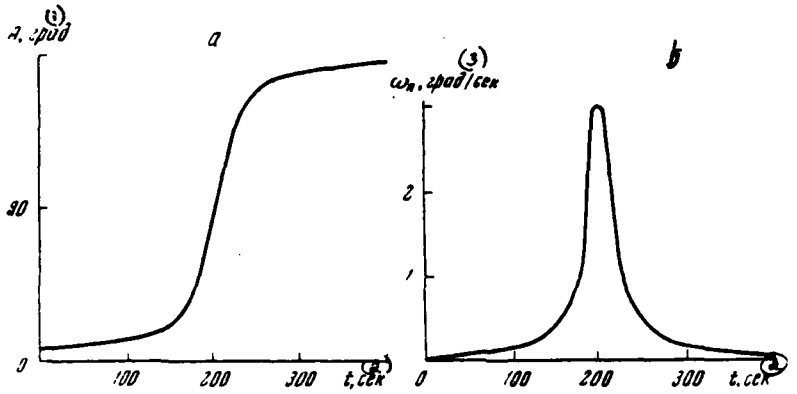

Fig. 7. Dependence of bearing angle (a) and azimuthal speed (b) on time.

Key: (1). deg. (2). s. (3). deg/s.

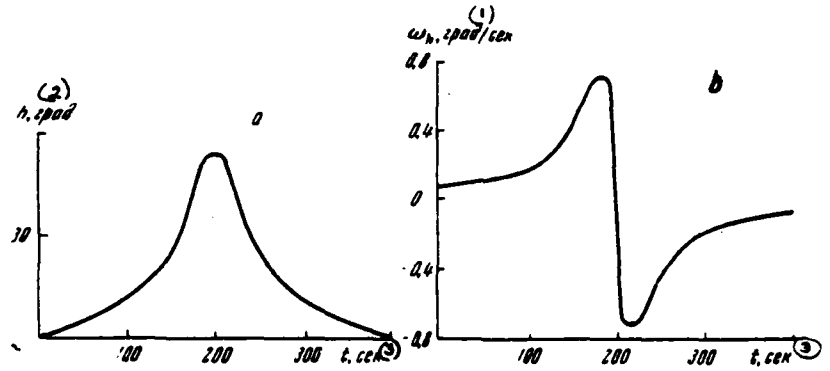

Fig. 8. Dependence of angle of elevation (a) and elevation speed (b) on time.

Key: (1). deg/s. (2). deg. (3). s.

Then the spectral densities of moments/torques, which correspond to correlation functions $R_{1.м.м}(\tau), R_{2.м.м}(\tau), R_{3.м.м}(\tau)$, take the form

$$G_{1.м.м}(\omega) = -2\pi_1 M_1^2\delta(\omega) + \mu_1 D_1\left[\frac{1}{\mu_1^2+(\beta_1-\omega)^2} + \frac{1}{\mu_1^2+(\beta_1+\omega)^2}\right] + D_2\left[\frac{\beta_2-\omega}{\mu_1^2+(\beta_2-\omega)^2} + \frac{\beta_2+\omega}{\mu_1^2+(\beta_2+\omega)^2}\right] + \mu_2 D_3\left[\frac{1}{\mu_2^2+(\beta_1-\omega)^2} + \frac{1}{\mu_2^2(\beta_1+\omega)^2}\right] + D_4\left[\frac{\beta_2-\omega}{\mu_2^2+(\beta_2-\omega)^2} + \frac{\beta_2-\omega}{\mu_2^2+(\beta_2-\omega)^2}\right] - \frac{2D_5\nu}{\nu^2+\omega^2},$$

$$G_{2.м.м}(\omega) = \mu_3 D_6\left[\frac{1}{\mu_3^2+(\beta_3-\omega)^2} + \frac{1}{\mu_3^2+(\beta_3+\omega)^2}\right] + \mu_4 D_7\left[\frac{1}{\mu_4^2+(\beta_3-\omega)^2} + \frac{1}{\mu_4^2+(\beta_3+\omega)^2}\right], \quad (39)$$

$$G_{3.м.м}(\omega) = 2\pi M_2^2\delta(\omega) + \frac{2\pi D_9\nu}{\nu^2+\omega^2},$$

where $\delta(\omega)$ - unit impulse function.

After the substitution of numerical values we will obtain

$$G_{1.м.м}(\omega) = -159\cdot10^6\delta(\omega) + 0{,}318\cdot10^8\left[\frac{1}{0{,}23\cdot10^{-6}+(0{,}00437-\omega)^2} + \frac{1}{0{,}2\cdot10^{-6}+(0{,}00437+\omega)^2}\right] + 6{,}62\cdot10^8\left[\frac{0{,}021-\omega}{0{,}23\cdot10^{-4}+(0{,}021-\omega)^2} + \frac{0{,}021-\omega}{0{,}23\cdot10^{-4}+(0{,}021+\omega)^2}\right] + 42{,}4\cdot10^8\left[\frac{1}{1+(0{,}00437-\omega)^2} + \frac{1}{1+(0{,}00437+\omega)^2}\right] + 4{,}24\cdot10^8\left[\frac{0{,}021-\omega}{1+(0{,}021-\omega)^2} + \frac{0{,}021-\omega}{1+(0{,}021+\omega)^2}\right] - \frac{32{,}6}{1+\omega^2},$$

$$G_{2.м.м}(\omega) = 0{,}123\cdot10^8\left[\frac{1}{9{,}85\cdot10^{-6}+(0{,}073-\omega)^2} + \frac{1}{9{,}85\cdot10^{-6}+(0{,}073+\omega)^2}\right] + 25{,}1\cdot10^8\left[\frac{1}{1+(0{,}073-\omega)^2} + \frac{1}{1+(0{,}073+\omega)^2}\right],$$

$$G_{3.м.м}(\omega) = 7{,}91\,\delta(\omega) + \frac{161}{1+\omega^2}.$$

The curves of a change in spectral densities $G_{1.м.м}(\omega), G_{2.м.м}(\omega)$ and

$G_{зим}(\omega)$ according to (39) are given in Fig. 6a, b, c.

Integration of the spectral density of moment/torque for all frequencies gives the mean square of moment/torque in (kg-m)^2 (Fig. 7):

$$\langle M_1^2(t)\rangle = M_1^2 + D_1 + D_2 + D_3 + D_4 - D_5 = 66{,}9\cdot 10^6,$$
$$\langle M_2^2(t)\rangle = D_6 + D_7 = 64{,}2\cdot 10^6,$$
$$\langle M_3^2(t)\rangle = M_2^2 + D_8 = 206{,}6\cdot 10^6.$$

The respectively rms values of moments/torques from the wind effects on the executive axis/axle of azimuthal drive are equal: with the tracking object $[\langle M_1^2(t)\rangle]^{1/2} = 82\cdot 10^3$ kg-m; during the motion with the constant maximum speed along azimuth $[\langle M_2^2(t)\rangle]^{1/2} = 80\cdot 10^3$ kg-m; with fixed antenna $[\langle M_3^2(t)\rangle]^{1/2} = 142\cdot 10^3$ kg-m (Fig. 8).

Conclusions/derivations.

1. Random disturbances, which affect guidance system of radiotelescope, are defined by both the fluctuations of windstream and by random character of change in aerodynamic coefficient of antenna.

2. Is given procedure of determination of statistical characteristics of change in aerodynamic moment coefficient in results of testing of model in wind tunnel of radiotelescope in wind tunnel.

3. Correlation functions of moments/torques on executive axis/axle of drive of guidance are damped cosine- exponential functions.

Page 132.

4. With solution of problems of determining statistical characteristics of disturbances/perturbations were not considered antennas filtering properties with respect to fluctuations of wind velocity. It was considered that energy of windstream it is linear, without the losses, it is converted by antenna. Therefore the results, obtained in the work in terms of the absolute values, are overstated, which, obviously, can be useful reserve during the planning.

The examination of antenna as the aerodynamic filter of windstream, which is changed in the value, is complicated independent goal.

APPLICATION/APPENDIX.

Kinematics of accompaniment ISZ by radiotelescope.

Let us examine kinematics of accompaniment by radiotelescope ISZ on the basis of the following assumptions: the Earth - sphere; the orbit of satellite - circular; the orbital plane passes through the center of the Earth. Let us designate R_3 -- radius of the Earth; H - height/altitude of the satellite above the surface of the Earth; v - linear rotation speed of satellite around the Earth (Fig. 9).

Spherical coordinates of radiotel scope (Fig. 10)

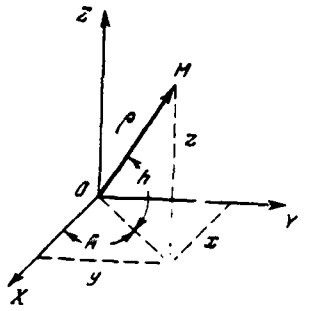

Figure 10. Diagram of the spherical coordinates system of radiotelescope.

$$x = \rho \cos h \cos A,$$
$$y = \rho \cos h \sin A,$$
$$z = \rho \sin h,$$
$$\rho = \sqrt{x^2 + y^2 + z^2},$$
$$A = \operatorname{arctg} \frac{y}{x},$$
$$h = \operatorname{arctg} \frac{z}{\sqrt{x^2 + y^2}}.$$

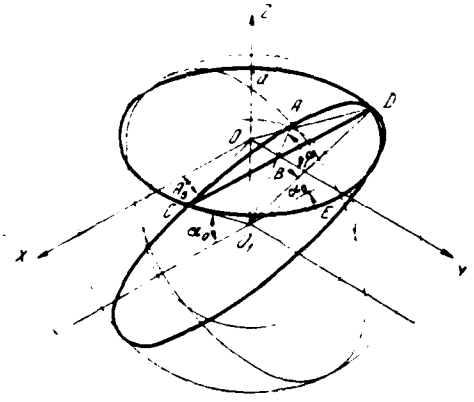

Fig. 9. Diagram for determining laws of motion of antenna with tracking for ISZ.

Page 133.

Let us find the equation of the trajectory of the motion of satellite relative to the system of coordinates X, Y, Z whose beginning coincides with the observation point.

Equation of the sphere of radius R_3+H

$$x^2 + y^2 + (z - R_3)^2 = (R_3 + H)^2. \qquad (\Pi.1)$$

Equation of plane CAD

$$z = y \operatorname{tg} \varphi - R_3. \qquad (\Pi.2)$$

Equation of the sphere

$$x^2 + y^2 + (z - R_3)^2 = R_3^2. \qquad (\Pi.3)$$

Equation of the plane of the horizon/level

$$z = 0. \tag{П.4}$$

Equation of the orbit of the satellite

$$\begin{gathered} x^2 + y^2 + (z - R_3)^2 = (R_3 + H)^2, \\ z = y \operatorname{tg} \varphi - R_3. \end{gathered} \tag{П.5}$$

Points of intersection of the plane of the horizon/level with the orbit of the satellite

$$\begin{aligned} &x_0^2 + y_0^2 + (z_0 - R_3)^2 = (R_3 + H)^2, \\ &z_0 = y_0 \operatorname{tg} \varphi - R_3, \\ &z_0 = 0. \end{aligned}$$

Hence

$$\begin{aligned} &y_0 = R_3 \operatorname{ctg} \varphi, \\ &x_0^2 = 2R_3H + H^2 - R_3^2 \operatorname{ctg}^2 \varphi, \\ &x_0 = \sqrt{(R_3 + H)^2 - R_3^2 \operatorname{cosec}^2 \varphi}, \\ &z_0 = 0. \end{aligned} \tag{П.6}$$

In the polar coordinate system

$$\begin{aligned} &A_0 = \operatorname{arctg} \frac{y_0}{x_0}, \\ &h_0 = 0. \end{aligned} \tag{П.7}$$

Coordinates of the point of determination of ISZ at the moment of the end of the period of communication

$$\begin{gathered} y_к = R_3 \operatorname{ctg} \varphi, \\ x_к = -\sqrt{(R_3 + H)^2 - R_3^2 \operatorname{cosec}^2 \varphi}, \\ z_к = 0 \end{gathered} \tag{П.8}$$

In the polar coordinate system

$$\begin{gathered} A_к = \operatorname{arctg} \frac{y_к}{x_к} = \operatorname{arctg} \left(- \frac{y_0}{x_0} \right) = \pi - \operatorname{arctg} \frac{y_0}{x_0}, \\ h_к = 0. \end{gathered} \tag{П.9}$$

Equation of motion of satellite relative to the center of the Earth

(Fig. 11)

$$x(t) = \frac{v}{R_3 + H} t. \qquad (\text{П.10})$$

Page 134.

Period of period of communication

$$T = \frac{x_к - x_0}{\omega_x} = \frac{\alpha_к - \alpha_0}{v/(R_3 + H)}, \qquad (\text{П.11})$$

where ω_x — angular rotation speed of ISZ around the Earth.

Let us find the projections of the motion of satellite on two mutually perpendicular directions m-m and n-n, parallel to the plane of orbit of ISZ (Fig. 12). Directions m-m belongs to the plane of orbit of ISZ and to the parallel line O_1A:

$$m(t) = (R_3 + H)\sin(\omega_x t + \alpha_0),$$

$$\sin(\alpha_0) = \frac{R_3}{R_3 + H} \frac{1}{\sin\varphi},$$

$$\alpha_0 = \arcsin \frac{R_3}{R_3 + H} \cos\varphi. \qquad (\text{П.12})$$

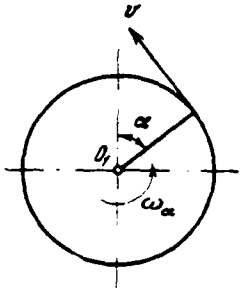

Fig. 11.

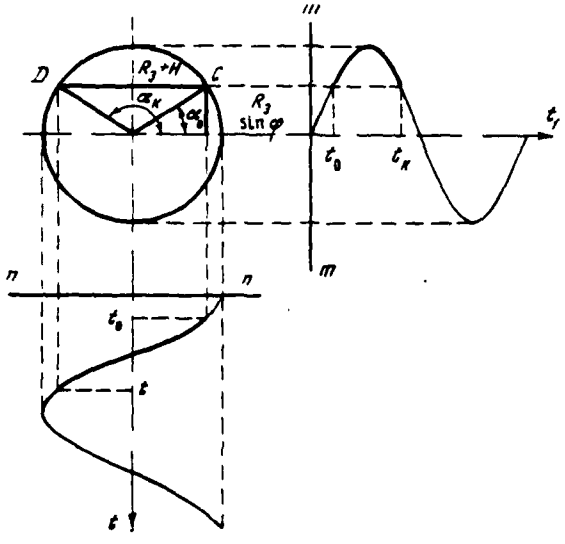

Fig. 12.

Fig. 11. Diagram to equation of motion of satellite.

Fig. 12. Diagram to determination of projections of motion of satellite on two mutually perpendicular directions.

Page 135.

n-n belongs to the orbital plane and is parallel to X axis:

$$n(t) = (R_3 + H)\cos(\omega_a t + \alpha_0),$$

gde n(t) - projection of instantaneous position of ISZ on the coordinate axis OX in the rectangular coordinate system as a result

of the fact that nn || CD, and CD || OX. Direction m-m comprises with the plane of the horizon/level angle φ.

$$\begin{aligned} y(t) &= m(t)\cos\varphi, \\ z(t) &= m(t)\sin\varphi - R_3, \end{aligned} \qquad (\text{П.13})$$

where y(t) and z(t) - the projection of the instantaneous position of satellite on the coordinate axes Y, Z, φ - the angle, formed by the plane of the horizon/level and by the plane of orbit of ISZ.

Thus, the equation of motion of satellite in the projections on the coordinate axes

$$\begin{aligned} x(t) &= (R_3+H)\cos\left[\frac{v}{R_3+H}t + \arcsin\frac{R_3\operatorname{cosec}\varphi}{R_3+H}\right], \\ y(t) &= (R_3+H)\cos\varphi\sin\left[\frac{v}{R_3+H}t + \arcsin\frac{R_3\operatorname{cosec}\varphi}{R_3+H}\right], \\ z(t) &= (R_3+H)\sin\varphi\sin\left[\frac{v}{R_3+H}t + \arcsin\frac{R_3\operatorname{cosec}\varphi}{R_3+H}\right] - R. \end{aligned} \qquad (\text{П.14})$$

In the spherical coordinates

$$\begin{aligned} A(t) &= \operatorname{arctg}\left[\cos\varphi\operatorname{tg}(\omega_\alpha t+\alpha_0)\right], \\ h(t) &= \operatorname{arctg}\frac{\sin\varphi\sin(\omega_\alpha t+\alpha_0) - \dfrac{R_3}{R_3+H}}{\sqrt{\cos^2(\omega_\alpha t+\alpha_0)+\cos^2\varphi\sin^2(\omega_\alpha t+\alpha_0)}}, \\ \omega_A(t) &= \frac{dA(t)}{dt} = \frac{\omega_\alpha\cos\varphi}{\cos^2(\omega_\alpha t+\alpha_0)+\cos^2\varphi\sin^2(\omega_\alpha t+\alpha_0)}, \qquad (\text{П.15}) \\ \omega_h(t) &= \frac{dh(t)}{dt} = \frac{\omega_\alpha\{\sin\varphi\cos(\omega_\alpha t+\alpha_0)[\cos^2(\omega_\alpha t+\alpha_0)+\cos^2\varphi\sin^2(\omega_\alpha t+\alpha_0)] - \\ \{\cos^2(\omega_\alpha t+\alpha_0)+\cos^2\varphi\sin^2(\omega_\alpha t+\alpha_0)+[\sin\varphi\sin(\omega_\alpha t+\alpha_0) - \\ -\frac{1}{2}\sin 2(\omega_\alpha t+\alpha_0)[\cos^2\varphi-1]\left[\sin\varphi\sin(\omega_\alpha t+\alpha_0) - \frac{R_3}{R_3+H}\right]\Big\} \\ \hline -\frac{R_3}{R_3+H}\Big]^2\Big\}\sqrt{\cos^2(\omega_\alpha t+\alpha_0)+\cos^2\varphi\sin^2(\omega_\alpha t+\alpha_0)} \end{aligned}.$$

Azimuthal speed reaches its maximum value Ω_A in moment/torque $\frac{T}{2} = \frac{\pi-2\alpha_0}{2\omega_\alpha}$:

$$\Omega_A = \frac{\omega_x \cos\varphi}{\cos^2\left(\omega_x \frac{T}{2} + x_0\right) + \cos^2\varphi \sin^2\left(\omega_x \frac{T}{2} + x_0\right)} = \frac{\omega_x \cos\varphi}{\cos^2\varphi} = \frac{\omega_x}{\cos\varphi},$$

whence

$$\cos\varphi = \frac{\omega_x}{\Omega_A},$$

$$\varphi = \arccos\frac{\omega_x}{\Omega_A}.$$

Page 136.

Then expression (P.15) is rewritten as

$$\omega_A(t) = \frac{\omega_x^2}{\Omega_A} \frac{1}{\cos^2(\omega_x t + x_0) + \frac{\omega_x^2}{\Omega_A^2}\sin^2(\omega_x t + x_0)},$$

$$\omega_h(t) = \frac{\omega_x\left\{\frac{\omega_x^2}{\Omega_A\,\omega_A}\sqrt{1-\frac{\omega_x^2}{\Omega_A^2}}\cos(\omega_x t + x_0) + \frac{1}{2}\left[1-\frac{\omega_x^2}{\Omega_A^2}\right]\sin 2(\omega_x t + x_0) \times \left[\sin(\omega_x t + x_0)\sqrt{1-\frac{\omega_x^2}{\Omega_A^2}} - \frac{R_3}{R_3+H}\right]\right\}}{\sqrt{\frac{\omega_x^2}{\omega_A\,\Omega_A}\left\{\frac{\omega_x^2}{\omega_A\,\Omega_A} + \left[\sqrt{1-\frac{\omega_x^2}{\Omega_A}}\sin(\omega_x t + x_0) - \frac{R_3}{R_3+H}\right]^2\right\}}}. \quad (\text{П}.16)$$

REFERENCES

1. Дж. К. Ньютон, Л. А. Гулд, Дж. Ф. Кайзер. Теория линейных следящих систем. Физматгиз, 1961.
2. Дж. Бендат. Основы теории случайных шумов и ее применения. Изд-во «Наука», 1965.
3. С. Л. Зубковский. Частотный спектр пульсаций горизонтальной компоненты скорости ветра в приземном слое атмосферы. Изд-во АН СССР, серия геофиз., № 10 (1962).
4. Л. Г. Лойцянский, И. Д. Повх. Аэродинамические характеристики некоторых конструкций. Отчет ЛПИ им. Калинина, 1961.
5. В. А. Барабанов, Е. А. Розенман. Вопросы радиоэлектроники, 5, 629 (1963).

Page 149.

Radiometers with the parametric amplifiers on wave 1.6 and 3.3 cm for radiotelescope RT-22.

V. P. Bibinova, A. D. Kuz'min, M. T. Levcenko, V. I. Pushkarev, A.Ye. Salomonovich, I. V. Shavlovskiy [deceased].

The radio-astronomical investigations of planets, discrete/digital sources and other objects in the centimeter band require a considerable improvement in the sensitivity of radiometric instrumentation.

As is known (for example, see [1]), one of the most effective methods of an improvement in the sensitivity of radiometer is the decrease of noise temperature of receiver. A supplementary improvement in the sensitivity can be also achieved/reached by the expansion of the passband of radiometer to the detector. In this connection in 1961 at the radio-astronomical station FIAN was carried out the work on an improvement in the sensitivity of the Dicke radiometers of ranges 3 and 1.6 cm of radiotelescope RT-22 by

applying the parametric amplifiers with the low noise level, and then broadband IF amplifier.

1. Diagrams of radiometers.

The block diagram of the radiometer of X-band is given in the figure. In the radiometer is used single-circuit reflecting parametric amplifier on the semiconductor diode (OPPU). For guaranteeing the quasi-degenerate and coherent mode/conditions of the work of amplifier pumping and heterodyning are conducted with the aid of one and the same klystron, and the frequency of pumping $f_н$, equal to the double frequency of heterodyne $2f_г$, is delayed by frequency doubler.

Under these conditions the amplification of noise signal with the spectral density constant in the passband is realized with the minimum noise factor in two sidebands of resonance characteristic OPPU, situated symmetrically relative to the central frequency of heterodyne. For frequency fixing of heterodyne and pumping is used the passive stabilizer of the frequency of klystron by the method of backlash by supporting high-Q resonator. Stabilization factor composes 15-20 with the power loss in the resonator 3-4 dB.

The radiometer of range 1.6 cm differs from the radiometer of

X-band in terms of the presence of separate klystron pump oscillator of parametric amplifier. The frequency of this generator is also stabilized by external reference cavity.

Page 150.

Structurally/constructurally parametric amplifiers of both ranges are carried out in the form of two waveguides, connected "overlap". Parametric diode is established/installed along the intersection of the planes of the symmetry of waveguides and during the tuning can be moved from the waveguide of signal into the waveguide of pumping. The free ends/faces of waveguides are shortened/shorted out by the plungers, which are effective tuning elements along the channels of pumping and signal. The diodes of parametric amplifier and frequency doubler work in the mode/conditions of automatic displacement. The efficiency of frequency doubler on the parametric diode composes 15o/o at the power output of 12-15 mW.

For decreasing the mutual effect pa-ametric amplifier, frequency doubler and reference cavity are unt: d by ferrite valves/gates. Special attention is turned to weakening of the power of heterodyne, which leaks to the input of radiometer. For this before the mixer is introduced ferrite valve/gate with the decoupling 60 dB.

The r-f unit of radiometer is placed about the primary focus of antenna RT-22. For decreasing the effect of a change in the ambient temperature parametric amplifier, frequency doubler and input ferrite devices/equipment are isolated/insulated from the heat-releasing nodes (klystron UPCh) and are placed in the special heat stabilized bellows. To the plumbing these nodes are connected by dielectric waveguides.

Radiometers of both ranges are modulation. For decreasing the effects of the background of the radio emission of sky, Earth and surrounding objects/subjects is used diagram modulation; equivalent is the auxiliary horn, arranged/located about the focus of antenna.

The calibration of radiometers is conducted with the aid of they are gas-discharge noise generators, connected through the directional couplers (30 dB) with the circuit of equivalent.

The radiometer of X-band works in the quasi-zero mode/conditions, i.e., with the equality of the noise radiation/emission, which enters the input of modulator through signal channels and equivalent. The latter is achieved by the introduction of special attenuator to the circuit of equivalent. For

the installation of quasi-zero mode/conditions this attenuator has remote control.

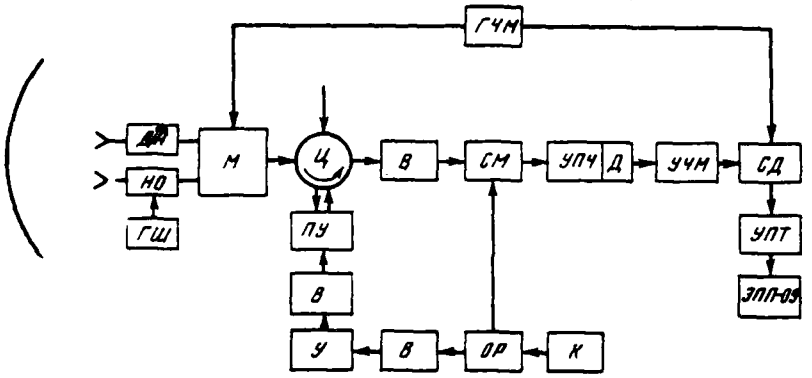

Fig. 1. Block diagram of the radiometer of X-band. NO - the directional coupler; GSh - gauging noise of generator; DA - the remotely/distance controlled attenuator for the installation of quasi-zero mode/conditions; M - modulator; Ts - circulator; PU - parametric amplifier; V - valve/gate; U - modulation frequency; UChM - amplifier of modulation frequency; SD - synchronous detector; UPT - dc amplifier.

Page 151.

2. Fundamental characteristics of radiometer.

The effective noise temperature of receiver with the high-frequency amplifier is determined by the known (for example, see [1]) by the relationship/ratio

$$T_{\text{ш}} = (L_{\text{т}}' - 1)\,T_0 + L_{\text{т}}' T_{\text{пу}} + \frac{L_{\text{т}}'}{G_{\text{пу}}}\left[(L_{\text{т}}' - 1)\,T_0 + L_{\text{т}}' T_{\text{ш}}\right].$$

Here $L_т'$ — path loss between the antenna and PU; $L_т''$ — path loss between PU and the mixer; T_0 - ambient temperature; $T_{пу}$ — noise temperature of parametric amplifier; $G_{пу}$ — amplification PU; $T_п$ — noise temperature of mixing receiver.

Taking into account that in the two-band mode of operation

$$T_п = \frac{1}{2}(F_п - 1)\,T_0,$$

where the factor of the noise of the mixing receiver

$$F_п = L(F_{упч} + t_м - 1),$$

and substituting the values of the parameters

$$L_т' = 1{,}2\ (0{,}8\ дб),\ L_т'' = 1{,}3\ (1{,}1\ дб),$$
$$T_{пу} = 150°\ \text{K},\ G_{пу} = 15{,}8\ (12\ дб).$$
$$L = 4,\ F_{упч} = 3{,}2,\ t_м = 1{,}7.$$

Key: (1). dB.

we will obtain $T_ш = 425°\text{K}$. In the passband UPCh Δf=60 MHz this corresponds to calculated fluctuation sensitivity of δT=0.09°K with τ=1 s.

For the range 1.6 cm

AD-A118 963 FOREIGN TECHNOLOGY DIV WRIGHT-PATTERSON AFB OH F/G 3/2
RADIO-ASTRONOMICAL INSTRUMENTS OBSERVATIONS (SELECTED ARTICLES)--ETC(U)
AUG 82 L I MATVEYENKO, G S MISEZHNIKOV
UNCLASSIFIED FTD-ID(RS)T-0564-82 NL

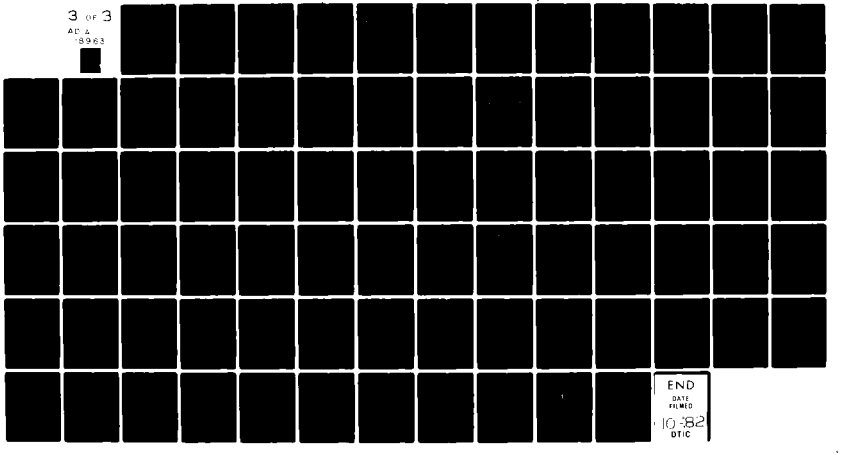

$L_\tau' = L_\tau^* = 1.2(0.8\ \overset{(1)}{\partial 6})$, $T_{\text{пу}} = 200°\text{K}$,

$G_{\text{пу}} = 12\ \partial 6$, $T_{\text{п}} = 3000°\text{K}$,

Key: (1). dB.

which gives $T_{\text{ш}} = 850°\text{K}$.

In Δf=56 MHz this corresponds to calculated fluctuation sensitivity of δT=0.2°K, with τ=1 s.

The measured fluctuation sensitivity of radiometers proved to be equal to 0.12 and 0.3°K with τ=1 s for λ=3.3 cm and λ=1.6 cm respectively, i.e., somewhat more than calculated.

Prolonged operation (since 1962) showed the stable operation of the radiometer of three-centimeter wave band under different weather and seasonal conditions. Relative changes of amplifying the radiometer during the continuous (6-8 hours) continuous operation comprised in average/mean 10^{-2} per hour of work. The total operating time of the radiometer between the maintenance and the tunings comprised usually about 1500 hours.

Use/application of a radiometer with the parametric amplifier on radiotelescope RT-22 made possible to carry out the systematic observations of the radio emission of Venus [2, 3] and some

discrete/digital sources, including which possess the anomalous dependence of the density of flow on the frequency (source 3C84, 3C273, 3C279) [4]. With the aid of the described radiometer were refined the polarizational characteristics of source Corpuscle-A [5].

Page 152.

The high sensitivity of radiometer made it possible to use the method of radio-guiding on the signal on the wave 3 cm of discrete/digital sources during the study of their radio emission in the millimetric wavelength range. Thus it was measured the radio emission of nebulae Orion and Omega [6] and distribution of the radio brightness of source Corpuscle-A. Subsequently on the base of the radiometer of three-centimeter s-band parametric amplifier was developed the radiometer for the spectral measurements, on which were discovered the spectral lines of the radiation/emission of excited hydrogen [7].

The radiometer of range 1.6 cm worked less reliably, but with its aid were also obtained the valuable data about the radio emission of Venus [3] and discrete/digital sources.

References.

1. А. Д. Кузьмин, А. Е. Саломонович. Радиоастрономические методы измерения параметров антенн. Изд-во «Советское радио», 1964.
2. В. П. Бибикова, А. Д. Кузьмин, А. Е. Саломонович, И. В. Шавловский. Астрон. ж., 39, 1083 (1962).
3. Ю. Н. Ветухновская, А. Д. Кузьмин, Б. Г. Кутуза, Б. Я. Лосовский, А. Е. Саломонович. Изв. вузов. Радиофизика, 6, 1054 (1963).
4. А. Х. Баррет, Б. Г. Кутуза, Л. И. Матвеенко, А. Е. Саломонович. Астрон. ж., 42, 527 (1965).
5. В. А. Удальцов. Дисс., ФИАН, 1966.
6. А. Д. Кузьмин, А. Е. Саломонович. Астрон. цирк., № 260 (1964).
7. Р. Л. Сороченко, Э. В. Бородзич. Докл. АН СССР, 163, 603 (1965).

Page 153.

Parametric amplifier to the wave 21 cm for the radio-astronomical investigations.

I. I. Berulis, B. Z. Kanevskiy, Ye. A. Spangenberg, I.A. Strukov.

The successes in the development of the spectral investigations of cosmic radio-frequency radiation are significantly determined by the possibilities of an improvement in the sensitivity of radio-astronomical equipment. One of the fundamental methods of sensitization is the use/application of the low-noise parametric amplifiers (PU) for the preliminary amplification in the high frequency. Despite the fact that the quantum paramagnetic amplifiers provide smaller noise temperature and successfully they are applied for the observations on the wave 21 cm [1, 2], due to the complexity of their operation in certain cases more is preferable (for the prolonged programs of the observations of the distribution of neutral hydrogen in the galaxy) the use/application of PU.

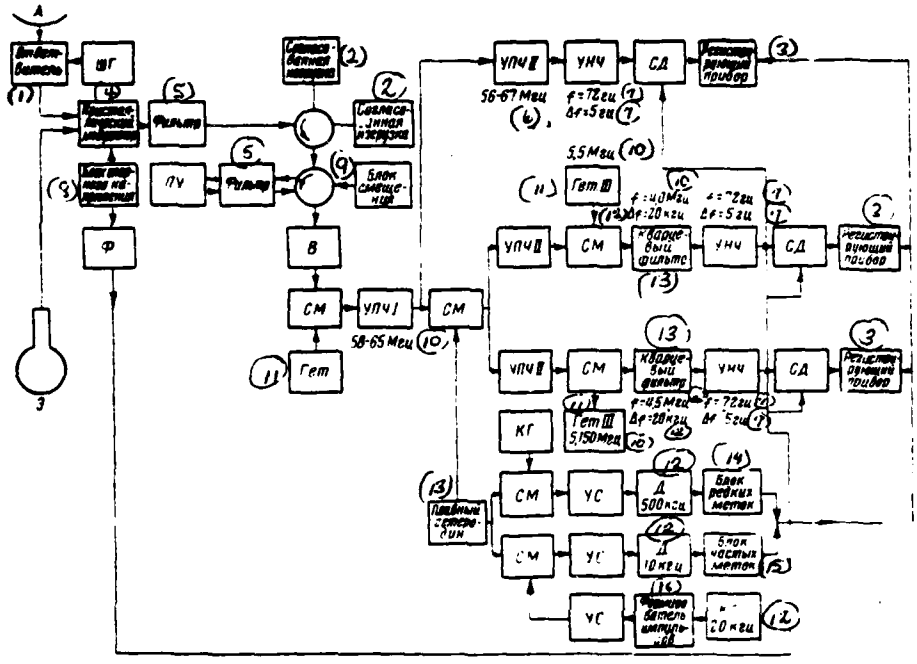

Fig. 1. Block diagram of radiometer with the parametric amplifier.

Key: (1). Coupler. (2). Matched load. (3). Recorder. (4). Crystal modulator. (5). Filter. (6). MHz. (7). Hz. (8). Block of reference voltage. (9). Block of displacement. (10). MHz. (11). het. (12). kHz. (13). Smooth heterodyne. (14). Block of rare markers. (15). Block of frequent markers. (16). Impulse shaper.

Page 154.

For this purpose in the beginning of 1966 on 22- metric

radiotelescope of FIAN of USSR [3] in the spectral radiometer to the wave 21 cm was established/installed by PU. The general/common/total block diagram of spectral radiometer with PU is represented in Fig. 1. This is modulation type superheterodyne receiver with the triple frequency conversion and a smooth change in the frequency in the second heterodyne. Modulation is realized by switching the input of receiver from the antenna to the equivalent whose effective temperatures are equalized before the observations. In the radiometer of PU it is connected into the circuit on the reflecting diagram with the aid of two ferrite circulators with the losses in one arm 0.3 dB. The remaining part of the radiometer is the microwave spectrometer, prepared for the observations without UHF [4].

1. Parametric amplifier.

During the analysis of noisiness and operational stability of PU of decimeter wave band, carried out in work [5], in PU to the wave 21 cm is used the current mode/conditions at which reaches the large depth of modulation of capacity/capacitance and the best stability. In this mode/conditions is utilized the accumulation of minority carriers in the base of diode.

During the detection of pumping on the straight/direct branch of the volt-ampere characteristic of diode together with charge

capacitance appears diffusion conductivity with capacitive and active components. In some types of diffusion parametric diodes in the base of diode there is a field, caused by the nonuniform distribution of admixtures/impurities. The presence of this field leads to the fact that the capacitive component of conductivity becomes more active, which makes it possible to utilize this conductivity for the parametric frequency conversion.

The noise temperature of amplifier with the work of diode in the current mode/conditions composes 100-150°K (with G=10-15 dB). During the use of diodes, which work with the negative bias voltage, it is theoretically possible to obtain PU noise temperature on the order of 30-50°K. However, current mode/conditions makes it possible to considerably raise the stability of amplification factor to the power drift of pumping and, consequently, also to the frequency drift of pump oscillator. Thus, with the factor of amplification 15 dB the power drift of pumping on 1 dB leads to the drift of amplification factor on 6 dB in the case of usual mode/conditions and on 2 dB in the case of current mode/conditions (Fig. 2). Furthermore, the use/application of current mode/conditions creates the very simple broadband (10-15o/o) construction/design of amplifier with a minimum number of elements/cells of tuning.

In the amplifier after the diode is arranged/located coaxial

loop by the length λ/4 in the idle frequency, that is inductance on the signal frequency. Pumping is supplied to the diode through the waveguide, formed by the continuation of the grounded plates. The waveguide of pumping is beyond the limits at the idle frequency.

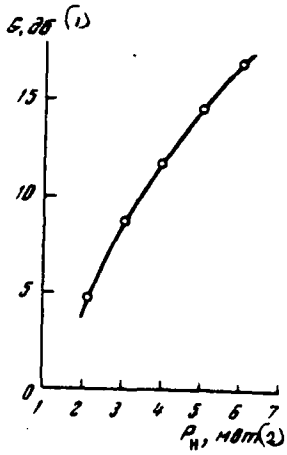

Fig. 2. Dependence of amplification factor on the power of pumping.

Page 155.

Idle duct/contour is formed only by the elements/cells of the housing of diode, since during the current mode/conditions capacity/capacitance p - n-transfer $C_п$ is considerably more than the capacity/capacitance of the receptacle of diode, and therefore the resonance frequency of idle duct/contour in essence is determined by the parasitic parameters of the housing of diode $L_{об}$ and $C_п$. In the small limits idle duct/contour can be reconstructed, connecting in parallel with the capacity/capacitance of housing small fine-adjustment capacity/capacitance.

Signal duct/contour is formed by the capacity/capacitance of p-n

junction and by the inductance of loop after the diode and by the cut of high-impedance line, connected between the diode and the traps. Fundamental characteristics of PU are the following:

(1) Входная частота, f_c . . . 1420, 405 *Мгц*
(2) Емкость $p-n$-перехода, C_{bb} . . . $0{,}22 \pm 0{,}04$ *пф*
(3) Температура шумов, $T_ш$ . . . 120°К
(4) Коэффициент усиления, $G_{ПУ}$ . . . 12 *дб*
(5) Потребляемая мощность накачки, $P_н$ . . . $\leqslant 5$ *мвт*

Key: (1). input frequency, f_c ... 1420, 405 MHz. (2). Capacity/capacitance of p-n junction, C_{bb} ... 0.22 +- 0.04 pF. (3). Noise temperature, $T_ш$ ... 120°K. (4). Amplification factor, $G_{ПУ}$ ... 12 dB. (5). Required power of pumping, $P_н$ ... $\leqslant$5 mW.

The amplitude-frequency characteristic of PU is given in Fig. 3. It should be noted that due to the narrow-band characteristic of decouplers of PU specially it was tuned to the narrow band. The use/application of current mode/conditions in the decimeter range makes it possible to obtain passband 10-15o/o without the supplementary compensating circuits in the presence of wide-band decouplings.

2. Noise measurements.

The sensitivity of radiometer in essence is determined by the fluctuations of internally-produced noise and by the instability of amplification factor. The fluctuation sensitivity, caused by

internally-produced noise, is determined by the relationship/ratio

$$\Delta T_{\text{мин}} \approx \frac{\pi}{2} \frac{T_{\text{ш}}}{\sqrt{\Delta f \tau}}, \qquad (1)$$

where $T_{\text{ш}}$ — general/common/total noise temperature of system; Δf - passband of receiver; τ - time constant.

When the fluctuations of factor of amplification are present, (G) the sensitivity deteriorates to the value, determined by the relationship/ratio

$$\Delta T_G = (\gamma - 1)(|T_a - T_э|), \qquad (2)$$

where γ=1+(ΔG/G) - the coefficient of the fluctuations of amplification; T_a — noise temperature of antenna; $T_э$ — noise temperature of equivalent.

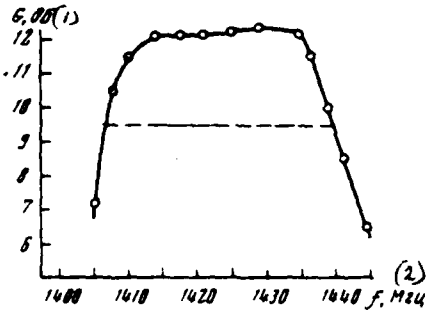

Fig. 3. amplitude-frequency characteristic of PU.

Key: (1). dB. (2). MHz.

Page 156.

As the equivalent was utilized the well matched load, cooled to the temperature of liquid nitrogen. The noise temperature of equivalent together with the coupling feeder composed 90°K; $T_э$ according to the measurements conducted, it was equal to 43°K. For obtaining the maximum sensitivity (according to equation (2) it is necessary to equate $T_э$ and $T_э$) into the circuit of antenna were introduced supplementary noises. The noise temperatures of antenna and equivalent it was possible to balance to 1.5°K. As a result the real sensitivity of radiometer can be recorded

$$\Delta T_0 = \Delta T_G + \Delta T_{\text{изм}}. \qquad (3)$$

The general/common/total noise temperature of the entire system of radiometer with PU is determined by the expression

$$T_{\text{ш}} = T_{\text{а}} + \frac{1}{q}\left[T_0(1-q) + T_{\text{пу}} + \frac{T_{\text{р}}}{G_{\text{пу}}}\right], \qquad (4)$$

where $T_{\text{пу}}$ — noise temperature of PU; $T_{\text{р}}$ — noise temperature of radiometer without PU; q - transmission factor of circuit to PU; $G_{\text{пу}}$ — factor of amplification of PU.

The noise temperature of radiometer with PU was measured with the aid of two noise equivalents - the well matched loads (KSVN [КСВН - VSWR] $\leq$ 1.04), one of which was located at a room temperature ($T_{\text{к}}$ =273° K $\pm$ t° C). another was cooled to the temperature of liquid nitrogen ($T_{\text{х}}$ = 77,3° K). Block diagram for the noise measurements is represented in Fig. 4.

Noise power from both loads alternately were connected to the system of circulators, were amplified by PU and second cascade/stage of amplification. As the second cascade/stage was utilized the radiometer with noise temperature $T_{\text{р}}$ = 1500° K. The precision attenuator connected to the detector made it possible to obtain identical power level at the output of receiver.

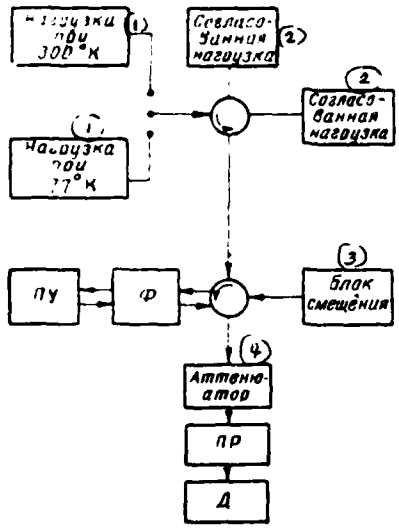

Fig. 4. Block diagram of installation for measuring the noise temperature of PU.

Key: (1). Load with 300°K. (2). Matched load. (3). Block of displacement. (4). Attenuator.

Page 157.

The difference in readings/indications of attenuator, which corresponds to the relation of the noise power N, is connected with the total noise temperature of two series-connected amplifiers with the simple correlation:

$$T_{\text{ш.с}} = \frac{T_{\text{к}} - NT_{\text{г}}}{N-1}, \qquad (5)$$

where

$$T_{ш.с} = T_{ПУ} - \frac{T_р}{G_{ПУ}}.$$

Equation (5) is conveniently represented in the form

$$T_{ПУ} = \frac{T_к - NT_г}{N-1} - \frac{T_р}{G_{ПУ}}. \qquad (6)$$

As a result of consecutive measurements was determined the noise temperature of PU at the different values of its amplification factors. The optimum parameters of PU, in which $\Delta T_э$ accepts smallest value, they proved to be: $T_{ПУ} = 120°$ K, $G_{ПУ} = 12$ dB, $\Delta f = 32$ MHz. In measurement $T_{ПУ}$ and $G_{ПУ}$ was checked the linearity of system after PU and in connection with the use/application of broadband loads entire system tested to the freedom from interference. The transmission factor of high-frequency circuit to PU was determined by losses in the modulator, the circulators and in coupling feeder lines ($q=0.82$). Substituting $T_а$, q, $T_{ПУ}$ and $T_р/G_{ПУ}$ in equation (4), we will obtain $T_ш = 420°$ K. which will agree well with measured data. Overall magnitude of error in the measurements did not exceed 5°K.

Before the observations conducted was investigated the lasting stability of amplifier. Fig. 5 gives the typical recording of output signal for the four hour old time interval with the factor of

amplification 12 dB.

As a result of numerous measurements of stability of PU with $G_{my} = 12$ dB the maximum drift of amplification factor during the long time (order 8 hour) was 0.5 dB. The fundamental source of slow instabilities was a change in the power of pumping. The oscillator frequency of pumping is stabilized.

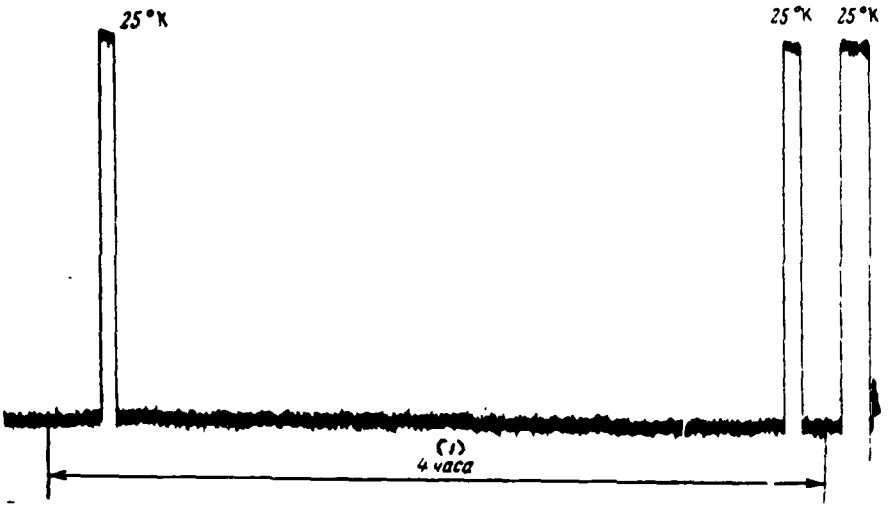

Fig. 5. Recording, which characterizes the stability of radiomete with PU in the continuous spectrum (time constant of 1 s).

Key: (1). hour.

Page 158.

In the process of work the adjustment of PU was not conducted. At a noise temperature of entire system of 420°K fluctuation sensitivity in the measurements in the continuous spectrum (τ=1 s and Δf=7 MHz) corresponded to 0.25°K, and for the observations in the radio link (τ=30 s and Δf=20 kHz) it was equal to $\Delta T_{\text{ш}}$=0.84°K, which will agree well with calculation data. Examples of recording in the radio link and in the continuous spectrum are shown in Fig. 6, 7.

Fig. 6 gives the recording of the radio emission of discrete/digital source virgin-A with coordinates $\alpha = 12^h29^m09^s$, $\delta = 12°34'32''$ (1966,5) in the continuous spectrum with the radiometer without PU and with the parametric amplifier. In Fig. 6 it is evident that the sensitivity of radiometer with PU increased 3.6 times in comparison with the radiometer without PU. The example to the recordings of radio link is given in Fig. 7. The calibratio of the intensity of the radio emission adopted with observation was conducted on the noise generator whose power was introduced into the circuit of the antenna through the directional coupler.

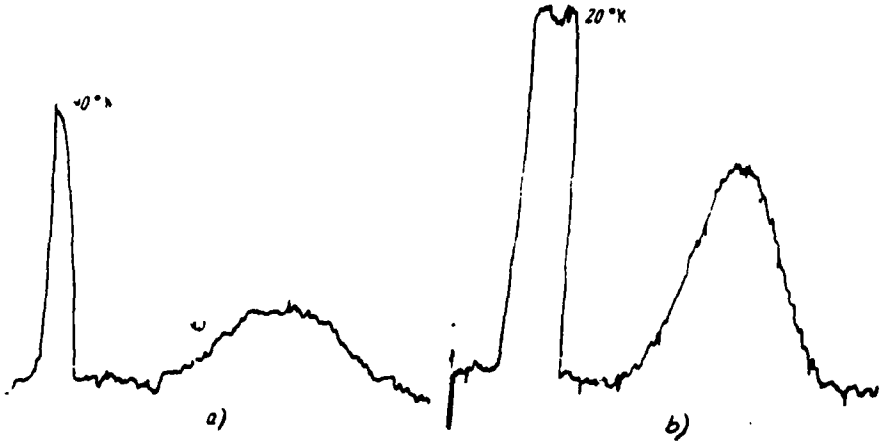

Fig. 6. Recording of radio source virgin-A in the continuous spectrum without PU (a) and with PU (b).

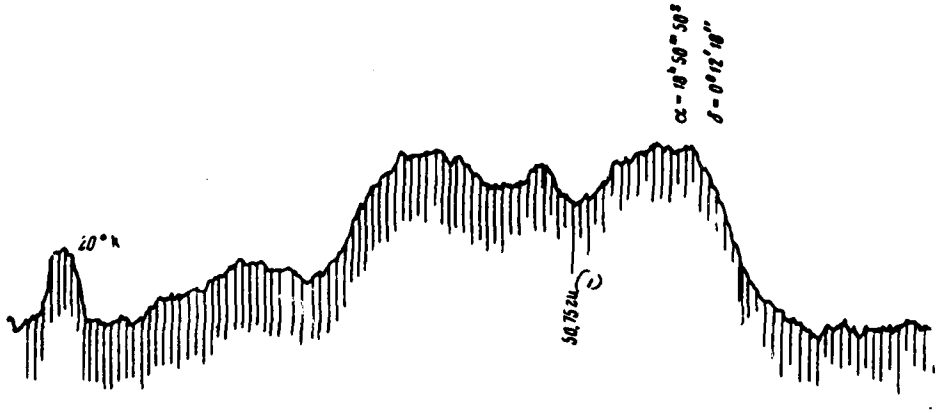

Fig. 7. Recording of profile/airfoil of line of radiation/emission of neutral hydrogen (frequency markers follow through 10 kHz).

Key: (1). Hz.

Page 159.

The conducte preliminary investigations of the radio emission of neutral hydrogen showed that the radiometer possesses high sensitivity with the narrow band of reception/procedure and it makes it possible to isolate the previously not noted thin parts in the form of lines and to in detail study the distribution of hydrogen in the galaxy.

The authors express deep appreciation to R. L. Sorochenko and V. S. Etkina for the discussion of the obtained results.

REFERENCES

1. T. V. Jelly. Microwave, J., 5, № 2 (1962).
2. Р. М. Мартиросян, А. М. Прохоров, Р. С. Сороченко. Докл. АН СССР, 156, 1326 (1964).
3. П. Д. Калачев, А. Е. Саломонович. Труды ФИАН, 17, 11 (1962).
4. Р. С. Сороченко. Канд. дисс., ФИАН, 1961.
5. К. С. Мосалян, А. И. Струков, В. С. Эткин (в печати).

Page 160.

Determination of the orientation of the electrical axis of curtain "east- west" of the crosslike radiotelescope DKR-1000 by means of the static [redacted]treatment of the observations of many discrete[redacted] sources.

V. V. Vitkevich, V. N. Kozhukhov.

1. Development of radio astronomy and, in particular, discovery on sphere of series/row of discrete/digital sources of radio emission celestially created new cart of possibility for research of antenna systems. Knowing the parameters of source, it became possible to determine efficient antenna area, to study the diagrams of radio reception, value and direction of minor lobes with the use of discrete/digital sources as the natural "radio transmitters" over a wide range of frequencies. Moreover the larger/coarser the antenna and the further arranged/located the distant zone, that the method indicated acquires larger value, to the form of the fact that the removal/taking the diagrams of large antennas with the help of the heterodynes requires the excessive removal/distance of the latter,

which strongly impedes and raises in price works.

Until recently most frequently was applied the method, based on the use of the separate, well studied discrete/digital sources, which have the greatest intensity (for example, see [1]). The difficulty which in this case appears, lies in the fact that we cannot change the coordinate of sources, and they are not always located, where it is necessary, moreover a number of them is small.

Another possibility lies in the fact that to use for the adjustment a large quantity of sources and to deduce from the observations the average/mean values of the unknown parameters. In this case the insufficient information about each source which in this case are used (the low accuracy of the determination of flow values, the low accuracy of the value of coordinates and sizes/dimensions), they are compensated by their large quantity, which gives the possibility to lead averaging according to a considerable number of observations.

The possibility indicated we used for determining the orientation of curtain of "east-west" of the range crosslike radiotelescope DKR-1000. As is known [2], this fabric is the parabolic cylinder with the size/dimension 40x1008 m^2 with the rotation on the angle of elevation. In this case, according to

geodetic data, its azimuth corresponded precisely to direction to the south, and western side it was elevated with respect to east at angle of 30' (which is caused by locality conditions).

In data finding as the basis is accepted the material of the first series of observations on the composition of the catalog of the discrete/digital sources of radio emission on the wave 3.5 m [3].

Page 161.

2. From observational data for each source was determined sidereal time s of its culmination, was located value $\Delta t=s-\alpha$ (α - right ascension) and was constructed graph/diagram of dependence Δt on declination δ. In the case of the absence any errors Δt it would be equal to zero, i.e., all sources simply would lie on the straight line, which coincides with the axis of abscissas.

Figure illustrates the results of the processing conducted. From the described ideal case it differs in two relations: first, curves do not coincide with the axis of abscissas (i.e. $\Delta t \neq 0$), there is a systematic difference, which depends on the declination, the reason for what is the fact that curtain "east- west" DKR-1000 it is oriented not accurately along the line an east-west and, furthermore, inclined; in the second place, point they lie down on the graph with

certain spread. The reasons for spread are caused by two groups of errors. The first group includes the errors, systematic with respect to this source, i.e., the possible errors in the coordinates of source and the effect of confusion in major lobe - result of the presence of other more or less strong source in immediate proximity of that studied. Let us note that during the observation of many sources these errors do not give the systematic contribution to the results. The second group - is the purely random errors which must vanish with the averaging of sufficiently great quantity of recordings. They include: the measuring errors, the effect of the ionosphere, the effect of confusion from the minor lobes (this occurs in such a case, when strong source falls into one of the minor lobes and if the latter is unstable), the disagreement/mismatch of the phases of fabrics.

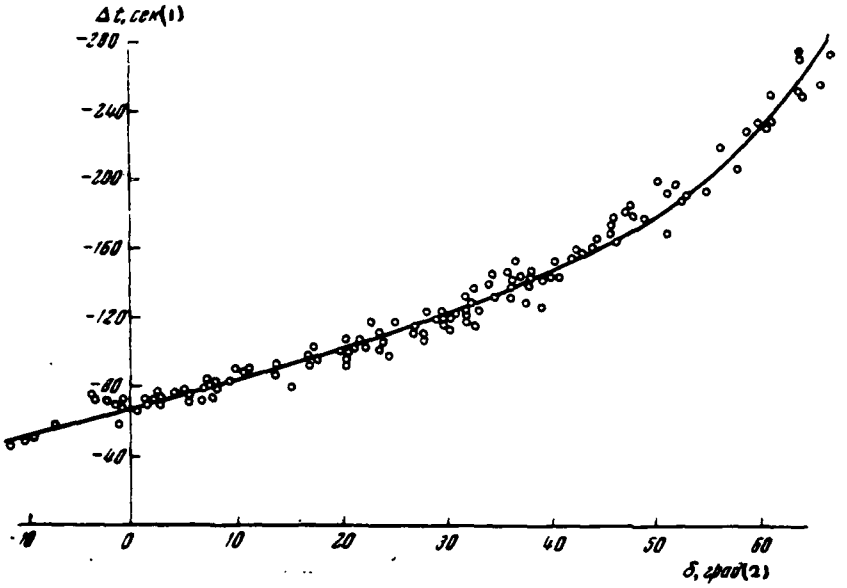

Fig. 1. Dependence of a difference in the actual transit time of the radio sources through the antenna radiation pattern and their right ascension ($\Delta t = s - \alpha$) on the declination δ. Crosses designated sources, on which was determined the orientation of curtain "east-west" DKR-1000; solid line - curve, obtained on the basis of the calculated parameters.

Key: (1). s. (2). deg.

Page 162.

The sufficiently large material of observations, obtained as a result of processing, made it possible to determine inclination/slope

and azimuth of curtain "east- west" DRK-1000. The effect of inclination/slope on the transit time of source is expressed by the formula

$$(\Delta t_1) = \frac{a \cos z}{\cos \delta}, \qquad (1)$$

where z - zenith distance; δ - declination of source; a - inclination/slope of fabric, expressed in the same unity, as value Δt.

The effect of azimuth is respectively expressed by the formula

$$(\Delta t)_2 = \frac{b \sin z}{\cos \delta}, \qquad (2)$$

where b - deviation of curtain "east- west" from the true direction the east - west. Joining (1) and (2), we have

$$\Delta t = (\Delta t)_1 + (\Delta t)_2 = \frac{a \cos z}{\cos \delta} + \frac{b \sin z}{\cos \delta}$$

or

$$a + b \operatorname{tg} z = \frac{\cos \delta}{\cos z} \Delta t. \qquad (3)$$

Hence by the method of least squares it is possible to determine the values of a and b interesting us. For this purpose it was used 131 sources, which was being observed in the period from March through May 1965. The results of calculations gave the following values:

a=29'10 "+-34" (western end is above),

b=24 "+-43" (western end was deflected to the south).

Figure gives calculated curve for obtaining the average/mean values of a and b.

The deviation of observational data from the theoretical curve comprises $\leqslant 10^{s}$. Taking into account that values Δt vary from the day to the day for one and the same source in the limits approximately/exemplarily 30^{s} and that the greatest number of averaging of one source is equal to 10, quadratic deviation in the figure must be about 10^{s}, i.e. all sources lie/rest within the limits of random errors. Thus, there are no foundations for considering that the errors of the first group (i.e. inaccuracy in the coordinates and confusion-effect) for the used sources are considerable on the wave λ=3.5 m.

REFERENCES

1. А. Д. Кузьмин, А. Е. Саломонович. Радиоастрономические методы измерений параметров антенн. Изд-во «Советское радио». 1964.
2. В. В. Виткевич, П. Д. Калачев. Труды ФИАН. 28, 5 (1965).
3. В. С. Артюх, В. В. Виткевич, Р. Д. Дагкесаманский. Астрон. ж., 44, 984 (1967).

Page 173.

Fundamental parameters of the antenna feeder "east- west" of range cross-shaped radiotelescope of FIAN.

1. Layout of irradiator.

N. P. Ilyasov.

Antenna "east-west" of cross-shaped radiotelescope of FIAN is parabolic cylinder with the sizes/dimensions of 1008 m on the generatrix and 40 m along the bracing chord with the wide-range irradiator, established/installed along the focal line of radiotelescope. According to the design considerations, in detail examined in [1], the antenna is divided in 36 sections with a length of 28 m each. Within one such part of the antenna is established/installed the section of irradiator of eight shunt radiators/resonators/elements with the broadband balancer. The parameters of this section are given in [2]. There it is shown that the section of irradiator provides the possibility of the simultaneous work of antenna over a wide range of the frequencies:

from 30 to 120 MHz.

From each section of irradiator on the dipole masts are laid the cables of a decrease in brand RKK-5/18 with length of 50 m each. Length their is identical, to the accuracy +-5 mm. The cables of decrease from two adjacent sections are conducted/supplied to the summing broadband transformers which are carried out in the form of conical coaxial lines by the length of 4 m. These transformers are established/installed directly in the earth/ground. From the summing transformers the cables of brand RKM-5/18 with a length of 465 m each are fed/conducted to the center of antenna. In all such cables 18, on nine from each side from the center of antenna. They are laid underground at the depth of approximately 1 m in the special asbestos-cement tubes for decreasing the change in their electrical length from a change in the temperature. The surplus lengths of cable from the central sections of irradiator are assembled on the drums, installed in the center of antenna in the special commutation basement. For the equalization of the electrical lengths of these cables are used the lines of variable/alternating length, established/installed at the ends/leads of 18 cables in this basement. Further association of all sections of irradiator is conducted in accordance with the diagram in Fig. 1 with the aid of the summing broadband transformers with the transformation of resistor/resistance from 25 to 75 ohms. These are conical coaxial

lines with the length of 4 m. In this switching circuit of antenna is provided the uniform cophasal excitation of all sections of irradiator with a good agreement over a wide range of frequencies.

As is evident in Fig. 1, switching circuit makes it possible to work as with the compensative ones and with the correlation radiometers.

Page 174.

Furthermore, this diagram makes it possible to form interferometers with any bases in the limits of entire antenna. As shown in [3], the divergence of diagram in the direction with the random phase errors in the feeder circuits of antenna for this switching circuit will be less than for the diagram with a smaller number of independent high-frequency cables, applied to the center of antenna for the addition.

2. Adjustment of irradiator.

Tuning the majority of the elements/cells of irradiator was conducted before their installation on the antenna. Shunt radiators/resonators/elements were collected on the special template/pattern. After assembly were checked their basic dimensions.

The deviation of sizes/dimensions was not more than +-1 cm. Before the assembly of sections of eight dipoles preliminarily on the single standard were tuned all entering there cuts of feeder. Then the assembled section finally was adjusted slightly with changes of the agreement and phasing over a wide range of frequencies. The accuracy of phasing on the absorbing loads, included instead of the dipoles to the period of the tuning (see [2]), was not worse than +-3°. After final checking without any dismantling the section of irradiator was assembled in the reflector. The broadband balancers (ShSU) and the summing transformers were checked in the range of the frequencies of 30-120 MHz using the agreement and amplitude-phase symmetry at the output. All cables RK-3, which connect the separate elements/cells of feeder circuit, were tuned on the common standards with the accuracy not worse than +-3 mm to usual procedure with the use/application of the grad line LI-3.

The fundamental feeder lines, packed underground, were checked and were tuned with the special thoroughness. Initial tuning was carried out by pulse method. Impulses/momenta/pulses the duration of 0.1 μs were supplied simultaneously to the "standard" and measured cables. On the pulses echo from the ends/leads of the cables the measured cable was equalized with the accuracy +-60 cm with respect to the standard. In these measurements was applied the high-speed/high-velocity dual-trace oscillograph DESO-1. Preliminary

they were removed all heterogeneities in the measured cable, the giving reflections are more than 0.1. Location it was possible to easily determine them on the temporary/time markers DESO-1.

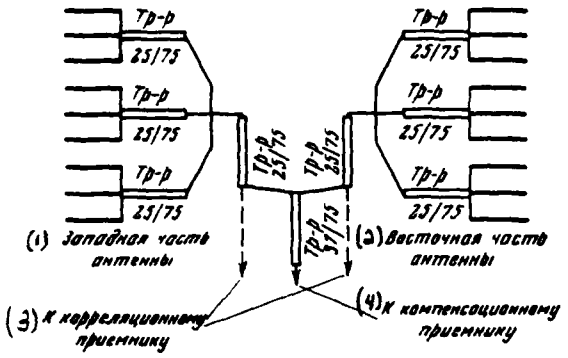

Fig. 1. Switching circuit of the sections of irradiator.

Key: (1). Western part. (2). Eastern part of antenna. (3). To correlation receiver. (4). To compensative receiver.

Page 175.

As a rule, the majority of heterogeneities appeared in the points of connection of different construction lengths of cables. The accuracy of the presetting of cables +-60 cm was determined by the rise time of sounding pulse, by the maximum speed of scanning/sweep DESO-1 and by the scale of its temporary/time markers. In our view, was provided the actually obtainable accuracy of reading, since leading front of the echo pulse depends on the length of cable due to the frequency course of attenuation in it. As showed calculations, for cable RKM-5/18 with a length of about 500 m the rectangular sounding pulse, after being reflected from the end/lead of the cable, would return by

that distorted with a duration of fronts on the order 0.075 μs.

Pulse method proved to be convenient and for the rough testing of the identity of attenuation in the cables. At slow scanning speeds it was possible to examine multiple reflections from both ends/leads of the cable whose envelope gave exponential curve. On the repeated reflections in the cables of decrease it was possible already in the process of test operation to reveal/detect and to remove the absence of contacts in the separate sections of irradiator. In this sense pulse method can be proposed as the convenient system of control/checking for similar type feeder circuits.

For the final phasing of subterranean cables was used the modulation method, similar to that described in [4]. This method of measurement unambiguously makes it possible to equalize/level electrical lengths in the limits only of half-wave difference in the lengths of these circuits. The major advantage of modulation method lies in the fact that it makes it possible with the high accuracy to phase long circuits with the high attenuation. In our case equivalent attenuation due to cable and measuring circuit was about 40 dB. As the load with the modulated reflection coefficient was utilized the tee, in one arm of which was connected the matched load, and in other - the semiconductor diode of model 1A501. The voltage/stress of modulation was supplied to this diode from the movable audiofrequency

oscillator, made on the transistors. Before the measurements the modulated loads of the measured and "standard" cables were checked and was determined an initial difference in their electrical lengths. The accuracy of method was not worse than +-0.5 cm in the measurements at one frequency.

It was shown that the measurements can be carried out, also, on the waves of decimeter s-band the same modulated loads. However, real tuning precision was limited not to the method of measurement, but by small heterogeneities of cable. At the different frequencies these heterogeneities, characterized by reflection coefficient not are more than 0.1, due to the different position in the circuit gave divergences of electrical length within limits of +5° (about 5 cm on the wave 3.6 m). In connection with this measurements it was necessary to carry out at three nonmultiple frequencies, and tuning - through an average/mean difference in the lengths.

Modulation method proved to be the method suitable for measuring small heterogeneities of circuits with the high attenuation of displacing the short-circuited piston. For these measurements between the modulated load and the cable was included the well matched line of variable/alternating length. With the aid of these two methods were inclined all subterranean cables with the accuracy not worse than +-5 cm (relative accuracy $+-10^{-4}$) with the heterogeneities in

the circuit not higher than 0.1 in the reflection coefficient. Attenuation measurings, conducted with the aid of the radiometer and the movable noise generator, showed that the divergence of the attenuation of cables from the tabular values not more than 20o/o.

Page 176.

Was measured the agreement of all sections of irradiator over a wide range of frequencies in the section in the first summing transformer. With the accuracy, determined by measuring error, it is possible to say that the results of measurement coincide. Fig. 2 gives one of such curves (results of measuring the agreement of section No. 7, numbering begins from the western end/lead of the antenna).

According to the results of measurement the agreements and on the data of the attenuation of cables and the measured transient weakenings in the feeders in the range of frequencies were designed by efficiency for the section of irradiator and for entire irradiator. The results of these calculations are given in Fig. 3. Dashed curves are given here for the case of the complete agreement of dipoles and feeders in entire frequency band. Here Fig. 3a gives the values efficiency, measured at several frequencies according to the galactic radio emission and averaged for several sections. The

coincidence of experimental values with the calculated ones is sufficiently satisfactory.

Were measured radiation patterns in E of the plane of several sections of antenna at the different frequencies in the operating range. Measurements were conducted through the radio emission of Cassiopeium-A. The results of measurement showed that the form of diagram was close to the calculated, and effective area corresponds to that expected in KIP of reflector on the order of 0.5.

After tuning of all subterranean cables was carried out the addition of the parts of the antenna and testing the radiation patterns of these parts in the stages of addition in accordance with the diagram in Fig. 1. Radiation patterns were measured by several to the powerful/thick sources of radio emission.

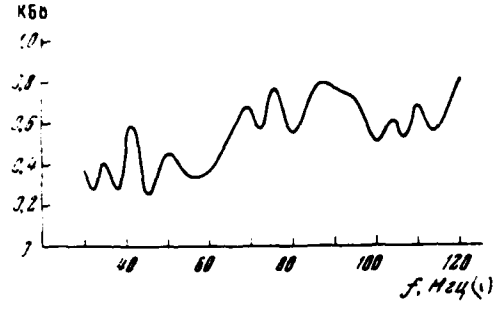

Fig. 2. Agreement of one of the sections of irradiator $K_{б.в} = F(l)$.

Key (1). MHz.

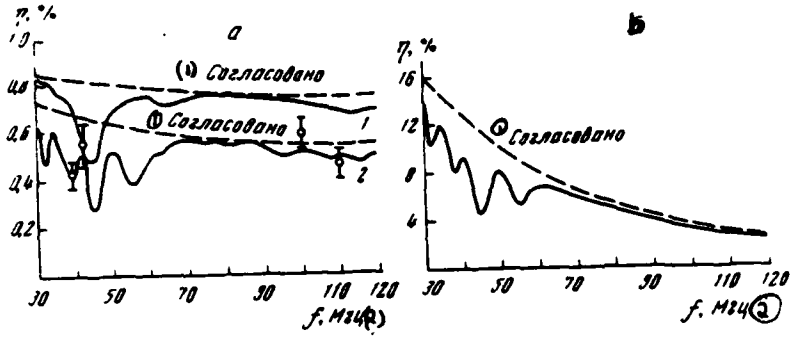

Fig. 3. Efficiencies of irradiator. a) the efficiency of the section of irradiator (1 - in the section in ShSU, 2 - in the section in transformer); b) the efficiency of the feeder circuit of irradiator.

Key: (1). It is matched. (2). MHz.

Page 177.

Fig. 4 gives the radiation pattern of entire antenna into E of plane, obtained at the frequency of 110 MHz on the basis of the source of Cassiopeium-A. The width of diagram according to half power 9'.0+-0'.3 (calculated width 9'.5), side-lobe level is not higher than 6o/o (calculated level 4o/o). The measurements of radiation

patterns in E of plane at other frequencies of operating range showed that their parameters were close to the calculated ones and at these frequencies.

For the purpose of the explanation of the cophasality of irradiator over a wide range of frequencies was measured the position of the maximum of diagram at the different frequencies according to the sources of Cassiopeium-A and Cygnus- A. The results of these measurements are represented in Fig. 5a. Fig. 5b gives the results of measuring the position of diagram at the different frequencies with different zenith distances. Processing results was conducted taking into account the existing inclination/slope of the axis of antenna to the east. Because of this inclination/slope the angle between the maximum of diagram and the meridian will change on the cosine of zenith distance. In the calculations the angle of the slope of axis was accepted by 30'. As showed measurements (Fig. 5a, b), the true angle of inclination/slope was about 28'. Furthermore, as can be seen from Fig. 5b, the axis of antenna is delivered not strictly in the direction an east-west, but it is deflected so that the eastern end/lead of the axis north of west to the angle of approximately 1'.

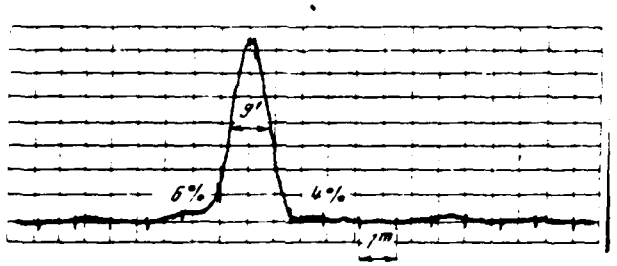

Fig. 4. Antenna radiation pattern "east-west" in E of plane at the frequency of 110 MHz.

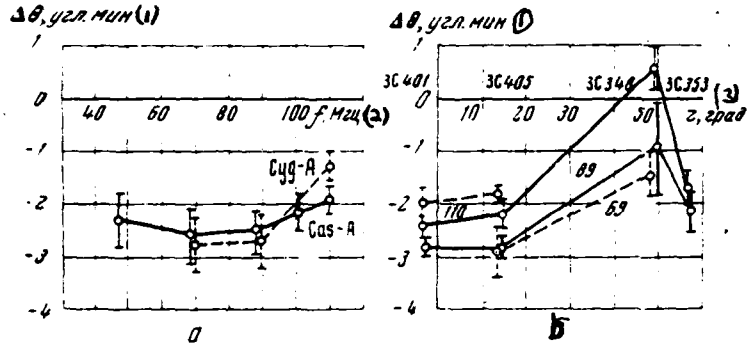

Fig. 5. Results of measuring position of radiation pattern a) in dependence on frequency; b) depending on zenith distance (calculated inclination/slope of axis "east- west" to horizon of 30°).

Key: (1). ugl. min. (2). MHz. (3). deg.

Page 178.

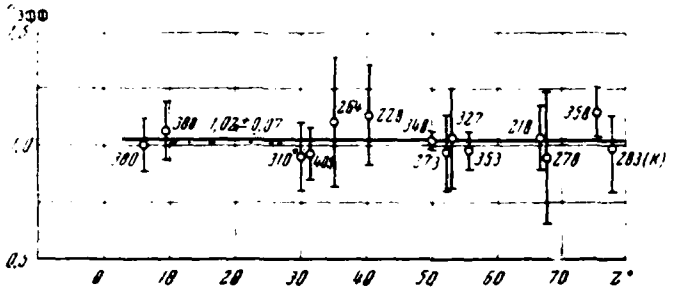

Fig. 6. Dependence of effective antenna area on zenith distance. Numerals in points - number of sources on the catalog ZS.

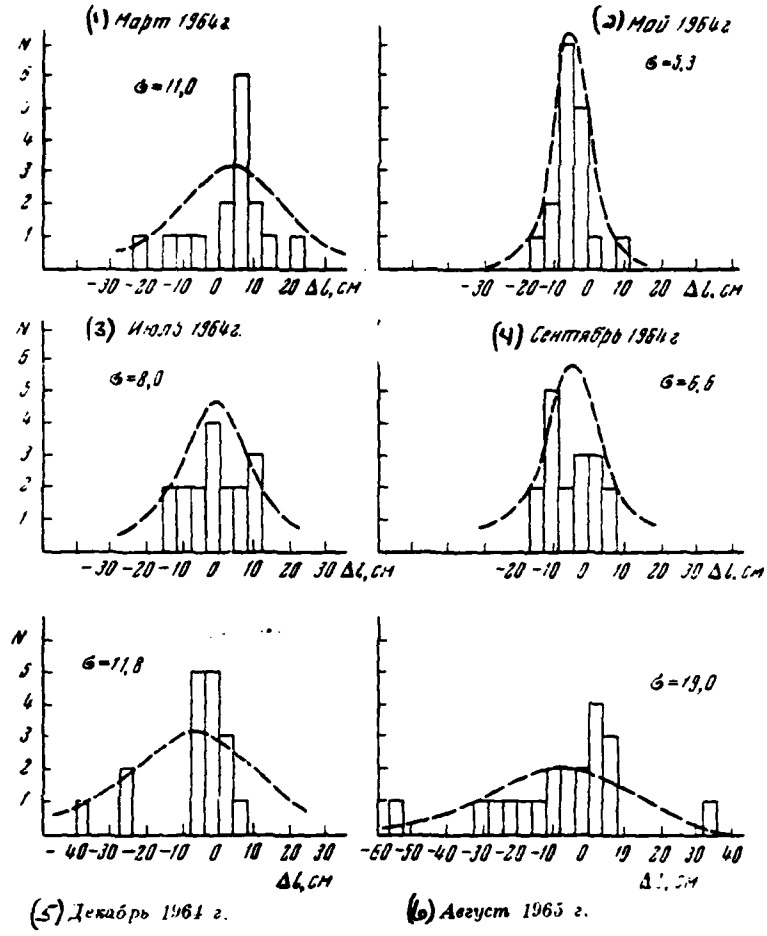

Fig. 7. Histograms of the scatter of the electrical lengths of subterranean cables.

Key: (1). March. (2). May. (3). July. (4). September. (5). December. (6). August.

Subsequent measurements, given according to a larger number of sources [5], gave the following values: the inclination/slope of axis with respect to horizon/level 29', 58+-0'.39; the rotation of axis 1'.85+-0'.43, i.e., the diagram of antenna at the horizon/level of divergence from the meridian to the east of this angle.

The measurements of effective antenna area, carried out on the basis of the intense sources on the wave 3.5 m, showed that for the zenith distances from 10 to 78° noticeable change in the effective area with the accuracy not worse than 7o/o it is not discovered. Fig. 6 gives the results of these measurements. Numerals in points designate the number of source on the catalog 3S.

In the process of operating the antenna "east-west" were conducted regular inspections of the electrical lengths of underground feeder circuits. It was explained that their electrical lengths changed relative to "standard" cable. As the "standard" was undertaken the cable, which goes to the central section of antenna, since it almost wholly was located in the commutation basement. The result of these investigations they are represented in the form of the series of histograms in Fig. 7. Along the axis of abscissas are deposited/postponed changes in the electrical length, along the axis

of ordinates - number of cables, which did not leave along the length beyond the limits of the assigned interval. In each histogram are given the values of standard deviation (σ) of each distribution of the scatter of electrical lengths. In the first approximation, it is possible to say that any seasonal behavior it was not observed. After each testing of scatter was conducted the tuning of the lengths of cables. With an increase in the time between the tunings the scatter of cables increased. The fundamental reason for a change in the electrical lengths of cables in our view is a change in the parameters of small heterogeneities, as a rule, in the sites of installation of high-frequency couplings. Were noted several cases when such heterogeneities, noted during the testing by pulse method and electrical lengths given drifts on the order of 20-30 cm, after elimination gave the considerably smaller drifts of length.

Due to a change in the lengths of cables was noted a change in the parameters of antenna. Increased side-lobe level to 8-10o/o, and a little decreased effective area. In connection with this was recommended the electrical length of cables check and to adjust slightly not less freqeuntly than one time in three months.

3. Sensitivity of antenna "east- west".

It is usually accepted to characterize antenna by the value of

its effective area. During the evaluation of the sensitivity of the knowledge of effective area and efficiency it is insufficient. For this in connection with the goals of radio astronomy it is necessary to know its noise temperature [6].

In the metric wave band the noise temperature of antenna is determined primarily by the brightness temperature of the radio emission of the background of galaxy, which from an increase in the frequency rapidly falls [7]. Since the brightness temperature is different by the celestial sphere, subsequently in the calculations we will take the maximum values of the temperature for the minimum sensitivity (in the direction to the center of galaxy) and minimum values - for the maximum sensitivity (in the direction to the pole of galaxy). Furthermore, as shown in [8] and [9], weak discrete/digital sources, which simultaneously fall into the diagram of antenna, give the fluctuation of their total flow due to the fluctuation of their number. It is obvious, this gives the fluctuation of readings/indications of output recorder and also is determined ultimate sensitivity of radiotelescope. It must be noted that the characteristic period of these fluctuations is determined by the transit time of sources on this declination through the diagram of antenna.

As shown in [9], for the evaluation of the sensitivity of radiotelescope it is convenient to characterize these fluctuations by equivalent noise temperature. For two possible laws of the dependence of a number of discrete/digital sources on their intensity were designed the equivalent noise temperatures, defined subsequently as $T_{\text{шс}}^{\max}$ and $T_{\text{шс}}^{\min}$. The values of these temperatures in the range of frequencies for the antenna "east- west" are given [1] in the table.

FOOTNOTE [1]. Values $T_{\text{шс}}$ are obtained by R. D. Dagkesamenskiy.
ENDFOOTNOTE.

The same table gives the values of the maximum and minimum brightness temperatures of the background of galaxy [7].

(1) МГц	$T_{нас}$, °K		$T_ф$, °K	
	min	max	min	max
30	40 500	82 500	10 000	120 000
40	22 500	54 000	5 000	61 000
50	12 000	40 500	2 900	37 000
60	6 000	30 000	1 900	24 500
70	1 500	24 000	1 300	17 500
80	0	19 500	960	13 000
90	0	15 000	720	10 000
100	0	12 800	570	7 800
110	0	9 500	420	6 000
120	0	7 800	360	5 000

Key: (1). MHz.

During calculations $T_{нас} = \frac{\Delta S A_{эфф} \sqrt{\Delta f \tau}}{2k}$ were accepted the following values: effective antenna area $A_{эфф} = 0.6\ A_{геом} = 24\,000\ м^2$, the band of radiometer Δf=300 kHz, time constant τ=10 s. The rms value of the fluctuations of average/mean flow was determined from [9]. The calculation of the critical angle of the discrete/digital source, recorded by radiotelescope with the signal-to-noise ratio, by the equal to 5, was performed for the radiometer with parameters $T_{пр} = 500°$ K (noise factor 2.6), passband Δf=300 kHz, time constant τ=10 s according to the usual formula

$$\Delta S_{пр} = 5 \frac{2k}{\sqrt{\Delta f \tau}} \frac{T_{пр} + (T_ф + T_{нас})\eta + T_0(1-\eta)}{A_{эфф}}.$$

Values efficiency η are undertaken from the graph/curve Fig. 3b, while values $A_{эфф}$ at the input of receiver/detector are designed taking into account this efficiency for the coefficients of the use

of a surface, which are found over a wide range of frequencies in limits of 0.6-0.53. Dependences $\Delta S_{\text{npminmin}}$ and $\Delta S_{\text{npmaxmax}}$ are given in Fig. 8. Is here given dependence $A_{\text{эфф}}$ over a wide range of frequencies. Points on the graph/curve noted experimental values $A_{\text{эфф}}$, the measured at the separate frequencies of operating range antennas. As can be seen from Fig. 8 coincidence of experimental values with the calculated ones completely satisfactory.

From Fig. 8 it is evident that in the range of the frequencies of 30-70 MHz the sensitivity of antenna is determined in essence by the radio emission of background and by the effect of saturation. Although the effective antenna area at the input of receiver decreases with an increase of the frequency due to the increase of losses in the feeder circuit however the sensitivity of radiotelescope is improved. In the range of the frequencies of 80-120 MHz the sensitivity of antenna with an increase in the frequency increasingly more is determined by the parameters of feeder circuit.

Page 181.

In this sense use/application of extension amplifiers [9] will give gain in the range 80-120 MHz and virtually will not improve sensitivity in the range 30-70 MHz. In that case the determination of the sensitivity of radiotelescope, in our opinion, is necessary

taking into account all factors in the working frequency band. The evaluation/estimate of the quality of antenna according to the effective area will be only incomplete. The observations, carried out on the wave 7.5 m, showed that actually/really the sensitivity of radiotelescope is determined by the radio emission of background and by the effect of saturation.

The creation of wide-range irradiator with the overlap in frequency 4:1 made it possible to more fully utilize possibilities of antenna. For this radiotelescope there are many goals which it is difficult to solve on the narrow-band instrument. In particular, the measurements of the spectral indices of many sources [5] it is most simple to carry out on one range instrument. Furthermore, the large freedom from interference of broadband antenna makes it possible to obtain more than information and to more completely utilize the expensive instrument.

In conclusion the author considers it his duty to express appreciation to leader to the doctor of physical-math. sciences V. V. Vitkevich for the constant attention to this work, doctor of physical-math. sciences A. D. Kuz'min for the useful discussions in the beginning of this work and wireless engineer V. T. Solodkov for the great assistance in the experimentation.

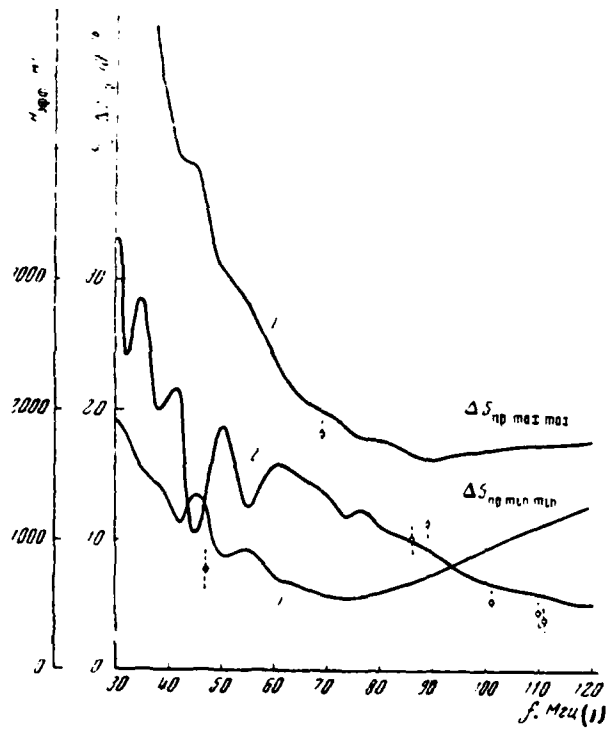

Fig. 8. Dependence of ultimate sensitivity of antenna "east- west" (1) and effective antenna area $A_{эфф}$ (2) on the frequency.

Key: (1). MHz.

Page 182.

REFERENCES

1. В. В. Вяткевич, П. Д. Калачев. Труды ФИАН, 28, 5 (1965).
2. Ю. П. Илясов, А. Д. Кузьмин. Труды ФИАН, 28, 14 (1965).
3. С. Н. Иванов, Ю. П. Илясов, Г. Н. Храмов. Труды ФИАН, 28, 22 (1965).
4. G. Swarup, K. S. Yang. IRE Trans. on Antennas and Prop., AP-9, № 1 (1961).
5. В. С. Артюх, В. В. Вяткевич, Р. Д. Дагкесаманский. Астрон. ж., 44, № 5 (1967).
6. Л. Д. Бахрах, К. И. Могильникова. Изв. вузов. Радиофизика, 7, 585 (1964).
7. H. K. Sutcliffe. RRE J., 50, october (1963).
8. S. von Hoerner. NRAO, 1, № 2, 1961.
9. Р. Д. Дагкесаманский, С. Н. Иванов, Ю. П. Илясов. Труды ФИАН, 38, 29 (1967).

Page 201.

INTERFEROMETER WITH THE RELAYING FOR THE METRIC RANGE.

G. I. Dobysh.

At present at the radio-astronomical station FIAN for the preliminary tests is prepared equipment of interferometer with the relaying. Predicted maximal value of base 40-50 km.

For some reasons the frequencies of the reception of the radio emission of sources were selected in the range 34-36 MHz (λ=8.2-8.8 m). The presence in this range of a comparatively high level of atmospheric and man-made interferences in many respects predetermined ways and methods of the technical solutions of separate nodes and units of equipment. In particular, one of the main conditions we considered the possibility of the smooth retuning of radio-astronomical receivers in the limits of 1-2 MHz for the possibility of selection in the range of the range of sections indicated with the smallest interference level.

General/common/total design principle of the construction of interferometers and separate results are well known from works [1-4]. However, the difficulties of practical design were determined by the absence of concrete/specific/actual norms to the series/row of the fundamental parameters of similar systems, and, first of all, on the relay equipment. In particular, were unknown such norms, as:

1) the acceptable noise levels, background and spurious radiations within the limits of the band of the operating frequencies:

2) the permissible coefficients of nonlinear distortions;

3) the nonuniformity of group time in the hf circuit, etc.

Unclear were also the questions, connected with the formation of the coherent frequencies of the heterodynes for the diverse radio-astronomical receivers. Therefore during the development of equipment as the base were accepted the recommendations of international consultative committee on radio communication (MKKR [International Radio Consultative Committee]) to the radio relay lines with the frequency division multiplex. However, finally to formulate and to refine norms and technical specifications will be only after the experimental check. This equipment is designed and

made taking into account this possibility.

Our version of interferometer is two diverse receivers of the radio emission of space sources (radio-astronomical receivers) with the coherent heterodyne. Heterodyne common to both receivers is located on the extension point/item (VP) and is transmitted by the radio relay line to the main post (OP) together with the signal of radio noise. Moreover relaying the signal of radio noise and transmission of the frequency of heterodyne are realized by one transmitter. The reception of these two signals on OP is also conducted by one receiver with their subsequent separation after demodulation and amplification.

Page 202.

The equipment part of the interferometer is made in the composition of the following basic building blocks:

a) on the extension point/item - radio-astronomic receiver, radio relay transmitter with the frequency modulation ($\tilde{f}_m$), the stabilized supplies of power and system of control/checking;

b) on the main post - radio-astronomical receiver, the receiver of the relayed signals, assembly of equalization and filters, line of

delay, low-frequency part, stabilized supplies of power and system of control/checking.

Block diagram VP and OP they are given respectively in Fig. 1 and 2.

Radio-astronomic receivers are made on the superheterodyne circuit with the frequency of heterodyne, located in the middle of the passband of amplifier of high frequency (uhf), i.e., the nominal value of the frequency of heterodyne $f_г$ in this case is determined by the relationship/ratio

$$f_г = \frac{f_в - f_н}{2},$$

where $f_н$ and $f_в$ - value of frequencies on the band edges of the transmission of uhf receiver. This method of transformation is used from the following considerations:

1) twice becomes narrow the passband of IF amplifier (UPCh), since the effective bandwidth, which is determining ultimate sensitivity of interferometer, is equal in this case $2\Delta f_{УПЧ}$;

2) relaying the low-frequency spectrum of zero signal to a certain extent it simplifies transmitter, decreases requirements for the series/row of characteristics it makes it possible to utilize (with its comparatively narrow band) for the simultaneous

transmission of the frequency of heterodyne and signal of noise;

3) the transfer of the spectrum of the noise signal into the region of low frequencies simplifies also the fulfillment of the delay line, necessary in this case for the compensation for the time of propagation of one of the signals of noise on the route of radio relay line.

The high-frequency part of the receiver consists of the preamplifier, arranged/located directly in antenna, and strictly the uhf receiver, made in the form of two parallel-connected amplifiers, included by choice, which have passbands on 1 MHz and inclined one on f_0=34.5 MHz, by another on f_0=35.5 MHz. Antenna amplifier has a passband 6 flat-topped MHz in the limits of 35+-1.5 MHz and a noise factor N=3.85. Thus is provided the possibility of the smooth tuning of receiver in the limits of 34-36 MHz without any retuning of uhf receiver with the sufficiently good selectivity of input part.

Further signal in the mixer with the aid of the frequency of heterodyne $f_r = 35 \pm 1.5$ MHz is converted into the intermediate frequency. Actually UPCh is UNCh with deep negative feedback ($k\beta$=120), the passband of which from 1 to 210 kHz. Strictly frequency receiver response in the intermediate frequency is formed/shaped in the region of lower frequencies with transient circuits, in the

region of higher frequencies - by three-link low-pass filter with a cutoff frequency of 135 kHz, connected after the mixer and of creating weakening 60 dB at the frequency 180 kHz. After filter at the input of UPCh is connected stepped gain control with a depth of adjustment of up to 30 dB.

Because of the strong negative feedback with a change in the voltages of supply (on the anode or the incandescence/filament) on +-20o/o amplification factor in PCh is changed by less than 1o/o.

Page 203.

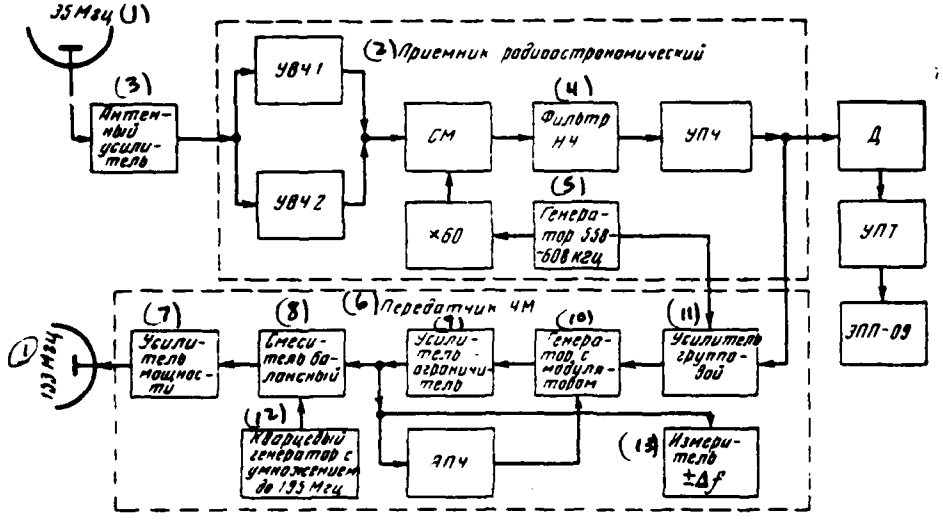

Fig. 1. Block diagram of equipment of extension point/item.

Key: (1). MHz. (2). Receiver, radio-astronomical. (3). Antenna amplifier. (4). Filter. (5). Generator 558-608 kHz. (6). Transmitter. (7). Amplifier of power. (8). Mixer, balance. (9). Amplifier limiter. (10). Generator with modulator. (11). Amplifier of group. (12). Crystal oscillator with multiplication to 195 MHz. (13). Meter +-Δf.

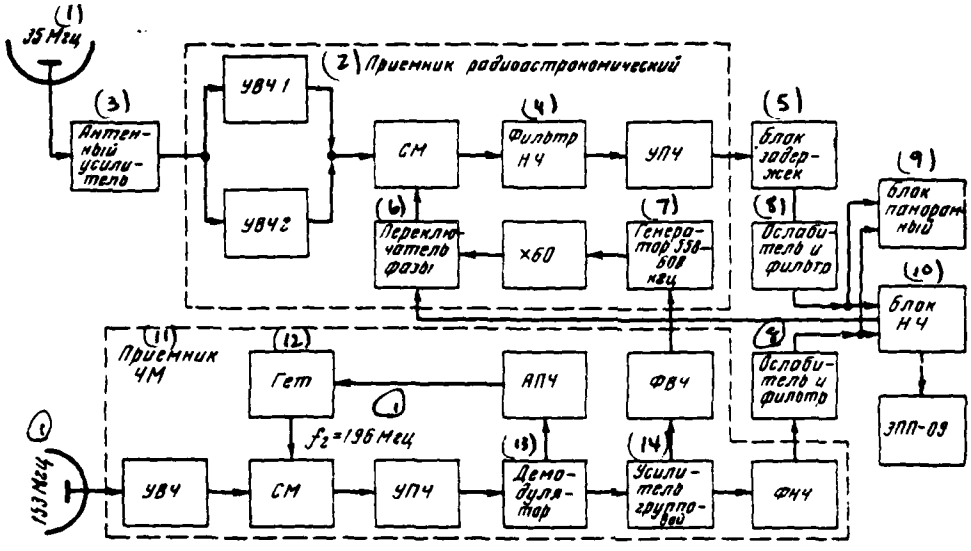

Fig. 2. Block diagram of equipment of main post.

Key: (1). MHz. (2). Receiver, radio-astronomical. (3). Antenna amplifier. (4). Filter. (5). Delay unit. (6). Phase reversing switch. (7). Generator 558-608 kHz. (8). Attenuator and filter. (9). Block, panoramic. (10). Block. (11). Receiver. (12). Het. (13). Demodulator. (14). Amplifier of group.

Page 204.

And, since in UPCh are absent resonant circuits, the form of its frequency characteristic and passband do not change upon the exchange

of tubes and during the gain control.

The voltage/stress of heterodyne with a frequency of 35+-1.5 MHz on the extension point/item is obtained via multiplication 60 times of oscillator frequency, reconstructed in the limits of 558-608 kHz. The reconstructed oscillator is made on the diagram of that making it possible with the appropriate heat stabilization to obtain lasting stability $1 \cdot 10^{-4}$.

The amplitude of the voltage/stress of heterodyne on the mixer is equal to $U_г = 12$ V. Therefore the conversion factor remains constant with change $U_г$ at least to +-30o/o. Thus, virtually is eliminated the effect of the amplitude instability of the block of the multipliers of heterodyne on the factor of amplification of radio-astronomical receiver.

From the output of radio-astronomical receiver VP noise signal with the spectrum from 1 to 135 kHz and part of the voltage of the generator 558-608 kHz fall on the modulator of the transmitter of radio relay line.

The transmitter of radio relay line operates at a frequency of 153 MHz. The peak power output of 50 W. Modulation is frequency.

The frequency of relaying 153 MHz was selected from those considerations, that on the ultrashort waves are absent rapid and deep signal fading on the route, of the caused by reflections from the heterogeneities tropospheres and change in the refraction. In the simplified form phase displacement between the straight/direct and reflected waves due to a path difference at the wavelength λ can be defined as

$$\Delta\varphi = \frac{2\pi}{\lambda_{\text{в}}}\Delta r(g),$$

where Δr(g) - a change in the path difference as the function, which depends on the lapse of dielectric permittivity of air g, the character of route, etc. Thus, for the average band of the Soviet Union with the route R=45 km Δr(g) it will be of the order 12 cm. Then for λ=10 cm Δφ=432°, and with change g is possible the appearance of the interference maximum and minimum, i.e., at the point of reception the strength of field is subjected to strong changes. With λ=2 m Δφ in all 21°,6, and level of signal at the point of reception will considerably less depend on the conditions of reception.

During the determination of the power output of transmitter, besides the account of all other factors, we proceeded from the possibility of work on comparatively simple antennas (for example, type "wave duct"), convenient during the transportation and the arrangement/position on the light supports. At the power of

transmitter 50 W for the base R=45 km the required antenna gain of radio relay line G=16 dB. Is preinspected the possibility of a smooth change of the power output of transmitter within the limits of 5-50 W.

As noted above, in the transmitter was used ChM (fm). Advantage of ChM over AM obviously and consists, first of all, in the possibility of the virtually complete elimination of parasitic amplitude modulation, caused by fadings on the route and the nonuniformity of the frequency characteristics of the hf circuits of transmitter and receiver. ChM modulator is made on the diagram of parallel circuits [5]. A similar diagram makes it possible to obtain the high degree of the linearity of modulation characteristic with the large deviations of frequency.

Central frequency of modulator f_0=42 MHz, the maximum deviation of frequency $\Delta f_{макс} = 1.2$ MHz. Fig. 3 gives the dependence obtained in the mock-up of the slope/transconductance of the modulation characteristic $d(\Delta f)/dU$ on the voltage on the input of modulator.

Page 205.

It is possible to see that the divergences from the linear law do not exceed 2o/o, to what corresponds percentage distortion in the second

and third harmonics of order 0.2o/o. During the more careful adjustment is possible obtaining the coefficient of nonlinear distortions less than 0.1o/o. The requirement of the high degree of the linearity of modulation characteristic is explained, first of all, by two-signal modulation of transmitter, since otherwise are possible mutual transient distortions and interferences in the channels of heterodyne and noise.

After amplification and limitation of ChM of oscillation/vibration with a central frequency of f_0=42 MHz and peak deviation $\Delta f_{max} = \pm 830$ kHz (+-360 kHz to the channel of noise and +-470 kHz to the channel of heterodyne) are supplied to the balance mixer where mix with a frequency of $f_r = 195$ MHz, obtained from the crystal oscillator after multiplication. The difference frequency

$$f_r - (f_0 \pm \Delta f_{max}) = 153 \pm 0{,}86 \text{ MHz}(1)$$

Key: (1). MHz.

it is further amplified to 50 W by the two-stage amplifier of power, made on the generator of VHF tetrodes of the type GU-29. The through frequency characteristic of transmitter is given in Fig. 4.

The system of the automatic tuning of central frequency (APCh) to 42 MHz, crystal oscillators for the frequency of 195 MHz they made

it possible to obtain the stability of the central frequency of transmitter $2 \cdot 10^{-5}$. During the work is realized continuous monitoring of the frequency deviation by the meter of deviation, combined with the system of APCh.

It is necessary to note the following fact. As showed the experiment, the presence of combination and side frequencies in the emission band of transmitter with the levels 60-65 dB from the level of central oscillation without modulation, which corresponds to the norms of MKKR, it is completely inadmissible, since it is possible to lead to the appearance of interferences in the channel of radio-astronomical receiver OP along the channel of the relayed frequency of heterodyne. The measurements conducted showed that the tolerance levels of combination frequencies are 80-90 dB.

The receiver of radio relay line, which is found on OP, has one cascade/stage of uhf/UVCh, mixer, heterodyne with the system APCh, six-stage UPCh, demodulator and group UNCh with the linear cascades/stages at the output.

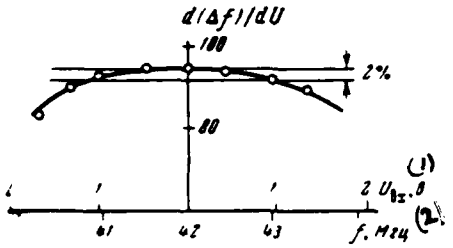

Fig. 3.

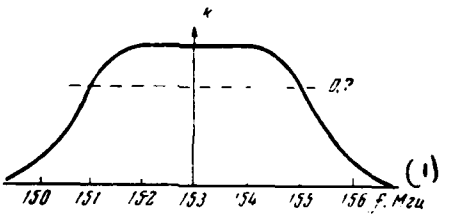

Fig. 4.

Fig. 3. Dependence of slope/transconductance of modulation characteristic of modulator of transmitter on frequency.

Key: (1). V. (2). MHz.

Fig. 4. Through frequency characteristic of transmitter.

Key: (1). MHz.

Page 206.

Receiver sensitivity 30 μV with 1 V of actual stress on the input of the limiters of demodulator. Noise factor N=3. Passband prior to the input of demodulator 4.7 MHz.

As is known, with ChM nominal width of band of system is

approximately equal to

$$2\Delta f = 2\,(\Delta f_{\text{пик}} + F_{\text{макс}}),$$

where $\Delta f_{\text{пик}}$ - peak deviation of frequency; $F_{\text{макс}}$ - highest frequency of the spectrum of the modulating signal. Due to an inaccuracy in tuning receiver, instability and nonuniformity of the characteristics of uhf/UVCh and UPCh, instability of the frequency of transmitter and heterodyne of receiver and series/row of other factors the bandwidth must be increased approximately/exemplarily 1.6 times. Thus, the final values of the band of ChM of receiver will compose value

$$3{,}2\,(\Delta f_{\text{пик}} + F_{\text{макс}}),$$

and in our case we will obtain $2\Delta f = 4.6$ MHz. For the stabilization of frequency and, that especially importantly with ChM, phase response the total values of the capacities/capacitances of ducts/contours of UPCh are selected order 50 pF. Because of this measure the form of frequency and phase responses of UPCh does not depend on changes in the modes of operation, ageing and exchanging the tubes.

For the distortion elimination due to the multiple-pronged reception and the fadings on the route in the demodulator is used two-stage broadband limitation. The characteristic of limiter is given in Fig. 5, where to point $U_{\text{вх}} = 1$ V corresponds signal at the input of receiver 30 μV. Limitation level, equal to 1.8 V at the input discriminators, is supported with the high degree of accuracy and stability due to the use as the sources of bias voltage of the

limiting diodes of dry cells of the type "Saturn" or "FBS". Since for the route R=45 km and λ=2 m the expected changes in the signal level, caused by fadings, will not exceed the value of 11 dB during 99.9o/o of time, which corresponds to change $E_{вх}$ of the receiver 3.55 times, they they will be completely suppressed, since signal level at the input of discriminator remains constant with a change in the signal at the input of limiter (counting from threshold level $U_{вх} = 1$ V) at least on 14 dB.

Discriminator is made on the detuned circuits. Mutual conductance of discriminator 200 m /MHz. Nonlinearity in the limits of +-2 MHz from the central frequency is the same as for the modulator of transmitter.

From the output of demodulator the signals of noise and heterodyne after amplification in the group amplifier, included by a deep negative feedback, to the levels 0.5-1 V, the signal of noise through the filter of lower frequencies ($f_{ср} = 180$ kHz), and the signal of the heterodyne through the high-pass filter ($f_{ср} = 450$ kHz) enter respectively: the first the unit of equalization and filters, the second to the unit of frequency multiplication of the heterodyne of radio-astronomical receiver OP.

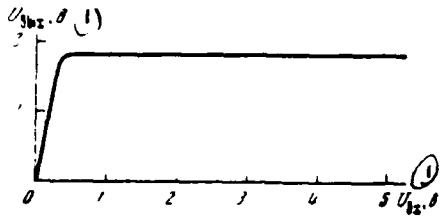

Fig. 5. Characteristic of limiter radio relay ChM of the receiver of main post.

Key: (1). V.

Page 207.

In this unit the frequency of 558-608 kHz relayed with VP is multiplied to the frequency of 35+-1.5 MHz (just as on VP the multiplication factor is equal to 60) and then after amplification it is utilized as the heterodyne voltage/stress of radio-astronomical receiver OP.

The expected variations in the phase of the frequency of heterodyne on the main post after multiplication to 35+-1.5 MHz, the caused by change "lengths" of route due to the refraction, will compose value $\Delta\varphi=2°,9$, which is completely admissible. However, as showed the first experiments, fundamental difficulty with the direct

multiplication of the relayed frequency of 583+-25 kHz consists not only in reaching/achievement of high phase stability, but also in obtaining of sufficiently free from the noises heterodyne voltage/stress, i.e., the voltage/stress of heterodyne on the mixer of radio-astronomical receiver OP with the large signal-to-noise ratio. For these purposes by us is now applied the synchronization of local oscillator by capturing its frequency by a frequency of the relayed voltage/stress of 558-608 kHz. Monitoring of the mode/conditions of synchronization is realized by an oscillograph. With the sufficiently rigid phase synchronization in this case nevertheless it is impossible to obtain high interference shielding on the heterodyne OP, although it substantially higher than with the direct multiplication.

Subsequently it is proposed to investigate the possibility of using the system of phase of APCh. In this case we proceed from the following considerations. The unit of multiplication for the possibility of changing the frequency of heterodyne has a passband on the input 0.1 MHz (respectively on the output 6 MHz). The majority of cascades/stages works in the sharply nonlinear mode/conditions. This leads to the fact that the signal-to-noise ratio at the output of unit deteriorates in comparison with the input on 10-15 dB. Even the insignificant noise level and interferences within the limits of the input band of multiplier greatly raises the inherent noise level of

radio-astronomical receiver OP, since noise components of heterodyne voltage/stress participate in the process of transformation on the level with the useful signal.

The most obvious and effective measure for noise reduction is in this case the contraction of the passband of the unit of multiplication. However, the execution of the narrow-band system of multiplication with the relatively larger multiplication factor, reconstructed in certain frequency band, and with the stable phase responses is extremely difficult goal.

The necessary ratio of the voltage/stress of heterodyne to its noises $(U_г/U_{ш.г})_{вых}$ on the output of the unit of multiplication and the input of the mixer of radio-astronomical receiver can be found from equation

$$\left(\frac{U_г}{U_{ш.г}}\right)_{вых} = 20\lg\frac{U_г}{2K_{увч}}\sqrt{\frac{P_{ш\,см}/P_{ш\,г}}{kT_0 2\Delta f_{увч} R_a (N-1)}}\ [\text{дб}], \qquad (1)$$

Key (1). dB

where $P_{ш\,см}$ - power of the noises, created by the hf/VCh part of radio-astronomic receiver, including mixer, with the heterodyne voltage/stress free from the noises; $P_{ш.г}$ - power of the noises of heterodyne voltage/stress; $K_{увч}$ - voltage amplification factor of uhf receiver of up to the grid of mixer. In order not to increase considerably the noise factor of radio-astronomical receiver, relation $P_{ш.см}/P_{ш.г}$ must be sufficient to large ones. Assigning $P_{ш.см}/P_{ш.г} = 10$, for our case we will obtain

$$(U_{\text{р}}/U_{\text{ш.г}})_{\text{вых}} = 100 \overset{(1)}{\text{дб}}.$$

Key: (1). dB.

Page 208.

If we now consider deterioration of signal-to-noise ratio due to the multiplication on 15 dB, then relation $(U_{\text{г}}/U_{\text{ш.г}})_{\text{вх}}$ at the input of the unit of multiplication must be not worse

$$(U_{\text{р}}/U_{\text{ш.г}})_{\text{вх}} \geqslant 115 \overset{(1)}{\text{дб}}. \qquad (2)$$

Key: (1). dB.

This relation must be fulfilled at the output of the receiver of ChM radio relay line for the channel of relaying oscillator frequency 558-608 kHz.

After using the results of work [6], we will obtain dependence $(P_{\text{с}}/P_{\text{ш}})_{\text{вых}}$ at the output of ChM receiver on $(P_{\text{с}}/P_{\text{ш}})_{\text{вх}}$ at the input and passbands of low-frequency part ΔF. In this case we consider that the deviation from the frequency of 558-608 kHz $\Delta f_{\text{с.г}}$ is less than half of the passband of UPCh receiver. Then

$$\left(\frac{P_{\text{с}}}{P_{\text{ш}}}\right)_{\text{вых}} = \frac{0{,}375\left(\frac{P_{\text{с}}}{P_{\text{ш}}}\right)_{\text{вх}} D^3}{D^2\left\{1 + 0{,}89\, D^2\left(\frac{P_{\text{с}}}{P_{\text{ш}}}\right)_{\text{вх}}\left[\exp\left(\frac{P_{\text{с}}}{P_{\text{ш}}}\right)_{\text{вх}} - 1\right]^{-1}\right\}}, \qquad (3)$$

where $D = \frac{2\Delta f_{\text{пч}}}{\Delta F}$ has idea of filtration factor, $B = \frac{\Delta f_{\text{пч}}}{\Delta f_{\text{с.г}}}$ can be defined as the coefficient of the use of a band.

Since us interests relation $(P_c/P_{\text{ш}})_{\text{вых}}$ with the sufficiently large ones $(P_c/P_{\text{ш}})_{\text{вх}}$ (usually for radio relay lines $(P_c/P_{\text{ш}})_{\text{вх}} > 30$ dB according to the peak relations), equation (1) we can simplify. We will obtain

$$\left(\frac{P_c}{P_{\text{ш}}}\right)_{\text{вых}} = 0{,}375\left(\frac{P_c}{P_{\text{ш}}}\right)_{\text{вх}} \frac{D^2}{B^2}. \qquad (4)$$

From equation (4) it is possible to see that the most effective means of an increase in the signal-to-noise ratio at the input of frequency multiplier of heterodyne OP is the contraction of the passband ΔF of the low-frequency part of ChM receiver along the channel of the frequency of 558-608 kHz. Utilizing equation (4), depending on ΔF were calculated relations $(P_c/P_{\text{ш}})_{\text{вых}}$ for two values $\Delta f_{\text{с.г}}$ in ratio $(P_c/P_{\text{ш}})_{\text{вх}} = 30$ dB, which corresponds to the worst conditions on the route R=45 km. The obtained dependences are given in Fig. 6. Thus, if necessary relation $(U_г/U_{\text{ш.г}})_{\text{вх}}$ is accepted with certain reserve, equal to 135 dB, then the passband of the low-frequency part of the receiver must be according to to Fig. 6 ΔF≤100 Hz.

The only actually feasible system of the tunable filter with this band at frequencies of 500-600 kHz - this is the system of phase self-alignment (FAP).

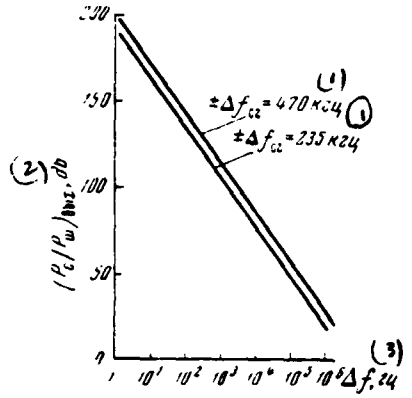

Fig. 6. Dependence of relation $P_c/P_ш$ at the output of UNCh of radio relay receiver on the passband of UNCh.

Key: (1). kHz. (2). dB. (3). Hz.

Page 209.

In practice does not present difficulties the execution of system of FAP with the interference suppression on 135-140 dB. In this case phase error and slow phase drifts of the synchronized oscillator will not exceed 4-5° after multiplication 60 times. Consequently, system of FAP is optimum version for the formation of the coherent voltage/stress of the heterodyne of radio-astronomical receiver of OP.

From the output of radio-astronomical receiver OP noise signal

enters the delay unit.

Delay unit is made in such a way that with a change in the delay time $\tau_з$ from 0 to 40 μs the transmission factor of unit remains equal to unity. This is reached by the fact that with the maximum $\tau_з$ fading signal is compensated by special amplifier, moreover the resulting transmission factor of delay unit is equal to K=1. Any disconnected component/link of delay line is replaced by U-shaped attenuator with the attenuation, equal to fading signal in the disconnected component/link.

Frequency characteristics, their dependence and dependence of K on $\tau_з$ are shown in Fig. 7. Because of the use/application of phase correctors the phase response for any $\tau_з$ in the limits of the service band of frequencies deviates from linear by no more than 0°,3. Delay line is made in the form of the set/dialing of the standard ones LC of delay units to 5 and 1 μs. Smooth change $\tau_з$ from 0 to 1 μs is realized by a delay line, that works according to the principle of capacitive slip ring [7]. Unit makes it possible to work with the bases to 10-12 km. Subsequently for the large bases is intended to utilize the magnetostrictive L3.

From LZ noise signal of OP and from the receiver of radio relay line noise signal VP they come the unit of equalization and filters.

In the unit of equalization and filters is possible a change of the transmission factor in each of two channels to 5 dB. The equality of signal levels at the output of unit is monitored by special differential voltmeter with an accuracy to 0.001 dB. In the same unit finally are formed/shaped the frequency characteristics of channels. For these purposes is utilized the unit of the interchangeable filters of lower and higher frequencies.

Since the passband of all preceding/previous devices/equipment for the noise signals of the sources of radio emission much wider than the passband of the unit of filters, effective band and form of the frequency characteristic of each channel is determined only by the unit of filters. For this is utilized the pair of three-link low-pass filters with $f_{cp} = 120$ kHz and the pair of three-link high-pass filters with $f_{cp} = 25$ kHz.

Thus are reached high identity and stability of passbands in both channels without depending on a change in parameters and modes of operation of all preceding/previous units.

Because of the interchangeability of filters possible to change the bandwidths without any retuning of equipment.
Structurally/constructurally all filters are made on the standard interchangeable cells from the electronic computer "Urals".

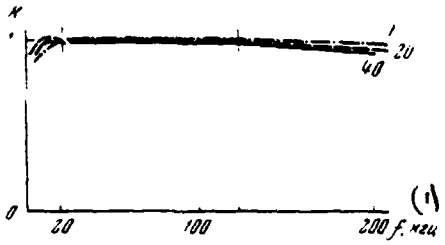

Fig. 7. Set of frequency characteristics of delay unit with different ones $\tau_з$ (delay factor they are indicated with numerals in μs).

Key: (1). kHz.

Page 210.

The through frequency characteristics of channels are given in Fig. 8. The sequence of the formation of the frequency characteristic of channel of OP is shown in Fig. 9.

The unit of equalization and filters has two pairs of outputs. From one pair of outputs noise signals enter the unit of 1f/NCh, where they are summarized, are squared, they are detected and after narrow-band RC- amplifier are supplied to the phase discriminator. Phase switching with a frequency of 30 Hz is realized in the frequency of heterodyne by the electronic switch.

The characteristic of the diagram of squaring has quadratic section with an accuracy to 0.5o/o in the limits of 1.5 V at the input summing cascades/stages (to 7 V at the input square-law function generators).

To another pair of the outputs of the unit of filters is connected the panoramic unit, which makes it possible to conduct continuous visual monitoring in the limits of the service band of each channel simultaneously.

Into the content of equipment of each point/item it enters power frame with electronic regulators of anodic and filament voltages/stresses. Are here placed the units of monitoring and signaling about the malfunction of all fundamental nodes of equipment.

On any of the points/items the signal adopted from the radio sources it is monitored via recording by its compensation method. In this time the equipment passes the stage of complex adjustment and testing. The tests conducted made it possible to refine requirements for the equipment on the series/row of the parameters, enumerated above. The sufficiently good coincidence of experimental data with the calculated ones makes it possible to hope for the possibility of observing the sources of radio emission for bases, also, to 50 km.

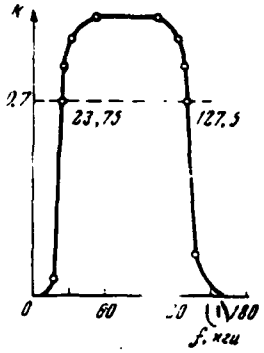

Fig. 8.

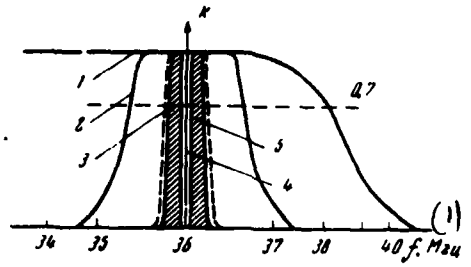

Fig. 9.

Fig. 8. Frequency characteristics of radio-astronomical receivers at output of unit equalization also of filters.

Key: (1). kHz.

Fig. 9. Sequence of formation of frequency characteristic of radio-astronomical receiver of main post. 1 - frequency characteristic (ChKh) of antenna amplifier; 2 - ChKh UVCh-1; 3 - ChKh UVCh-2; 4 - frequency of heterodyne; 5 - ChKh of the unit of filters.

Key: (1). MHz.

In conclusion the author thanks the doctor of physical-math. sciences V. V. Vitkevich for the theme proposed, attention to the work and concrete/specific/actual propositions during the selection, the discussion and the preparation of equipment for the operation. The author expresses his gratitude to engineers to M. T. Rezepin, V. A. Frolov and colleagues of the department "Radio engineering" of Tula polytechnic institute for the great assistance during development and production of the equipment part of the interferometer.

REFERENCES.

1. В. В. Виткевич. Астрон. ж., 29, вып. 4 (1952).
2. В. В. Виткевич, Р. С. Сороченко. Астрон. ж., 30, вып. 6 (1953).
3. R. N. Brown, R. Q. Twiss. Phil. Mag., 45, N 336 (1954).
4. O. Elgaroy, D. Morris, B. Rowson. Monthly Notices, 124, N 5 (1962).
5. Ж. Фаго, Ф. Мань. Частотная модуляция в радиорелейных линиях. Изд-во «Советское радио», 1964.
6. Э. С. Элинсон, А. С. Ларионов. Радиотехника, 22, № 2 (1967).
7. А. Г. Голубков. Изв. вузов. Радиотехника, 5, № 4 (1962).


ATE
LME